UNIVERSITAT POLITÈCNICA DE VALÈNCIA

Doctoral Dissertation

PhD in Design, Manufacture and Management of Industrial Projects

Experimental and numerical study of the thermo-fluid dynamics of borehole heat exchangers incorporating advanced materials to be optimized for use as thermal energy storage (BTES)

Estudio teórico-experimental de la termo-fluidodinámica de intercambiadores de calor de geotérmicos que incorporan materiales avanzados para su optimización como almacenamiento de energía térmica (BTES)

Author: Hossein Javadi

Directors: Prof. Dr. Javier Fermín Urchueguía Schölzel

Prof. Dr. Borja Badenes Badenes

February 2024

Abstract

Due to severe environmental pollution and worldwide energy deficiency, exploiting renewable energies has become more critical than ever. Shallow geothermal energy (SGE) is considered a sustainable and renewable energy source with significant advantages in space heating and cooling, industrial applications, greenhouses, electricity production, agriculture industry devices, and hot water production, among others.

The ground source heat pump (GSHP) system is a promising technology for utilizing SGE. In this system, a borehole heat exchanger (BHE) plays an important role and directly influences the coefficient of performance (COP) of this shallow geothermal system.

Different approaches have been carried out to enhance the performance of the BHE, including using advanced materials for pipes, heat transfer fluids, and backfill/grout, designing new geometries, and optimizing the BHE to be used as borehole thermal energy storage (BTES) systems.

Drilling costs, heat pump electricity consumption, and borehole thermal resistance can be reduced using materials with appropriate thermo-physical properties like nanofluids and heat storage materials. This results in not only a more significant heat transfer between the heat transfer fluid, the backfill/grout, and the soil but also lessens the thermal effect on the surroundings.

Heat transfer fluid is one of the factors in optimizing the BHE to be used for thermal energy storage (TES). Increased thermal conductivity in the heat transfer fluid enhances heat transfer efficiency between the fluid and the heat storage materials, leading to a more rapid attainment of the phase change temperature in the storage materials. In essence, when employing a heat transfer fluid with superior thermal conductivity, the temperature of the heat storage material experiences quicker fluctuations, resulting in a significant reduction in the duration required for a complete phase change.

Moreover, the use of phase change material (PCM) as a heat storage medium instead of conventional backfill/grout enables the BHE to be beneficial and applicable as a BTES system. In addition to decreasing the required borehole depth considerably, the BTES system can store and release energy daily and seasonally to reduce the load during peak hours.

However, there is a notable gap in the literature concerning exploring and applying new heat storage and heat transfer fluid materials in BHEs to render them suitable for TES purposes. While various approaches have been undertaken to enhance BHE performance, including using advanced materials and design optimizations, most research has concentrated on the conventional goal of BHEs. More attention should be given to the potential advantages of these heat exchangers by applying nanofluids and PCMs as heat transfer fluids and heat storage media, respectively. As mentioned above, these materials possess superior thermo-physical properties that can lead to more efficient heat transfer, reduced drilling costs, lower electricity consumption in heat pumps, and diminished borehole thermal resistance. This research gap necessitates an in-depth investigation to determine the feasibility and practicality of implementing these advanced materials in BHEs, ultimately facilitating their transformation into reliable BTES systems. The outcomes of such research endeavors hold the promise of addressing environmental concerns and global energy deficiencies by advancing the utilization of renewable energy sources like SGE sustainably and effectively.

Therefore, the main objectives of this doctoral dissertation are to study experimentally and numerically the impacts of using advanced materials for heat transfer fluid and backfill/grout, such as nanofluids and PCMs, on the performance of the BHE as BTES systems. The study aims to select the most favorable materials, making it a practical and reliable reference for future projects and industry sectors.

Resumen

Debido a la grave contaminación ambiental y a la crisis energética mundial, la explotación de las energías renovables se ha vuelto más esencial que nunca. La energía geotérmica somera (EGS) se considera una fuente de energía sostenible y renovable con importantes ventajas en la calefacción y refrigeración de edificios, aplicaciones industriales, invernaderos, producción de electricidad, industria agrícola y producción de agua caliente, entre otros.

El sistema de bomba de calor geotérmica (GSHP) es una tecnología prometedora para utilizar EGS. En este sistema, un intercambiador enterrado de calor de perforación (BHE) desempeña un papel principal e influye directamente en el coeficiente de rendimiento estacional (SCOP) de este sistema geotérmico poco profundo.

Se han llevado a cabo diferentes estudios para mejorar el rendimiento del BHE, incluyendo el uso de materiales avanzados para el plástico de las tuberías, uso de fluido caloportador (o de transferencia de calor) y de relleno/grouting, de mayor transferencia de calor, diseño de nuevas geometrías, y la optimización del BHE para ser utilizado como sistemas de almacenamiento de energía térmica (BTES).

Los costes de perforación, el consumo eléctrico de las bombas de calor y la resistencia térmica de las perforaciones pueden reducirse utilizando materiales con propiedades termofísicas adecuadas, como los nanofluidos y los materiales de almacenamiento térmico. De este modo, no sólo se produce una transferencia de calor más significativa entre el fluido caloportador, el relleno y el terreno, sino que también se reduce el efecto térmico sobre el entorno.

El fluido de transferencia de calor es uno de los factores de optimización de la BHE que se utilizará para el almacenamiento de energía térmica (TES). Una mayor conductividad térmica en el fluido de transferencia de calor mejora la eficacia de la transferencia de calor entre el fluido y los materiales alrededor, lo que lleva a alcanzar con mayor rapidez la temperatura de cambio de fase en los materiales de almacenamiento. Cuando se usa un fluido de transferencia de calor con una conductividad térmica superior, la temperatura del material de almacenamiento de calor experimenta fluctuaciones más rápidas, lo que reduce significativamente la duración necesaria para un cambio de fase completo.

Además, usar materiales de cambio de fase (PCM) para almacenar calor en lugar del relleno convencional permite aprovechar el BHE como sistema BTES. Además de disminuir considerablemente la profundidad de perforación necesaria, el sistema BTES puede almacenar y liberar energía diaria y estacionalmente para reducir la carga durante las horas punta.

Sin embargo ,hay un vacío notable en la bibliografía sobre la exploración y aplicación de nuevos materiales de almacenamiento de calor y fluidos de transferencia de calor en las BHE para hacerlas aptas para fines de BTES. Aunque se han aplicado diversas innovaciones para mejorar el rendimiento de los BHE, como el uso de materiales plásticos avanzados y la optimización del diseño, la mayor parte de la investigación se ha centrado en el uso convencional de los BHE .Debería prestarse más atención a las ventajas potenciales del aprovechamiento de los intercambiadores de calor mediante la aplicación de nanofluidos y PCM como fluidos de transferencia de calor y medios de almacenamiento de calor, respectivamente. Como ya se ha mencionado, estos materiales poseen propiedades termofísicas superiores que pueden dar lugar a una transferencia de calor más eficiente, una reducción de los costes de perforación, un menor consumo de electricidad en las bombas de calor y una disminución de la resistencia térmica de la perforación .Esta laguna en la investigación hace necesaria una investigación en profundidad para determinar la viabilidad y factibilidad de la aplicación de estos materiales avanzados en las BHE, facilitando en última instancia su transformación en sistemas BTES fiables .

Por lo tanto, los principales objetivos de esta tesis doctoral son estudiar experimental y numéricamente los impactos del uso de materiales avanzados para el fluido caloportador y el relleno/grouting tales como nanofluidos y PCMs, en el rendimiento del BHE como sistemas BTES. El estudio pretende seleccionar los materiales más favorables, convirtiéndose en una referencia práctica y fiable para futuros proyectos y sectores industriales.

Resum

A causa de la greu contaminació ambiental i a la crisi energètica mundial, l'explotació de les energies renovables s'ha tornat més essencial que mai. L'energia geotèrmica succinta (EGS) es considera una font d'energia sostenible i renovable amb importants avantatges en la calefacció i refrigeració d'edificis, aplicacions industrials, hivernacles, producció d'electricitat, industria agrícola i producció d'aigua calenta, entre altres.

El sistema de bomba de calor geotèrmica (GSHP, en anglès) és una tecnologia prometedora per a utilitzar *EGS. En este sistema, un bescanviador enterrat de calor de perforació (BHE, en anglès) exercix un paper principal i influïx directament en el coeficient de rendiment estacional (SCOP) d'este sistema geotèrmic poc profund.

S'han dut a terme diferents estudis per a millorar el rendiment del *BHE, incloent-hi l'ús de materials avançats per al plàstic de les canonades, ús de fluid termòfor (o de transferència de calor) i de grouting, de major transferència de calor, disseny de noves geometries, i l'optimització del *BHE* per a ser utilitzat com a sistemes d'emmagatzematge d'energia tèrmica (BTES, en anglès).

Els costos de perforació, el consum elèctric de les bombes de calor i la resistència tèrmica de les perforacions poden reduir-se utilitzant materials amb propietats termo-físiques adequades, com els *nanofluids* i els materials d'emmagatzematge tèrmic. D'esta manera, no sols es produïx una transferència de calor més significativa entre el fluid termòfor, el farciment i el terreny, sinó que també es reduïx l'efecte tèrmic sobre l'entorn.

El fluid de transferència de calor és un dels factors d'optimització de la *BHE que s'utilitzarà per a l'emmagatzematge d'energia tèrmica (*TES). Una major conductivitat tèrmica en el fluid de transferència de calor millora l'eficàcia de la transferència de calor entre el fluid i els materials al voltant, la qual cosa porta a aconseguir amb major rapidesa la temperatura de canvi de fase en els materials d'emmagatzematge. Quan s'usa un fluid de transferència de calor amb una conductivitat tèrmica superior, la temperatura del material d'emmagatzematge de calor experimenta fluctuacions més ràpides, la qual cosa reduïx significativament la duració necessària per a un canvi de fase complet.

A més, usar materials de canvi de fase (PCM, en anglès) per a emmagatzemar calor en lloc del farciment convencional permet aprofitar el *BHE* com a sistema *BTES*. A més de disminuir considerablement la profunditat de perforació necessària, el sistema *BTES* pot emmagatzemar i alliberar energia diària i estacionalment per a reduir la càrrega durant les hores punta.

No obstant això, hi ha un buit notable en la bibliografia sobre l'exploració i aplicació de nous materials d'emmagatzematge de calor i fluids de transferència de calor en les *BHE* per a fer-les aptes per a fins de *BTES*. Encara que s'han aplicat diverses innovacions per a millorar el rendiment dels *BHE*, com l'ús de materials plàstics avançats i l'optimització del disseny, la major part de la investigació s'ha centrat en l'ús convencional dels *BHE*. Hauria de prestar-se més atenció als avantatges potencials de l'aprofitament dels bescanviadors de calor mitjançant l'aplicació de *nanofluids* i *PCM* com a fluids de transferència de calor i mitjans d'emmagatzematge de calor, respectivament. Com ja s'ha esmentat, estos materials posseïxen propietats termofísiques superiors que poden donar lloc a una transferència de calor més eficient, una reducció dels costos de perforació, un menor consum d'electricitat en les bombes de calor i una disminució de la resistència tèrmica de la perforació. Esta llacuna en la investigació fa necessària una investigació en profunditat per a determinar la viabilitat i factibilitat de l'aplicació d'estos materials avançats en les *BHE*, facilitant en última instància la seua transformació en sistemes *BTES* fiables.

Per tant, els principals objectius d'esta tesi doctoral són estudiar experimental i numèricament els impactes de l'ús de materials avançats per al fluid termòfor i el *grouting* com ara *nanofluids* i *PCMs*, en el rendiment del *BHE* com a sistemes *BTES*. L'estudi pretén seleccionar els materials més favorables, convertint-se en una referència pràctica i fiable per a futurs projectes i sectors industrials.

Acknowledgements

To begin, I would like to express my gratitude to my supervisors, Prof. Dr. Javier F. Urchueguía and Prof. Dr. Borja Badenes, for their invaluable expertise and support in the research methodology and achievement of results. I appreciate the time and effort they dedicated to enhancing my knowledge in this field.

I would also like to extend my appreciation to the external reviewers for taking the time to review my dissertation and providing constructive feedback that significantly improved its quality.

I want to acknowledge my colleagues from the Institute of Information and Communication Technologies (ITACA), specifically those who collaborated with me on this research project - Miguel Á., Bruno, Aroa, José M., Lenin, Álvaro, and also Oliver, Teresa, Pep, Celia, Marta, Helena, Giuseppe, Alessandro, and others. I admire your contributions and teamwork.

Furthermore, I am grateful to the GEMINIS TOOLS company, particularly Mr. Romero and Mr. Toldrá, the Department of Applied Physics, and the Doctoral Program in Design, Manufacture, and Management of Industrial Projects for their unwavering support.

Lastly, I would like to express my appreciation to my family members, my parents, sister, and nephew for their continuous support throughout my journey.

Table of Contents

References

References

List of Figures

XIII

List of Tables

Nomenclature

C_p	Specific heat ($J \cdot kg^{-1} \cdot K^{-1}$)
C_{mush}	Mushy zone constant
d_h	Hydraulic diameter (m)
E	Effectiveness
$\vec{g}$	Gravitational acceleration ($m \cdot s^{-2}$)
H	Borehole depth (m)
h	Heat transfer coefficient ($W \cdot m^{-2} \cdot K^{-1}$)
h_t	Total enthalpy ($J \cdot kg^{-1}$)
h_{sens}	Sensible heat enthalpy ($J \cdot kg^{-1}$)
h_{lat}	Latent heat enthalpy ($J \cdot kg^{-1}$)
h_{ref}	Reference enthalpy ($J \cdot kg^{-1}$)
k	Thermal conductivity ($W \cdot m^{-1} \cdot K^{-1}$) "Chapter 3"
l	Length of the U-tube (m)
L_f	Latent heat of phase change material ($J \cdot kg^{-1}$)
$\dot{m}$	Mass flow rate ($kg \cdot s^{-1}$)
Nu	Nusselt number
n	Shape factor
P	Pressure (Pa)
Q	Heat exchange rate (W)
R	Thermal resistance ($K \cdot m \cdot W^{-1}$)
r	Radius (m)
S_e	Source term of energy equation
S_i	Source term of momentum equation
T	Temperature (K)
t	Time (s)
u	Velocity ($m \cdot s^{-1}$) "Chapter 2"
$\vec{v}$	Velocity vector ($m \cdot s^{-1}$)
v_i	velocity component of the i direction ($m \cdot s^{-1}$)
v	Circulation fluid velocity ($m \cdot s^{-1}$) "Chapter 5"
v_p	Velocity of solidified material moving throughout the computational cells ($m \cdot s^{-1}$)

Greek Symbols

β	Thermal expansion coefficient (K^{-1}) "Chapter 2"
	Liquid fraction of phase change material "Chapter 5"
λ	Liquid fraction "Chapter 3"
	Thermal conductivity ($W \cdot m^{-1} \cdot K^{-1}$) "Chapter 5"
ΔP	Pressure drop (Pa)
μ	Dynamic viscosity ($Pa \cdot s$)
ρ	Density ($kg \cdot m^{-3}$)
ϕ	Volume fraction of nanoparticle
η	Coefficient of performance-improvement factor

f	Friction factor

Subscripts

HNF	Hybrid nanofluid
NP	Nanoparticle
BF	Base fluid
s	Soil
a	Average
MAX	Maximum
0	Reference "Chapter 2" Original "Chapter 3"
ref	Reference
tot	Total
lat	Latent heat
sens	Sensible heat
m	Melting

Abbreviation

BHE	Borehole heat exchanger
BTES	Borehole thermal energy storage
COP	Coefficient of performance
CFD	Computational fluid dynamics
GHE	Ground heat exchanger
GSHP	Ground source heat pump
MPCM	Microencapsulated phase change material
MWCNT	Multi-wall carbon nanotube
NEPCM	Nano-enhanced phase change material
PCM	Phase change material
SSPCM	Shape stabilized phase change material
SGE	Shallow geothermal energy
SOTA	State of the art
TES	Thermal energy storage
TRT	Thermal response test

Chapter 1

1 Introduction

The emission of greenhouse gases (GHG) from fossil fuels is widely acknowledged as a leading cause of climate change, environmental pollution, global warming, and energy scarcity. This has prompted searching for alternative technologies and renewable energy sources to achieve more efficient energy conversion [1]. *Energy scarcity* is a significant issue that has compelled countries to prioritize renewable energy supply [2-5]. Combining energy efficiency and renewable energies offers a viable and practical approach to reducing the impact of these problems. In response to the environmental problems caused by traditional power generation systems, the improvement and application of renewable energy sources, e.g., solar energy [6], wind [7], and geothermal [8], are increasing. Adopting any of these renewable energy technologies can significantly contribute to future generations' welfare while reducing fuel expenses.

A heat pump (HP) system can be considered a renewable energy technology under specific circumstances commonly used to heat and cool buildings. The mechanism of these systems involves gathering thermal energy from the environment surrounding the building, like water, ground, or air, and intensifying it for internal use. [9]. HPs are categorized into water source, ground source, and air-to-air. Among these, ground-source heat pump systems (GSHPs) are top-rated due to their high coefficient of performance, environmental friendliness, ease of integration with other energy systems, and low operational costs [10,11]. They are considered promising renewable energy technology for residential and commercial buildings, and their installation is growing continuously [12]. GSHP systems utilize shallow geothermal energy (SGE) resources and are cleaner and more energy-efficient than conventional air conditioning systems. For several years, these systems have been a substitute or an addition to customary heating and cooling systems in many countries.

GSHPs can reduce energy use compared to air-source heat pumps and conventional heating, ventilation, and air conditioning (HVAC) systems by 44% and 72%, respectively [13]. By employing GSHPs instead of traditional HVAC systems, which depend on fossil fuels, the emission of GHG can be decreased by about 66% [9]. By consuming less energy compared to conventional heating/cooling systems, this technology can assist in lowering the emission of dangerous gases such as sulfur dioxide (SO_2), nitrogen oxides (NO_x), and carbon dioxide (CO_2). GSHP systems run exclusively on electricity and usually generate three to six times more heat than the electrical energy they consume to function. Despite higher installation costs than traditional systems, GSHPs require less maintenance and can offer dependable, eco-friendly heating/cooling for more than 50 years. This technology operates on the principle that the ground maintains a consistent temperature at a certain depth, which is warmer and colder than the ambient temperature during cold and hot seasons, respectively. Therefore, a GSHP can collect thermal energy from the ground, known as heat extraction, and transfer it to the house, as well as dissipate thermal energy from the application to the ground, known as heat injection, without the need for specific geological anomalies such as hot springs. GSHPs can be installed in many world regions using shallow trenches, ponds, lakes, or boreholes. In winter, GSHPs use the ground, groundwater, or both as a heat "source"; in summer, they use them as a "sink" to remove heat from the hot source. The system is advantageous because it can perform heating and cooling, reducing the need for independent HVAC and central heating systems. Generally, GSHP systems are categorized into three systems: open, closed, or other systems (neither open nor closed).

> *Open systems*: Open-loop GSHP systems extract heat from underground water or surface water, such as lakes, instead of using a heat-transfer fluid like closed-loop systems. These systems generally include extraction and reinjection wells or surface water. The extracted underground water can either be released into a surface water network or injected back into the ground via distinct wells as an

alternative option. The main characteristic of this system is the natural flow of underground water, which serves as a medium to convey heat to the surrounding solids while acting as a heat sink/source. There is also a third category of GSHP systems that do not clearly fall into either open or closed-loop systems.

Closed systems: To describe closed systems of GSHPs, there are three essential components, including the HP, the ground heat exchanger (GHE), and the distribution system. The GHE connects the HP and the ground, enabling thermal energy dissipation or extraction to or from the surrounding soil. It is typically situated underground in a vertical or horizontal manner, in which a working fluid is circulating within it to transfer heat between the underground and the HP. As the GHE separates the circulating fluid from the soil and underground water, it is known as a "closed system". Horizontal and vertical configurations are as follows:

Horizontal configuration: In the center and west of Europe, when installing the horizontal GHE, the pipes are closely spaced due to area restrictions, and they are connected in series or parallel. However, due to the lower land cost in the North of Europe, pipes are laid in wider trenches. Special GHEs have been developed to save surface area, and they are appropriate for cooling and heating systems that do not require regular temperature recovery of the soil. When there is abundant land area, and the water table is high enough, horizontal systems are favored over other types. However, this system requires longer pipes than vertical wells, a large ground area, and ground temperature variations, resulting in lower system efficiency.

Vertical configuration: The temperature at a certain depth (around 5-10 meters) stays constant throughout the year, making vertical GHEs, also called borehole heat exchangers (BHEs), a favorable option due to the need for adequate thermal energy exchange capability within a limited available land. BHEs commonly involve the installation of pipes (typically made of polyethylene or polypropylene) in boreholes, which are then filled with a backfill/grout material. Various kinds of BHEs have been tested. Three fundamental concepts can be employed:

- U-pipes are composed of two straight pipes linked by a bend at the base.

- Coaxial or concentric pipes can be created in a basic manner by using two straight pipes with varying diameters or in more intricate configurations used in heat exchangers in Europe.

- Helical pipes.

When the land surface is restricted, vertical loops are usually preferred. These loops utilize the least amount of pumping energy among closed systems, and compared to most of the configurations in closed systems, the total length of pipe required is lower. Additionally, the ground temperature typically does not experience seasonal variations. However, BHEs require specialized drilling equipment, and drilling expenses are often higher than horizontal trenching.

Other systems: It is not always possible to precisely categorize a system into one of the abovementioned categories. For instance, there may be a distinction between underground water and the working fluid, even though no tangible barrier exists. Such systems include tunnel water, mine water, and standing column wells.

To select the appropriate system for a particular installation, various aspects must be considered, such as the ground's hydrogeology and geology, the ground surface's usage and area, the cooling and heating features of

the house, and the presence of possible heat sources (e.g., mines). Precise information about the significant factors related to the selected technology is crucial during the planning stage to scale the GSHP system appropriately, guaranteeing the best possible performance while keeping expenses to a minimum. For more detailed information, one may be interested in reading the previously published comprehensive review of GHEs conducted by Javadi et al. [1].

In a GSHP system, the electricity is not converted to heat but is used to transfer heat from one location to another, resulting in a higher coefficient of performance (COP). Consequently, the higher the heat exchange of the BHE, the greater the efficiency of the closed-loop GSHP system [14-16]. Hence, the BHE plays a crucial role in the system. There have been many ways to enhance the BHE efficiency, including changing the heat carrier fluid.

In general, BHEs use pure water as the working fluid because it is readily available and inexpensive [1]. Several studies have compared different heat carrier fluids, including water, gasoline, and glycol, and found that water is more efficient in exchanging thermal energy [17]. Other working fluids used in BHEs include antifreeze-water [18-20], methanol/water antifreeze mixture [21], ethylene glycol solution (EGS) [22,23], and aqueous ethanol solution [24,25]. Casasso and Sethi [26] concluded that the working fluid velocity optimization could decrease the borehole thermal resistance, so more HP power will not be required. Maintaining an appropriate viscosity level in the working fluid mixture utilized in BHEs is crucial [27]. A calcium chloride solution (CCS) may be more efficient than a propylene glycol solution (PGS) thanks to the higher thermal conductivity and lower viscosity. Using saline solutions with low viscosities can also help to reduce total energy losses compared to ethanol and glycol. In a study conducted by Zhang et al. [28], EGS, CCS, and a sodium chloride solution (SCS) were examined. The study found that SCS and CCS have high thermal conductivity and are safe and non-toxic. However, metal corrosion may occur in the presence of air. The study also found that EGS has a high thermal conductivity, but its viscosity increases at low temperatures, leading to increased flow resistance. Neuberger et al. [29] studied the outlet temperature of the working fluid for a BHE, in which it was shown that ethanol concentration was increased by about 33%. It was found that the major contributing factors to this were the increased thermal resistance between the pipe and the heat carrier fluid and the heat carrier fluid's heightened kinematic viscosity and reduced thermal conductivity.

In addition, nanofluids have been introduced as working fluids in BHEs. Diglio et al. [30] conducted a study where a nanofluid was used as a working fluid in a BHE. Changes in the heat transfer coefficient and volumetric heat capacity were observed in the analysis, depending on the nanofluid concentration. The maximum heat transfer coefficient was found in a nanofluid containing Ag, followed by a nanofluid containing Cu. Daneshipour and Rafee [31] numerically examined the utilization of water-based nanofluids containing CuO and Al_2O_3 as heat carrier fluids in a coaxial BHE. The study determined that as the volume fraction of nanofluids increases, there is a proportional linear increase in pressure drop. Additionally, the water-based nanofluid having CuO could achieve the highest heat transfer coefficient while the pressure drop was substantial. The borehole depth for a BHE could be decreased by 1.3% using a water-based nanofluid containing Al_2O_3 [32]. Despite this rather marginal decrease, these studies justify the interest to investigate whether the use of nanofluids as circulation fluids for BHEs could lead to further improvements of the heat transfer efficiency and effectiveness of GSHP systems.

Additional investigations on nanofluids led to the development of a new type known as hybrid nanofluids. The fluids are produced by dispersing multiple nanoparticles into the foundation fluid instead of basic nanofluids that frequently do not possess appealing rheological or thermal characteristics. Hybrid nanofluids showcase physical and chemical attributes in a consistent phase, leading to concurrently integrating the extra

4

nanoparticles' qualities into the underlying fluid. Since projects often require tradeoffs between different characteristics, hybrid nanofluids play a significant role in meeting such criteria. Hybrid nanofluids typically demonstrate high mechanical resilience, thermal conductivity, chemical durability, physical potency, and other significant characteristics in contrast to simple nanofluids [33-39].

In the present doctoral dissertation, the first step was evaluating numerically the utilization of a new type of heat carrier fluid named hybrid nanofluid in the single U-tube BHE, which had not been studied before in the GSHP systems.

Moreover, backfill/grout material is known to be one of the most influential components of a BHE, and consequently, it has been widely studied by scholars over the past years. Pure backfill materials, including cementitious [40] and sand soil [41] types, have been extensively investigated in previous studies. The thermal conductivity range of pure backfill materials is reported to be between 0.8 and 2.4 W/(m·K) [42]. A rise in the thermal conductivity of the backfill/grout causes a decrease in the BHE's overall length. The impact of variations in backfill material thermal conductivity is more significant on BHEs having larger pipe diameters than those with smaller pipe diameters [43]. Some pure backfill materials, such as saturated sand and protoplasm, are only suitable for heating mode. In contrast, others, such as clay, bentonite, gravel, coarse/fine sand, quartz sand, and silica sand, are suitable for both heating and cooling modes.

Also, mixed materials consisting of pure materials were introduced and utilized as backfill/grout materials in BHEs. In the late 1980s, granular bentonite-water mixes were used as backfill materials, but their thermal conductivity range was insignificant, up to 0.9 W/(m·K) [44]. To improve this, Remund and Lund [45] evaluated several mixtures by adding quartzite, limestone, and masonry sand to bentonite and found up to 100% augmentation in some mixtures' thermal conductivity. In recent years, the mixtures containing graphite were predominantly utilized to enhance the thermal conductivity of grouts. In general, according to academic investigations, it has been ascertained that graphite is one of the most impactful supplements to augment bentonite's thermal conductivity. However, it is important to note that graphite is expensive, and using graphite to achieve high thermal conductivity can significantly increase the backfill material's viscosity [46]. Various mixed materials are used as backfill materials, such as clay-bentonite, quartzite-bentonite, cement admixtures, homemade mixtures containing graphite, gravel-sand, and sand-clay. For more detailed information on backfill materials, interested individuals can refer to the comprehensive review conducted by Javadi et al. [47].

Recently, there has been much interest in the advantages of combining phase change materials (PCMs) with GSHPs. PCMs are typically classified into four categories: organic, inorganic, hygroscopic, and solid-solid materials. Due to their ability to store thermal energy as latent heat, PCMs possess a greater energy density, rendering them suitable for energy storage with high density. When a PCM undergoes a phase change, latent heat is absorbed or released. Throughout the process of melting and solidifying, the temperature of the PCM remains fixed, leading to better performance of GSHPs. Furthermore, incorporating the PCM in a BHE as a backfill can reduce temperature fluctuations in the adjacent ground, thus diminishing the necessity for the land area [48].

Despite engineers' widespread use of organic PCMs, prior research has revealed that these substances encounter specific issues [49]. One of the primary problems is that organic PCMs have low thermal conductivity (0.235 W/(m·K)). To increase organic PCMs' thermal conductivity, additives such as high thermally conductive metal compounds, carbon fiber, and graphite have been developed. Organic PCMs' phase transition involves solid-liquid, which can result in PCM leakage into the borehole and adversely affect heat transfer, damaging the surrounding soil. Two techniques have been introduced to prevent the adverse effects of PCM leakage, which involve PCM microencapsulation and promoting PCM incorporation with some

additives such as polyethylene and silica to create shape-stabilized PCM (SSPCM). Generally, the improved PCMs used as backfill materials include microencapsulated PCM (MPCM), SSPCM, paraffin RT27, and acid, which have only been used in the BHEs for the summer season [47].

Further, there is a modern type of PCMs known as nano-enhanced PCM (NEPCM), produced by blending nanoparticles with a pure PCM. The addition of nanoparticles into PCM was first explored by Khodadadi and Hosseinizadeh [50], who demonstrated that NEPCM has superior thermal conductivity and a greater thermal energy storage (TES) capacity than traditional PCMs. NEPCM has brought various advantages to electronic devices [51], buildings [52], TES [53], solar systems [54], and heat exchangers [55].

Hence, in the present doctoral dissertation, the second step was applying numerically this novel form of backfill materials named NEPCM in the single U-tube BHE, which is the first time these materials have been applied in the context of GSHP systems.

It is crucial to underscore that the primary role of TES is to address the imbalance between energy production and demand rather than mitigating heating and cooling disparities that may accumulate within materials if left unaddressed. Given the pronounced differences in cooling and heating requirements within various building types throughout the year, integrating GSHP systems with supplementary TES systems is paramount, especially in areas where either heating or cooling predominates. Continuous operation and prolonged periods of unbalanced loads can significantly diminish the SGE potential of GSHPs. Notably, in regions where heating takes precedence, the heat absorbed by the soil and injected into the ground fails to achieve an annual equilibrium. This persistent asymmetry in production and demand of energy reduces ground temperature and lowers the COP value. It is widely acknowledged that TES systems play a pivotal role in efficiently utilizing renewable energies [56]. By aligning energy supply with demand, TES systems unlock the potential to harness a diverse array of energy resources. Various TES systems, including solar collectors, ice storage tanks, PCM, water, and soil, can seamlessly complement GSHPs. Ice storage containers prove invaluable during the warmer seasons, while solar collectors come to the forefront during colder periods. Notably, PCM, water, and soil offer versatile support for either the cooling or heating operation modes of GSHPs.

Underground TES systems are specifically engineered to facilitate the subterranean storage of thermal energy, with the aim of its subsequent utilization in heating or cooling applications. Over the years, these systems have been extensively developed based on either boreholes or aquifers. Borehole TES (BTES) systems are a combination of closed borehole loops and storage media that can be applied to various ground conditions. BTES systems typically comprise one or multiple wells to accumulate energy subsurface for subsequent usage, predominantly on a seasonal cycle. The scale of these systems may differ, ranging from tiny individual constructions to more giant commercial edifices or district heating networks attached to GSHPs. To enhance the thermal storage capacity of BTES and make it more cost-effective, researchers are exploring using materials such as PCMs. The concept of PCMs' latent heat storage revolves around the absorption or release of thermal energy during the conversion of PCM from one phase to another, such as solid-liquid or liquid-solid. The considerable thermal energy storage capacity and the ability to store thermal energy at a steady temperature or within a narrow temperature variety corresponding to the material's phase transition temperature make latent heat storage an attractive option. Accordingly, PCMs are gaining popularity as suitable for latent heat storage in BTES applications.

TES technologies, particularly when coupled with SGE and BTES, are of utmost importance to Europe's energy crisis mitigation strategies. European countries have made significant strides in harnessing the Earth's natural heat through shallow geothermal systems and integrating them with BTES systems. This approach allows for the efficient storage of excess heat generated during periods of renewable energy abundance and its

subsequent use during high-demand periods or when renewables are less productive. The commitment to BTES technology, which stores heat in the subsurface through boreholes, exemplifies Europe's dedication to sustainable energy solutions. BTES systems not only enhance energy grid stability but also enable greater utilization of renewable energy sources, reducing reliance on fossil fuels and bolstering Europe's resilience in the face of energy shortages and environmental challenges. Europe's focus on TES, coupled with SGE and BTES, points out its commitment to leading the way in sustainable energy innovation and combating the energy crisis.

Therefore, in the third and final step of this doctoral dissertation, as the title indicates, the use of advanced materials like PCMs in the BHEs to be optimized for use as BTES has been studied experimentally and numerically. Worth mentioning that the improved materials evaluated in the final chapter of this research were produced and tested during a European project named GEOCOND that we (Universitat Politècnica de València (UPV)) participated in.

It should be noted that there is a difference between applying a conventional BHE and a converted BHE into a BTES. A BHE and a BTES system serve different purposes in SGE applications. A BHE primarily functions as a heat exchange system, facilitating thermal energy transfer between the ground and fluid circulating within the borehole. This system is commonly employed for heating and cooling applications in buildings. On the other hand, a BTES system goes beyond the immediate exchange of thermal energy; it is designed to store excess thermal energy for later use. In essence, a BTES system acts as a thermal reservoir, allowing the accumulation of surplus heat during periods of abundance and its retrieval when demand arises. While both systems involve boreholes and thermal energy exchange, the key distinction lies in the storage capability of a BTES system, making it a valuable component for optimizing energy efficiency and addressing fluctuating energy demands in various applications.

In summary, the doctoral dissertation under consideration presents an overview of its objectives and research path, as depicted in Figure 1-1. The initial phase involves an examination of the technology and current state of the art (SOTA) of SGE systems, with particular emphasis on the BHE, which holds significant importance within GSHP systems (Chapter 1). The dissertation then proceeds with two distinct sets of objectives: firstly, the general goal of enhancing thermal performance of BHEs, and secondly, the specific aim of exploring the feasibility of converting a BHE into a BTES. In light of these objectives, a novel heat carrier fluid known as hybrid nanofluid is introduced, and its application within a single U-tube BHE is investigated through numerical analysis (Chapter 2). Subsequently, Chapters 3 to 6 delve into the utilization of innovative backfill/grout materials to address the specific research objectives. In Chapter 3, numerical simulations are employed to evaluate the suitability of a modern type of PCMs called NEPCM as a backfill material for a BHE. Additionally, newly developed materials, namely MPCM, SSPCM, and thermally-enhanced grout, are subjected to both experimental and numerical scrutiny in Chapters 4 to 6. These materials are investigated using a combination of computational fluid dynamics (CFD) modeling, sandbox tests, and field studies. Furthermore, the conclusions drawn from these investigations are discussed, along with suggestions for future research endeavors.
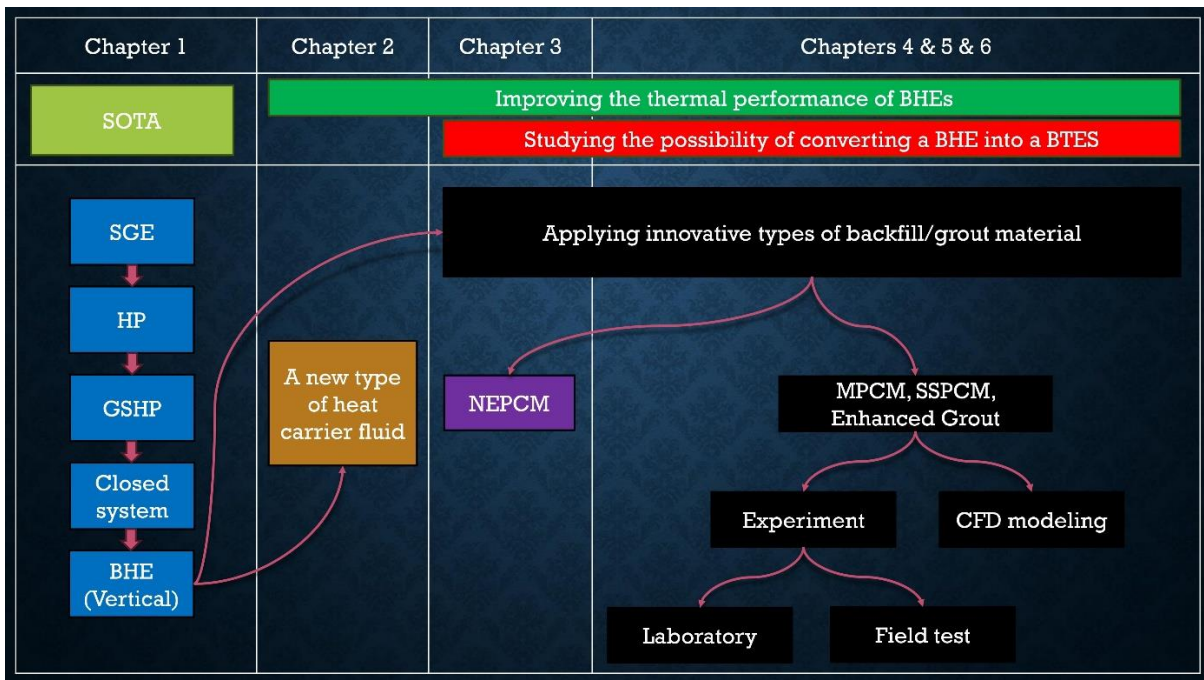
Figure 1-1: The graphical abstract of the present doctoral dissertation.

References

1. Javadi, Hossein, Seyed Soheil Mousavi Ajarostaghi, Marc A. Rosen, and Mohsen Pourfallah. "Performance of ground heat exchangers: A comprehensive review of recent advances." *Energy* 178 (2019): 207-233.

2. Yuan, Yanping, Xiaoling Cao, Liangliang Sun, Bo Lei, and Nanyang Yu. "Ground source heat pump system: A review of simulation in China." *Renewable and Sustainable Energy Reviews* 16 (2012): 6814-6822.

3. Hackel, Scott, and Amanda Pertzborn. "Effective design and operation of hybrid ground-source heat pumps: three case studies." *Energy and Buildings* 43 (2011): 3497-3504.

4. Miyara, Akio, Koutaro Tsubaki, Shuntaro Inoue, and Kentaro Yoshida. "Experimental study of several types of ground heat exchanger using a steel pile foundation." *Renewable Energy* 36 (2011): 764-771.

5. Esen, Mehmet, and Tahsin Yuksel. "Experimental evaluation of using various renewable energy sources for heating a greenhouse." *Energy and Buildings* 65 (2013): 340-351.

6. Deng, Hongling, Xiaohong Yang, Rui Tian, Junhu Hu, Bo Zhang, Fangda Cui, and Guangyu Guo. "Modeling and optimization of solar thermal-photovoltaic vacuum membrane distillation system by response surface methodology." *Solar Energy* 195 (2020): 230-238.

7. Gualtieri, Giovanni. "A comprehensive review on wind resource extrapolation models applied in wind energy." *Renewable and Sustainable Energy Reviews* 102 (2019): 215-233.

8. Hou, Gaoyang, Hessam Taherian, Longjun Li, Jordan Fuse, and Lee Moradi. "System performance analysis of a hybrid ground source heat pump with optimal control strategies based on numerical simulations." *Geothermics* 86 (2020): 101849.

9. Heinonen, Everett W., Maurice W. Wildin, Andrew N. Beall, and Robert E. Tapscott. "Assessment of antifreeze solutions for ground-source heat pump systems." *ASHRAE Transactions* 103 (1997): 747.

10. Wang, Zhihua, Fenghao Wang, Jun Liu, Zhenjun Ma, Ershuai Han, and Mengjie Song. "Field test and numerical investigation on the heat transfer characteristics and optimal design of the heat exchangers of a deep borehole ground source heat pump system." *Energy Conversion and Management* 153 (2017): 603-615.

11. Qi, Di, Liang Pu, Zhenjun Ma, Lei Xia, and Yanzhong Li. "Effects of ground heat exchangers with different connection configurations on the heating performance of GSHP systems." *Geothermics* 80 (2019): 20-30.

12. Sarbu, Ioan, and Calin Sebarchievici. "General review of ground-source heat pump systems for heating and cooling of buildings." *Energy and Buildings* 70 (2014): 441-454.

13. Rezendes, Victor S. "Geothermal Energy: Outlook Limited for Some Uses but Promising for Geothermal Heat Pumps". *United States General Accounting Office: Washington DC, DIANE Publishing* (1994).

14. Badenes, Borja, Burkhard Sanner, Miguel Ángel Mateo Pla, José Manuel Cuevas, Flavia Bartoli, Francesco Ciardelli, Rosa M. González et al. "Development of advanced materials guided by numerical simulations to improve performance and cost-efficiency of borehole heat exchangers (BHEs)." *Energy* 201 (2020): 117628.

15. Carnieletto, Laura, Borja Badenes, Marco Belliardi, Adriana Bernardi, Samantha Graci, Giuseppe Emmi, Javier F. Urchueguía et al. "A European database of building energy profiles to support the design of ground source heat pumps." *Energies* 12 (2019): 2496.

16. Badenes, Borja, Miguel Ángel Mateo Pla, Teresa Magraner, Javier Soriano, and Javier F. Urchueguía. "Theoretical and experimental cost–benefit assessment of borehole heat exchangers (BHEs) according to working fluid flow rate." *Energies* 13 (2020): 4925.

17. Dada, M. A., and A. Benchatti. "Assessment of heat recovery and recovery efficiency of a seasonal thermal energy storage system in a moist porous medium." *International Journal of Heat and Technology* 34 (2016): 701-708.

18. Bakirci, Kadir, and Derya Colak. "Effect of a superheating and sub-cooling heat exchanger to the performance of a ground source heat pump system." *Energy* 44 (2012): 996-1004.

19. Bakirci, Kadir. "Evaluation of the performance of a ground-source heat-pump system with series GHE (ground heat exchanger) in the cold climate region." *Energy* 35 (2010): 3088-3096.

20. Maestre, Ismael R., F. Javier González Gallero, Pascual Álvarez Gómez, and J. Daniel Mena Baladés. "Performance assessment of a simplified hybrid model for a vertical ground heat exchanger." *Energy and Buildings* 66 (2013): 437-444.

21. Olfman, Maeir Zalman, Allan D. Woodbury, and Jonathan Bartley. "Effects of depth and material property variations on the ground temperature response to heating by a deep vertical ground heat exchanger in purely conductive media." *Geothermics* 51 (2014): 9-30.

22. Dehghan, Babak. "Experimental and computational investigation of the spiral ground heat exchangers for ground source heat pump applications." *Applied Thermal Engineering* 121 (2017): 908-921.

23. Zhao, Qiang, Fang Liu, Chunwei Liu, Maocheng Tian, and Baoming Chen. "Influence of spiral pitch on the thermal behaviors of energy piles with spiral-tube heat exchanger." *Applied Thermal Engineering* 125 (2017): 1280-1290.

24. Spitler, Jeffrey D., Saqib Javed, and Randi Kalskin Ramstad. "Natural convection in groundwater-filled boreholes used as ground heat exchangers." *Applied Energy* 164 (2016): 352-365.

25. Acuña, José, and Björn Palm. "Comprehensive summary of borehole heat exchanger research at KTH." In *IIR/Eurotherm Sustainable Refrigeration and Heat Pump Technology Conference*, pp. 1-8. 2009.

26. Casasso, Alessandro, and Rajandrea Sethi. "Sensitivity analysis on the performance of a ground source heat pump equipped with a double U-pipe borehole heat exchanger." *Energy Procedia* 59 (2014): 301-308.

27. Erol, Selçuk, and Bertrand François. "Freeze damage of grouting materials for borehole heat exchanger: Experimental and analytical evaluations." *Geomechanics for Energy and the Environment* 5 (2016): 29-41.

28. Zhang, Wenke, Hongxing Yang, Lin Lu, and Zhaohong Fang. "Investigation on influential factors of engineering design of geothermal heat exchangers." *Applied Thermal Engineering* 84 (2015): 310-319.

29. Neuberger, Pavel, Radomír Adamovský, and Michaela Šed'ová. "Temperatures and heat flows in a soil enclosing a slinky horizontal heat exchanger." *Energies* 7 (2014): 972-987.

30. Diglio, Giuseppe, Carlo Roselli, Maurizio Sasso, and Umavathi Jawali Channabasappa. "Borehole heat exchanger with nanofluids as heat carrier." *Geothermics* 72 (2018): 112-123.

31. Daneshipour, Mahdi, and Roohollah Rafee. "Nanofluids as the circuit fluids of the geothermal borehole heat exchangers." *International Communications in Heat and Mass Transfer* 81 (2017): 34-41.

32. Narei, Hamid, Roghayeh Ghasempour, and Younes Noorollahi. "The effect of employing nanofluid on reducing the bore length of a vertical ground-source heat pump." *Energy Conversion and Management* 123 (2016): 581-591.

33. Sarkar, Jahar, Pradyumna Ghosh, and Arjumand Adil. "A review on hybrid nanofluids: recent research, development and applications." *Renewable and Sustainable Energy Reviews* 43 (2015): 164-177.

34. Leong, K. Y., KZ Ku Ahmad, Hwai Chyuan Ong, M. J. Ghazali, and Azizah Baharum. "Synthesis and thermal conductivity characteristic of hybrid nanofluids–a review." *Renewable and Sustainable Energy Reviews* 75 (2017): 868-878.

35. Hamzah, Muhammad Hafiz, Nor Azwadi Che Sidik, Tan Lit Ken, Rizalman Mamat, and Gholamhassan Najafi. "Factors affecting the performance of hybrid nanofluids: a comprehensive review." *International Journal of Heat and Mass Transfer* 115 (2017): 630-646.

36. Minea, Alina Adriana. "Challenges in hybrid nanofluids behavior in turbulent flow: recent research and numerical comparison." *Renewable and Sustainable Energy Reviews* 71 (2017): 426-434.

37. Gupta, Munish, Vinay Singh, Satish Kumar, Sandeep Kumar, Neeraj Dilbaghi, and Zafar Said. "Up to date review on the synthesis and thermophysical properties of hybrid nanofluids." *Journal of Cleaner Production* 190 (2018): 169-192.

38. Sajid, Muhammad Usman, and Hafiz Muhammad Ali. "Thermal conductivity of hybrid nanofluids: a critical review." *International Journal of Heat and Mass Transfer* 126 (2018): 211-234.

39. Kumar, D. Dhinesh, and A. Valan Arasu. "A comprehensive review of preparation, characterization, properties and stability of hybrid nanofluids." *Renewable and Sustainable Energy Reviews* 81 (2018): 1669-1689.

40. Allan, Marita L., and Steve P. Kavanaugh. "Thermal conductivity of cementitious grouts and impact on heat exchanger length design for ground source heat pumps." *Hvac&R Research* 5 (1999): 85-96.

41. Kara, Yusuf Ali. "Experimental performance evaluation of a closed-loop vertical ground source heat pump in the heating mode using energy analysis method." *International Journal of Energy Research* 31 (2007): 1504-1516.

42. Erol, Selçuk, and Bertrand François. "Efficiency of various grouting materials for borehole heat exchangers." *Applied Thermal Engineering* 70 (2014): 788-799.

43. Zhang, Wenke, Hongxing Yang, Lin Lu, and Zhaohong Fang. "Investigation on influential factors of engineering design of geothermal heat exchangers." *Applied Thermal Engineering* 84 (2015): 310-319.

44. Eckhart, Frank. "Grouting procedures for ground-source heat pump systems". *Ground Source Heat Pump Publications, Oklahoma State University*, 1991.

45. Remund, Charles P., and James T. Lund. "Thermal enhancement of bentonite grouts for vertical GSHP systems." *In Proceedings of the Heat Pump and Refrigeration Systems, Design, Analysis, and Applications, ASME Winter Annual Meeting, New Orleans, LA, USA, 28 November–3 December 1993; Volume 29, pp. 95–106.*

46. Delaleux, Fabien, Xavier Py, Régis Olives, and Antoine Dominguez. "Enhancement of geothermal borehole heat exchangers performances by improvement of bentonite grouts conductivity." *Applied Thermal Engineering* 33 (2012): 92-99.

47. Javadi, Hossein, Seyed Soheil Mousavi Ajarostaghi, Marc A. Rosen, and Mohsen Pourfallah. "A comprehensive review of backfill materials and their effects on ground heat exchanger performance." *Sustainability* 10 (2018): 4486.

48. Yang, Weibo, Lulu Sun, and Xuan Wu. "Energy storage and heat transfer characteristics of ground heat exchanger with phase change backfill materials." *Transactions of the Chinese Society of Agricultural Engineering* 30 (2014): 193-199.

49. Li, Xiangli, Cang Tong, Lin Duanmu, and Liangkan Liu. "Study of a U-tube heat exchanger using a shape-stabilized phase change backfill material." *Science and Technology for the Built Environment* 23 (2017): 430-440.

50. Khodadadi, J. M., and S. F. Hosseinizadeh. "Nanoparticle-enhanced phase change materials (NEPCM) with great potential for improved thermal energy storage." *International Communications in Heat and Mass Transfer* 34 (2007): 534-543.

51. Farzanehnia, Amin, Meysam Khatibi, Mohammad Sardarabadi, and Mohammad Passandideh-Fard. "Experimental investigation of multiwall carbon nanotube/paraffin based heat sink for electronic device thermal management." *Energy Conversion and Management* 179 (2019): 314-325.

52. Kalaiselvam, S., R. Parameshwaran, and S. Harikrishnan. "Analytical and experimental investigations of nanoparticles embedded phase change materials for cooling application in modern buildings." *Renewable Energy* 39 (2012): 375-387.

53. Ramakrishnan, Sayanthan, Xiaoming Wang, Jay Sanjayan, and John Wilson. "Heat transfer performance enhancement of paraffin/expanded perlite phase change composites with graphene nano-platelets." *Energy Procedia* 105 (2017): 4866-4871.

54. Rufuss, D. Dsilva Winfred, L. Suganthi, S. Iniyan, and P. A. Davies. "Effects of nanoparticle-enhanced phase change material (NPCM) on solar still productivity." *Journal of Cleaner Production* 192 (2018): 9-29.

55. Pahamli, Y., M. J. Hosseini, A. A. Ranjbar, and R. Bahrampoury. "Effect of nanoparticle dispersion and inclination angle on melting of PCM in a shell and tube heat exchanger." *Journal of the Taiwan Institute of Chemical Engineers* 81 (2017): 316-334.

56. Gao, Qing, Ming Li, Ming Yu, Jeffrey D. Spitler, and Y. Y. Yan. "Review of development from GSHP to UTES in China and other countries." *Renewable and Sustainable Energy Reviews* 13 (2009): 1383-1394.

Chapter 2

2 Impact of a new heat carrier fluid on a borehole heat exchanger

Article

Impact of Employing Hybrid Nanofluids as Heat Carrier Fluid on the Thermal Performance of a Borehole Heat Exchanger

Hossein Javadi [1,*](D), Javier F. Urchueguia [1](D), Seyed Soheil Mousavi Ajarostaghi [2](D) and Borja Badenes [1](D)

1 Information and Communication Technologies versus Climate Change (ICTvsCC), Institute of Information and Communication Technologies (ITACA), Universitat Politècnica de València (UPV), Camino de Vera s/n, 46022 Valencia, Spain; jfurchueguia@fis.upv.es (J.F.U.); borbaba@upv.es (B.B.)
2 Department of Energy Conversion, Faculty of Mechanical Engineering, Babol Noshirvani University of Technology, Babol 47148-71167, Iran; s.s.mousavi@stu.nit.ac.ir
* Correspondence: hjavadi@upv.es; Tel.: +34-963-877-000 (ext. 75247)

Abstract: In this numerical study, 4 types of hybrid nanofluid, including Ag-MgO/water, TiO_2-Cu/water, Al_2O_3-CuO/water, and Fe_3O_4-multi-wall carbon nanotube/water, have been considered potential working fluid in a single U-tube borehole heat exchanger. The selected hybrid nanofluid is then analyzed by changing the volume fraction and the Reynolds number. Based on the numerical results, Ag-MgO/water hybrid nanofluid is chosen as the most favorable heat carrier fluid, among others, considering its superior effectiveness, minor pressure drop, and appropriate thermal resistance compared to the pure water. Moreover, it was indicated that all cases of Ag-MgO/water hybrid nanofluid at various volume fractions (from 0.05 to 0.20) and Reynolds numbers (from 3200 to 6200) could achieve better effectiveness and lower thermal resistances, but higher pressure drops compared to the corresponding cases of pure water. Nevertheless, all the evaluated hybrid nanofluids present lower coefficient of performance (COP)-improvement than unity which means that applying them as working fluid is not economically viable because of having higher pressure drop than the heat transfer enhancement.

Keywords: borehole heat exchanger; hybrid nanofluid; numerical modeling; thermal resistance; pressure drop; effectiveness

*Javadi H, Urchueguia Scholzel JF, Ajarostaghi SSM, Badenes B. Impact of employing hybrid nanofluids as heat carrier fluid on the thermal performance of a borehole heat exchanger. **Energies**. **Impact Factor: 3.252**, **Nivel R2**.*

2.1 Introduction

Shallow geothermal energy is one of the renewable and sustainable energy resources with numerous applications in different areas, such as heating and cooling of buildings, electricity production, agriculture, etc. The ground-source heat pump (GSHP) system is a promising technology in shallow geothermal energy exploitation [1]. In this system, the ground heat exchanger (GHE) is considered one of the main components that directly impacts the coefficient of performance of the GSHP. The GHE is classified into horizontal and vertical. The vertical GHE, also called borehole heat exchanger (BHE), has various configurations such as U-tube, W-tube, helix, and coaxial U-tube BHEs are found to be the most studied types [2].

Over the years, different criteria and methods have been studied by researchers to design a more efficient GSHP system coupled to a BHE. The BHE overall length can be calculated by the American society of heating, refrigerating and air-conditioning engineers (ASHRAE) scheme where the working fluid temperature, borehole effective thermal resistance, building thermal load, and ground properties play a significant role in the BHE performance and coefficient of performance (COP) of the GSHP system. Philippe et al. [3] suggested a new method for designing single and multiple borefields, which was found to be in excellent agreement with commercial borehole sizing software. Fossa and Rolando [4] presented a precise and reliable technique for calculating the temperature penalty index, i.e., a parameter for BHE field design introduced in the ASHRAE. The total length of BHE and the temperature penalty term were estimated with high accuracy using the developed method. A simulation-based tool for designing the length of the BHE was compared to the ASHRAE design approach by Cullin et al. [5]. Based on the outcomes, the simulation-based tool (with an error of 6%) could estimate the BHE length with higher precision than the ASHRAE (with errors from – 21% to 167%). Rolando et al. [6] proposed a g-function-based approach that could design the GSHP system considering various parameters, including temperature penalty term, thermal resistance, and building thermal load. Spitler and Bernier [7] reviewed different BHE design methods such as the ASHRAE method and g-function-based methods. It was concluded that despite presenting various techniques for designing the BHE, the lack of validation and comparison with experimental data still exists in the literature. Fossa and Rolando [8] proved their new technique consistency in designing the actual BHE field when different values have been selected for the building thermal load, ground properties, and the BHE length. Staiti and Angelotti [9] conducted a comparison between two different design procedures of BHE, including the ASHRAE method and the professional ground loop heat exchanger design software (GLHEPRO). According to the results, it was shown that the ASHRAE method overestimates the borehole size by 28% compared to that when using GLHEPRO. Fossa et al. [10] carried out a comparative analysis between different techniques such as the improved ASHRAE method, earth energy design (EED) code, and TecGeo proprietary code for predicting the total length of the BHE field over 10 years. It was indicated that the developed approach could estimate the BHE overall length with a percent error of 8% compared to the EED code as a reference. Further investigations can be found in the references of [11–14].

There have been many studies focusing on various methods to enhance the performance of BHEs [2,15–20]. Pure water is reported to be the most commonly applied working fluid in the BHEs [2]; nevertheless, nanofluids' applications in the BHEs as working fluid has recently been under evaluation. Bobbo et al. [21] studied preliminarily and theoretically Al_2O_3/water nanofluid at different volume fractions to be used as a working fluid in the BHE. The results indicated that nanofluid use with a lower volume fraction is beneficial at higher temperatures for the system, but more analysis should be undertaken. The use of Al_2O_3/water nanofluid as a working fluid in a single U-tube BHE is theoretically conducted by Narei et al. [22]. Based on the results, the borehole depth decreases by 1.3% when using nanofluid instead of pure water. According to a

comparison made numerically between the CuO/water and Al_2O_3/water nanofluids as the working fluids in the coaxial BHE, CuO/water nanofluid proved to have better potential in the heating operation of the system [23]. Sui et al. [24] analyzed the influence of using Al_2O_3/water nanofluid as a working fluid on the performance of a coaxial BHE numerically. It was shown that there could be more heat extraction (about 11%) when using Al_2O_3/water nanofluid than pure water. Diglio et al. [25] numerically investigated the addition of 7 nanoparticles, including SiO_2, CuO, Cu, Al, Ag, graphite, and Al_2O_3, to the water to be used as the working fluid in the single U-tube BHE. The outcome demonstrated that the highest heat exchange rate and the highest decrease in the borehole thermal resistance is obtained by Ag/water and Cu/water nanofluids, respectively. A numerical study of Fe_3O_4/water and Al_2O_3/water nanofluids' suspension stability in a coaxial BHE is conducted by Sun et al. [26]. It was suggested that in addition to the geometry optimization of the bottom of BHE, the pulsed fluid flow should be conducted to guarantee the tremendous operational reliability of the coaxial BHE. Peng et al. [27] evaluated Cu/water nanofluid in a single U-tube BHE at various volume fractions and nanoparticles' size. It was illustrated that the performance of the BHE improves when using Cu/water nanofluid rather than pure water.

Moreover, there are a limited number of articles concerning the use of nanofluids in the horizontal GHE. The influence of using three nanofluids, including Al_2O_3/water, CuO/water, and SiO_2/water as the working fluid in the horizontal GHE at different volume fractions is theoretically investigated by Mishra et al. [28]. Based on the results, the use of CuO/water nanofluid at a 4% volume fraction leads to the highest heat exchange rate than that of 2 other nanofluids. Du et al. [29,30] experimentally and numerically studied the effect of using CuO/water nanofluid as a working fluid in 2 double U-tube horizontal GHE. It was concluded that the heat exchange rate could be enhanced by up to 40% by CuO/water nanofluid compared with pure water. They also reported that the best nanoparticle diameter and shape are 40 nm and sphere, respectively.

Further research on the nanofluids has resulted in the invention of a new type of nanofluid, i.e., hybrid nanofluids, which can be generated by dispersing 2 or more nanoparticles into the base fluid. Since the simple nanofluids do not possess any desirable feature necessary for a particular objective, they are likely to lack either rheological or thermal properties. In contrast, the chemical and physical properties of hybrid nanofluids are provided in a homogeneous phase by a simultaneous combination of added nanoparticles' properties to the base fluid. Considering that one of the essential criteria in actual projects is the tradeoff between various characteristics, the significant role of hybrid nanofluids can be indicated. Hybrid nanofluids generally have superior chemical stability, thermal conductivity, mechanical resistance, physical strength, etc., than simple nanofluids [31–37]. Suresh et al. [38] analyzed the application of Al_2O_3-Cu/water hybrid nanofluid experimentally in a straight tube at fixed heat flux. Labib et al. [39] simulated Al_2O_3-carbon nanotube (CNT)/water hybrid nanofluid in a horizontal straight tube under the tube wall's constant heat flux. Numerical simulation of the laminar flow of Al_2O_3-Cu/water hybrid nanofluid inside a corrugated box with a fixed heat source is carried out by Takabi and Salehi [40]. Sundar et al. [41] experimentally evaluated Fe_3O_4-multi-wall CNT (MWCNT)/water hybrid nanofluid flowing through a horizontal straight tube at fixed heat flux. The impact of using TiO_2-Cu/water hybrid nanofluid on the performance of a tubular heat exchanger is examined experimentally by Madhesh et al. [42]. An experimental investigation on Graphene nanoplatelet-Ag/water hybrid nanofluid application in a horizontal straight tube under constant heat flux is conducted by Yarmand et al. [43]. The influence of different volume fractions on the thermophysical properties of Ag-MgO/water hybrid nanofluid is experimentally investigated by Esfe et al. [44]. Toghraie et al. [45] added ZnO and TiO_2 nanoparticles experimentally to ethylene glycol (EG) and studied the effects of various volume fractions and temperatures on the thermal conductivity of the hybrid nanofluid. Van Trinh et al. [46] also conducted an

16

experiment in which 3 nanoparticles, such as graphene, MWCNT, and Cu are combined with EG and then examined the effect of different volume fractions. In an experimental investigation done by Sundar et al. [47], the dispersion of Co_3O_4 and graphene oxide nanoparticles into EG, water, and a mixture of water/EG are evaluated at various temperatures and volume fractions. Sahoo and Sarkar [48] numerically studied the addition of TiO_2, SiC, CuO, Cu, Al_2O_3, and Ag to EG to be used as a coolant in an automobile radiator. Mousavi Ajarostaghi et al. [49] compared numerically 2 types of hybrid nanofluid including Ag-Hydrogen Exfoliated Graphene (HEG)/water and Fe_3O_4-MWCNT/water at different volume fractions in a straight tube which was equipped with a turbulator. Hashemi Karouei et al. [50] evaluated the laminar heat transfer and the use of hybrid nanofluids (Fe_3O_4-MWCNT/water and Ag-HEG/water) in a helical double pipe heat exchanger equipped with a new helical turbulator. Moreover, in addition to the aforementioned works, some other studies have proven that numerical simulation is an efficient method to evaluate utilizing different nanofluids (single or hybrid) in various applications [51–53].

Given the literature reviewed and to the best of our knowledge, it is necessary to highlight that there has been no previous study yet reported on using any hybrid nanofluids as the working fluid in the BHEs. Hence, this research work aims at the numerical investigation of comparing 4 types of hybrid nanofluids, including Ag-MgO/water, TiO_2-Cu/water, Al_2O_3-CuO/water, and Fe_3O_4-MWCNT/water as a working fluid in a single U-tube BHE. Then, the selected hybrid nanofluid is evaluated at various volume fractions. After that, the impact of an increase in the Reynolds number of hybrid nanofluid on the BHE thermal performance is studied.

2.2 Geometry and boundary conditions

In this research, a three-dimensional unsteady state numerical model of a single U-tube BHE is built and analyzed by Ansys Fluent commercial software, which uses the finite volume method. Figure 2-1 shows the schematics of the BHE under study and indicates its different regions. Geometric and operating parameters and study variables are demonstrated in Table 2-1. The thermo-physical properties of the U-tube, casing, backfill, and the surrounding soil are given in Table 2-2. The casing is placed between the backfill and soil, and note that the borehole depth and the U-tube length are the same. As shown in Figure 2-1, the U-tube and casing materials are considered to be polyethylene (PE) and steel, respectively. Moreover, the backfill material is silica sand, and the soil around the BHE comprises 2 parts, including clay (L_1) and sandy-clay (L_2). In this study, 4 types of hybrid nanofluids are evaluated to be applied as working fluids in a single U-tube BHE. Eight nanoparticles, such as Ag, Al_2O_3, Cu, CuO, MgO, MWCNT, TiO_2, and Fe_3O_4 have been dispersed equally into the water to create 4 types of hybrid nanofluid of Ag-MgO (50 : 50 vol.%)/water, TiO_2-Cu (50 : 50 vol.%)/water, Al_2O_3-CuO (50 : 50 vol.%)/water, and Fe_3O_4-MWCNT (50 : 50 vol.%)/water. Thermo-physical properties of the base fluid and nanoparticles are presented in Table 2-3. The BHE operates 24 h a day in the cooling mode where the inlet temperature is set to 300.15 K. The velocity inlet and pressure outlet are chosen for the inlet and outlet boundary conditions, respectively. The standard k-epsilon model is selected for the turbulent fluid flow inside the U-tube, and for the velocity-pressure condition, we applied the SIMPLE algorithm. The time step size is 60 s. The relaxation factors in the spatial discretization of momentum and energy equations done by second-order upwind are 0.7 and one, respectively. Considering the residuals of 10^{-6} for energy equation and 10^{-3} for k, epsilon, momentum, and continuity equations, the numerical simulations' convergence has been achieved.
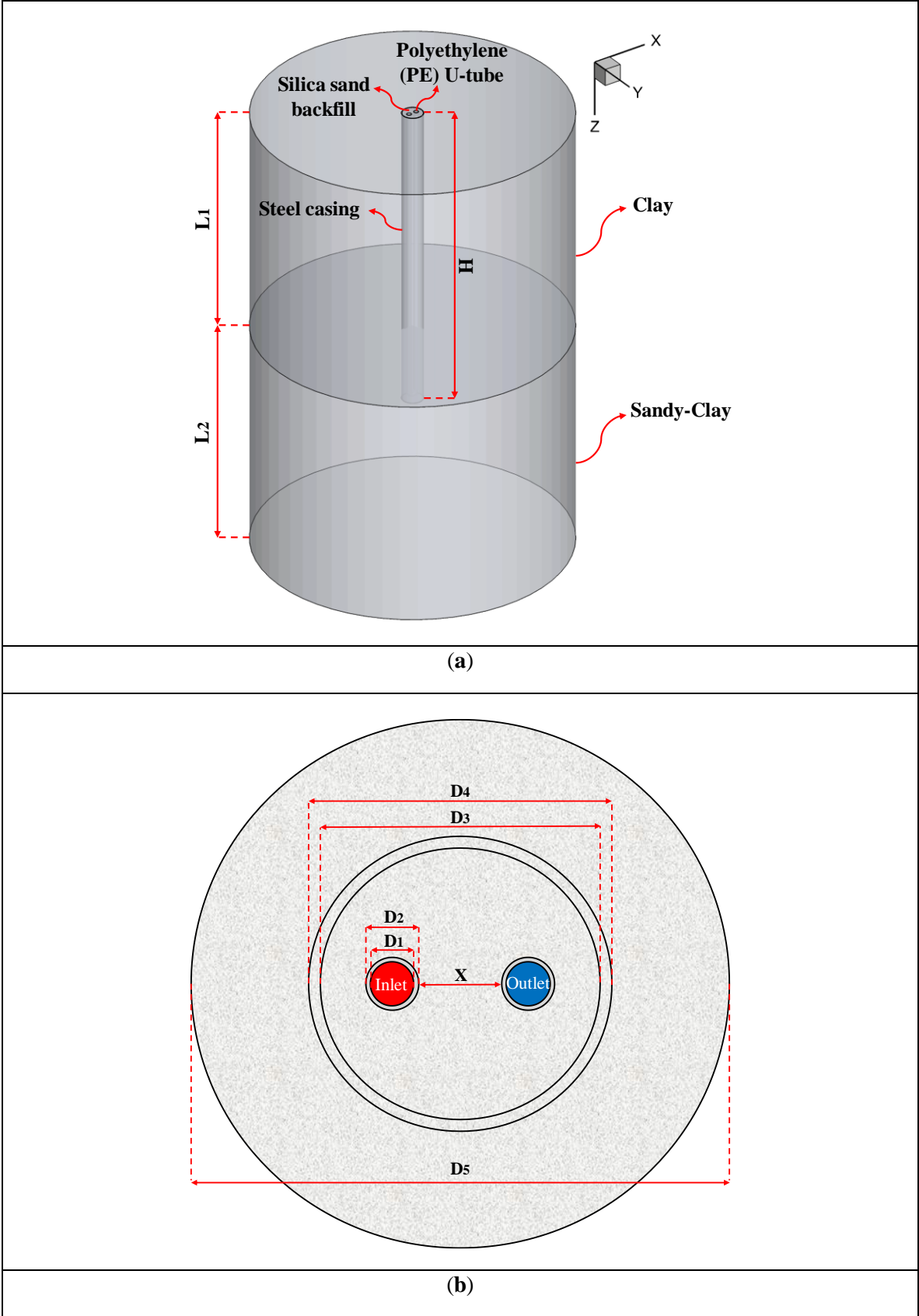
Figure 2-1: Schematic of the borehole heat exchanger (BHE): (a) 3D view, and (b) 2D view (ground surface).

Table 2-1: Geometric and operating parameters and studied variables.

Parameters	Value
Soil Diameter, D_5	2 m
Casing Outer Diameter, D_4	0.1398 m
Casing Inner Diameter, D_3	0.1298 m
U-tube Outer Diameter, D_2	0.033 m
U-tube Inner Diameter, D_1	0.026 m
Clay Length, L_1	1.5 m
Sandy-Clay Length, L_2	1.5 m
Borehole Depth, H	2 m
U-tube Length	2 m
Leg Spacing of U-tube, X	0.02 m
Inlet Temperature	300.15 K
Operating Duration	24 h
Operating Mode	Cooling
Hybrid Nanofluids	Ag-MgO (50 : 50 vol.%)/Water
	TiO_2-Cu (50 : 50 vol.%)/Water
	Al_2O_3-CuO (50 : 50 vol.%)/Water
	Fe_3O_4-MWCNT (50 : 50 vol.%)/Water
Volume Fractions of Nanoparticles	0.05, 0.10, 0.15, 0.20
Reynolds Numbers	3200, 4200, 5200, 6200

Table 2-2: Thermo-physical properties of U-tube, casing, backfill, and soil [18].

Parameters	Value
Polyethylene (PE)	
Density (kg/m^3)	920
Specific Heat Capacity (J/(kg·K))	2300
Thermal Conductivity (W/(m·K))	0.35
Steel	
Density (kg/m^3)	8030
Specific Heat Capacity (J/(kg·K))	502.48
Thermal Conductivity (W/(m·K))	16.27
Silica Sand	
Density (kg/m^3)	2210
Specific Heat Capacity (J/(kg·K))	750
Thermal Conductivity (W/(m·K))	1.4
Clay	
Density (kg/m^3)	1700
Specific Heat Capacity (J/(kg·K))	1800
Thermal Conductivity (W/(m·K))	1.2
Sandy-Clay	

Density (kg/m³)	1960
Specific Heat Capacity (J/(kg·K))	1200
Thermal Conductivity (W/(m·K))	2.1

Table 2-3: Thermo-physical properties of base fluid and nanoparticles.

Property	Base Fluid	Nanoparticles							
	Water	Cu [54]	CuO [54]	Al₂O₃ [54]	TiO₂ [54]	Fe₃O₄ [41]	MWCNT [41]	Ag [44]	MgO [44]
Density (kg/m³)	998.2	8933	6510	3880	4175	5180	1600	10,500	3580
Specific Heat Capacity (J/(kg·K))	4182	385	540	792	692	670	796	235	874
Thermal Conductivity (W/(m·K))	0.6	401	18	42.34	8.4	9.7	3000	429	55
Viscosity (Pa·s)	0.001003	–	–	–	–	–	–	–	–

2.3 Thermo-physical properties and studied factors

The conservation equations for energy, momentum, and continuity are given below:

$$\frac{\partial \rho}{\partial t} + \nabla\nabla \cdot (\rho \vec{v}) = S_m \tag{1}$$

$$\frac{\partial (\rho \vec{v})}{\partial t} + \nabla \cdot (\rho \vec{v}\vec{v}) = -\nabla P + \nabla(\overline{\overline{\tau}}) + \rho \vec{g} + \vec{F}, \overline{\overline{\tau}} = \mu\left[\nabla\vec{v} + \nabla\vec{v}^T - \frac{2}{3}\nabla \cdot \vec{v}I\right] \tag{2}$$

$$\frac{\partial (\rho E)}{\partial t} + \nabla \cdot (\vec{v}(\rho E + P)) = \nabla\left[k_{HNF}\nabla T - \sum_j h_j \vec{J}_j + (\overline{\overline{\tau}}_{HNF} \cdot \vec{v})\right] + S_h \tag{3}$$

The thermo-physical properties of hybrid nanofluid can be estimated with the following equations.

The density of hybrid nanofluid (ρ_{HNF}) [55]:

$$\rho_{HNF} = \phi_{NP1}\rho_{NP1} + \phi_{NP2}\rho_{NP2} + (1 - \phi_{NP1} - \phi_{NP2})\rho_{BF} \tag{4}$$

The specific heat capacity of hybrid nanofluid ($(C_p)_{HNF}$) [55]:

$$(C_p)_{HNF} = \frac{\phi_{NP1}(\rho C_p)_{NP1} + \phi_{NP2}(\rho C_p)_{NP2} + (1 - \phi_{NP1} - \phi_{NP2})(\rho C_p)_{BF}}{\rho_{HNF}} \tag{5}$$

The thermal conductivity of hybrid nanofluid (k_{HNF}) [55]:

$$k_{HNF} = \cfrac{2\left(\phi_{NP1}k_{NP1}+\phi_{NP2}k_{NP2}\right)-2k_{BF}\left(\phi_{NP1}+\phi_{NP2}\right)+2k_{BF}+\left[\cfrac{\phi_{NP1}k_{NP1}+\phi_{NP2}k_{NP2}}{\phi_{NP1}+\phi_{NP2}}\right]}{-\left(\phi_{NP1}k_{NP1}+\phi_{NP2}k_{NP2}\right)-k_{BF}\left(\phi_{NP1}+\phi_{NP2}\right)+2k_{BF}+\left[\cfrac{\phi_{NP1}k_{NP1}+\phi_{NP2}k_{NP2}}{\phi_{NP1}+\phi_{NP2}}\right]} \tag{6}$$

The viscosity of hybrid nanofluid (μ_{HNF}) [55]:

$$\mu_{HNF} = \frac{\mu_{BF}}{(1-\phi_{NP1}-\phi_{NP2})^{2.5}} \tag{7}$$

The thermal expansion of hybrid nanofluid (β_{HNF}) [55]:

$$\beta_{HNF} = \frac{\phi_{NP1}(\rho\beta)_{NP1}+\phi_{NP2}(\rho\beta)_{NP2}+(1-\phi_{NP1}-\phi_{NP2})(\rho\beta)_{BF}}{\rho_{HNF}} \tag{8}$$

The subscripts of *HNF*, *BF*, *NP1*, and *NP2* indicate hybrid nanofluid, base fluid, nanoparticle 1, and nanoparticle 2. ϕ represents the volume fraction of nanoparticles. It should be emphasized that an equal volume of 8 nanoparticles has been dispersed into the base fluid, which resulted in the formation of 4 types of hybrid nanofluid (see Table 2-1).

Factors under study in this work include the pressure drop, thermal resistance, and effectiveness, as follows:

The pressure drop of working fluid flows through the U-tube (ΔP) [18]:

$$\Delta P = P_1 - P_2 \tag{9}$$

P_1 is the inlet pressure (Pa), and P_2 is the outlet pressure (Pa).

The total thermal resistance of the borehole and the surrounding soil (R) [18]:

$$R = \frac{T_s - T_a}{Q_H} \tag{10}$$

T_s and T_a indicate the surrounding soil's initial temperature (K) and working fluid's average temperature between inlet and outlet (K), respectively. Q_H is the heat exchange rate per unit BHE depth, which is calculated by dividing Q (heat exchange rate, W) by H (BHE depth, m) [18]:

$$Q_H = \frac{Q}{H}, where \rightarrow Q = \dot{m}C_p(T_1 - T_2) \tag{11}$$

Furthermore, $\dot{m}$ and C_p show the mass flow rate (kg/s) and the specific heat capacity (J/(kg·K)) of the working fluid, respectively. T_1 is the inlet temperature (K) and T_2 is the outlet temperature (K). Besides, the effectiveness is considered as a non-dimensional factor for evaluating the heat transfer efficiency of the BHE changing from 0 to 1 [18]:

$$E = \frac{Q_{\text{Real}}}{Q_{MAX}} = \frac{\dot{m}C_p(T_1 - T_2)}{\dot{m}C_p(T_1 - T_s)} = \frac{(T_1 - T_2)}{(T_1 - T_s)} \tag{12}$$

Q_{Real} and Q_{MAX} demonstrate the real heat exchange rate and the highest heat exchange rate, respectively. COP improvement (η) factor considers the impact of applying the hybrid nanofluids on the BHE operation in terms of both pressure drop and heat transfer [49,56]:

$$\eta = \left[\frac{Nu}{Nu_0}\right]\left[\frac{f_0}{f}\right]^{1/3} \tag{13}$$

The subscript of 0 refers to pure water as a working fluid at the Reynolds number of 3200 in Sections 2.5.1 and 2.5.2, and the cases of pure water at each specific Reynolds number considered in Section 2.5.3. Nu and f are Nusselt number and friction factor which are defined as follows, respectively [49,56]:

$$Nu = \frac{h_a d_h}{k} \tag{14}$$

$$f = \frac{2d_h \Delta P}{\rho u^2 l} \tag{15}$$

h_a and d_h are the average heat transfer coefficient (W/(m²·K)) and the U-tube hydraulic diameter (m), respectively. u is the working fluid velocity (m/s), and l is the length of the U-tube (m).

2.4 Mesh topology and validation

The generated grid for the single U-tube BHE is illustrated in Figure 2-2a,b. As can be seen, the working fluid and U-tube meshing are done by structured methods, while the other regions are meshed by the unstructured methods. Because the volumes inside the borehole are of high importance compared to the outside, finer grids have been applied for these regions. Besides, the boundary layer meshes are generated for the interfaces between the working fluid and U-tube as well as the U-tube and backfill, with 3 layers and a growth rate of 1.2. The grid independence test of the model is also conducted, as shown in Figure 2-2c. Different numbers of grids, from 334,473 to 2,129,847, have been evaluated for the model in terms of the working fluid's outlet temperature. The third type of mesh with the orthogonal quality of 0.22, skewness of 0.82, and the grid number of 1,573,132 is chosen for the numerical modeling of hybrid nanofluids in the BHE. This numerical study is verified with an experiment conducted in Japan by Jalaluddin et al. [57] (see Figure 2-3). All the geometric parameters and test conditions are similar to what is stated in Section 2.2, except for the borehole depth and soil diameter, 20 m and 10 m, respectively, with the pure water flowing through the U-

tube. It is shown that there is an excellent agreement between the numerical results and the experimental data verifying the reliability of the numerical model being studied.
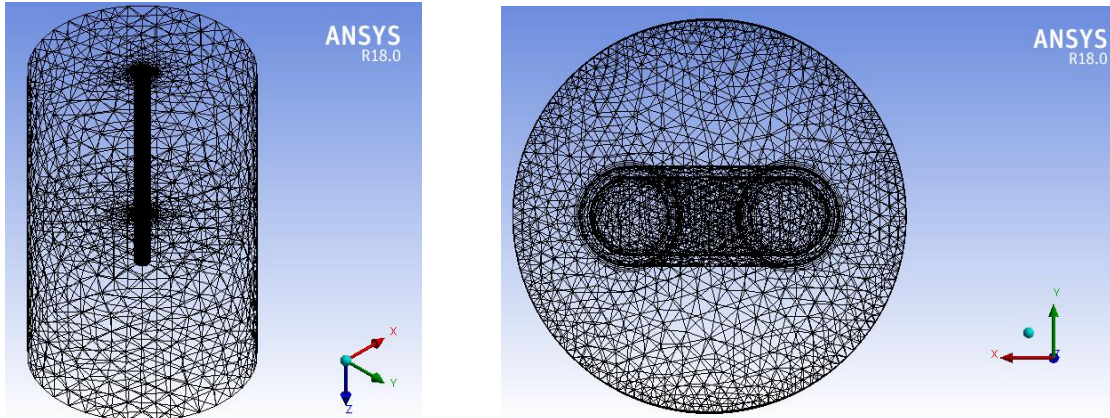
(**a**)   (**b**)
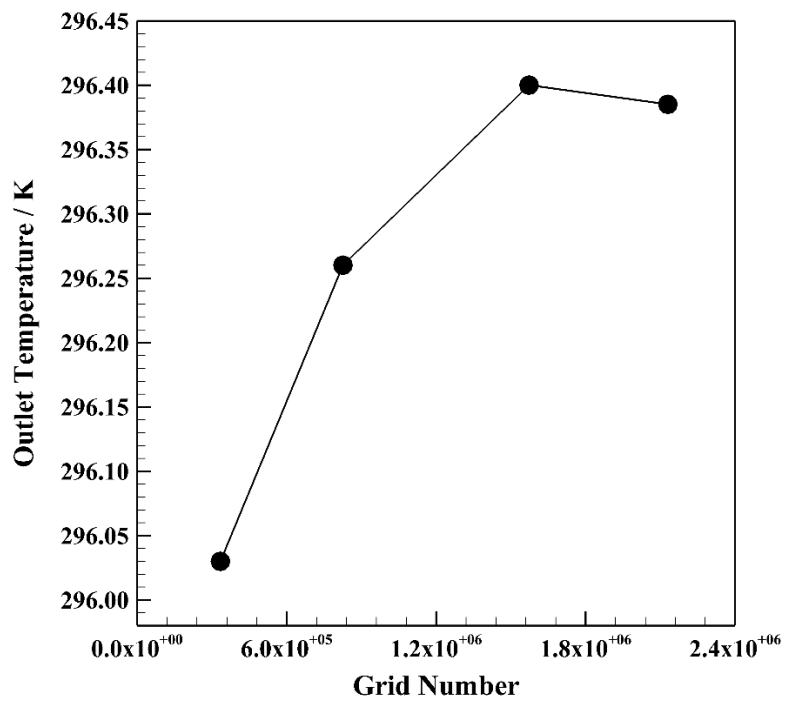
(**c**)

Figure 2-2: Generated grid for the BHE and the grid independence test: (a) 3D view, (b) 2D view, and (c) the grid independence test.
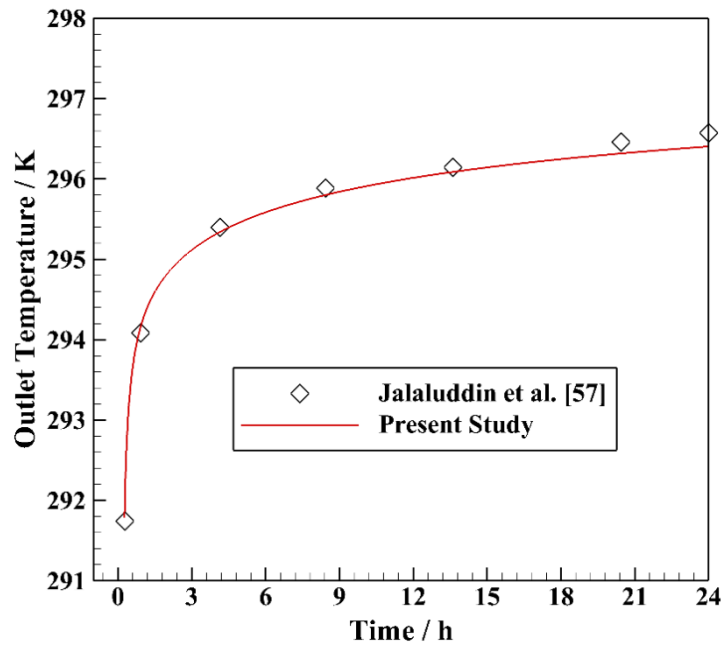
Figure 2-3: Verification of this numerical study with the experimental data.

2.5 Results and discussion

In this study, several types of hybrid nanofluids such as Ag-MgO/water, Al$_2$O$_3$-CuO/water, Fe$_3$O$_4$-MWCNT/water, and TiO$_2$-Cu/water are numerically examined to be used as working fluid in a single U-tube BHE. After comparing, the selected hybrid nanofluid is evaluated at various values of volume fractions and Reynolds numbers. Also, the obtained numerical results of hybrid nanofluids have been compared with the case of pure water.

2.5.1 Comparing various types of hybrid nanofluid

Thermo-physical properties of various hybrid nanofluids at $\phi = 0.15$ calculated by Equations (4)– (8) are given in Table 2-4. The variation of the outlet temperature with operating time using various hybrid nanofluids at $\phi = 0.15$ and Re = 3200 is illustrated in Figure 2-4. Accordingly, it can be seen that at the beginning of the operation, the differences between the various cases are not notable. However, all hybrid nanofluids show lower outlet temperature than pure water, except for Fe$_3$O$_4$-MWCNT/water. Moreover, the results show that the lowest outlet temperature belongs to the case with Ag-MgO/water hybrid nanofluid followed by TiO$_2$-Cu/water hybrid nanofluid.

Table 2-4: Thermo-physical properties of various hybrid nanofluids at $\phi = 0.15$.

Property	Hybrid Nanofluids			
	Ag-MgO (50 : 50 vol.%)/Water	TiO$_2$-Cu (50 : 50 vol.%)/Water	Al$_2$O$_3$-CuO (50 : 50 vol.%)/Water	Fe$_3$O$_4$-MWCNT (50 : 50 vol.%)/Water
Density (kg/m^3)	2810.74	2664.94	2257.24	1715.74
Specific Heat Capacity (J/(kg·K))	1338.2930	1452.7067	1732.3743	2117.8970
Thermal Conductivity (W/(m·K))	2.2769	2.2753	2.2183	2.2842
Viscosity (Pa·s)	0.0024	0.0024	0.0024	0.0024
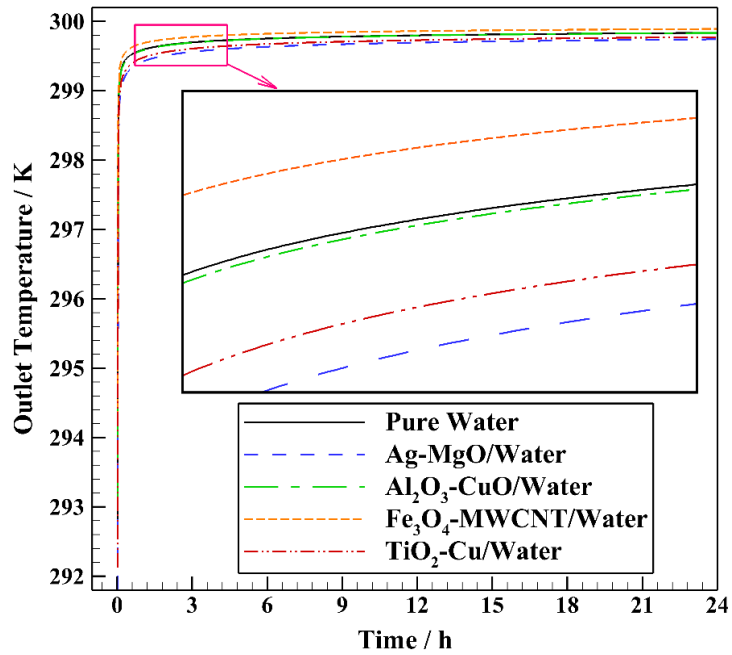
Figure 2-4: The variation of the outlet temperature with operating time using various hybrid nanofluids at ϕ = 0.15 and Re = 3200.

The effectiveness (E) for various hybrid nanofluids at ϕ = 0.15 and Re = 3200 is depicted in Figure 2-5. It can be concluded that the hybrid nanofluids have higher effectiveness than pure water, while the corresponding value for Fe_3O_4-MWCNT/water is lower than pure water. For instance, the effectiveness of cases with Ag-MgO/water, Al_2O_3-CuO/water, and TiO_2-Cu/water are 29.81, 0.48, and 19.71% more than pure water; however, the effectiveness of Fe_3O_4-MWCNT/water is lower by 17.79%. According to Equation (12), the effectiveness is the ratio of the real heat exchange rate to the highest heat exchange rate. Since the mass flow rate and the specific heat capacity are simplified in the numerator and denominator of the fraction, they do not influence the estimated effectiveness. Therefore, the inlet and outlet temperature difference plays the primary role here (see Figure 2-4 and Figure 2-5). The total thermal resistance of the borehole and the surrounding soil and the heat exchange rate per unit BHE depth for various hybrid nanofluids at ϕ = 0.15 and Re = 3200 are shown in Figure 2-6.

25
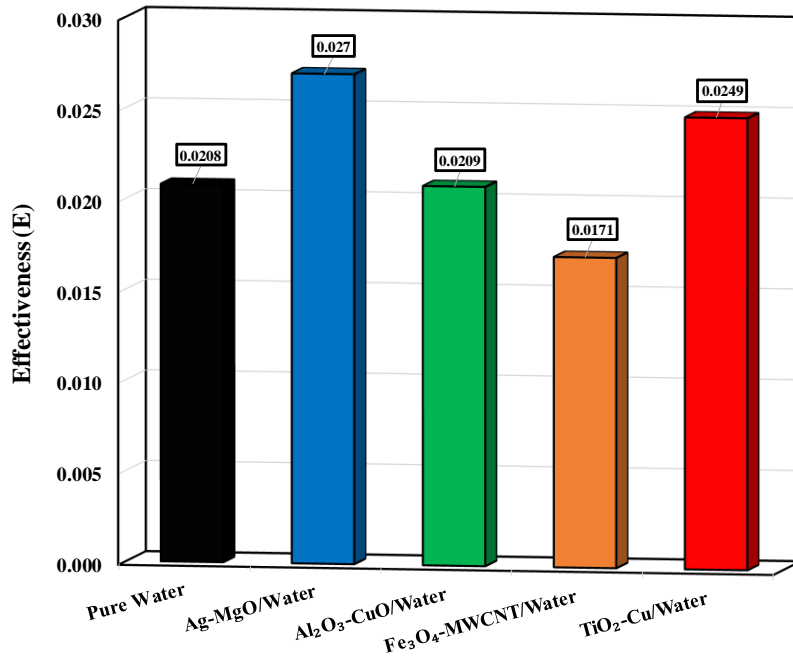
Figure 2-5: Effectiveness for various hybrid nanofluids at ϕ = 0.15 and Re = 3200.
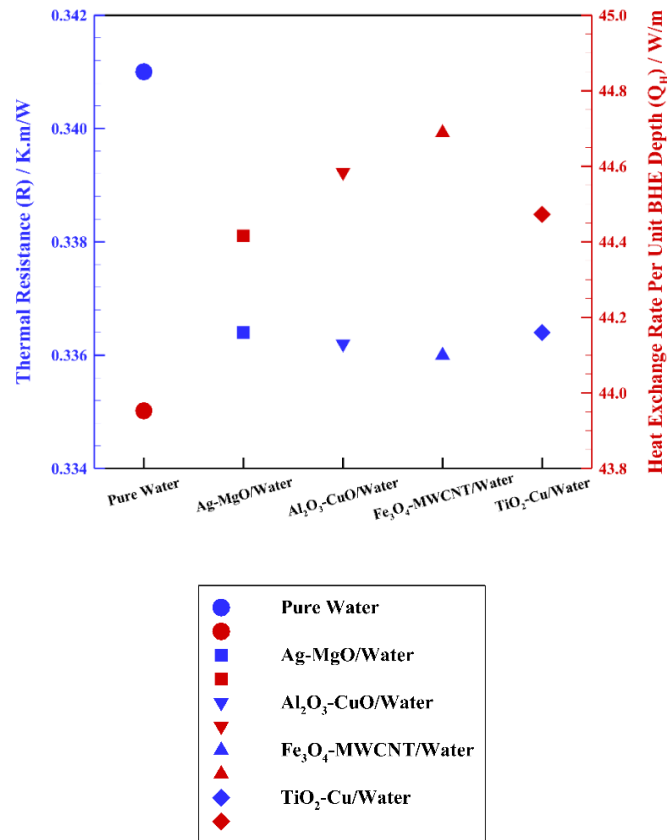
Figure 2-6: The total thermal resistance of the borehole and the surrounding soil and the heat exchange rate per unit BHE depth for various hybrid nanofluids at ϕ = 0.15 and Re = 3200.

Figure 2-6 shows that all hybrid nanofluids being studied have lower thermal resistance and higher heat exchange rate per unit BHE depth than the pure water as the working fluid. Consequently, hybrid nanofluids' thermal resistances, including Ag-MgO/water, Al_2O_3-CuO/water, Fe_3O_4-MWCNT/water, and TiO_2-Cu/water, are less than pure water by 1.35, 1.41, 1.47, and 1.35%, respectively. Furthermore, it can be seen that the differences between the calculated thermal resistance of various hybrid nanofluids are not considerable. However, the lowest one belongs to the case with Fe_3O_4-MWCNT/water working fluid. The thermal resistance and the heat exchange rate per unit BHE depth have been calculated by Equations (10) and (11). In these equations, the specific heat capacity and the density of the hybrid nanofluids significantly impact the estimated results. For instance, Fe_3O_4-MWCNT/water has the minimum effectiveness, but it could achieve the highest heat exchange rate, which can be related to its higher values of specific heat capacity and thermal conductivity compared to the others (see Table 2-4, Figure 2-5 and Figure 2-6).

The pressure drop for various hybrid nanofluids at $\phi = 0.15$ and Re = 3200 is illustrated in Figure 2-7. It is indicated that using hybrid nanofluid instead of pure water as a working fluid results in higher rates of pressure drop. The pressure drops of hybrid nanofluids, including Ag-MgO/water, Al_2O_3-CuO/water, Fe_3O_4-MWCNT/water, and TiO_2-Cu/water, are higher than pure water by 111.41, 163.12, 246.25, and 122.8%, respectively. The maximum and minimum values of pressure drop among hybrid nanofluids belong to the cases with Fe_3O_4-MWCNT/water and Ag-MgO/water, respectively.
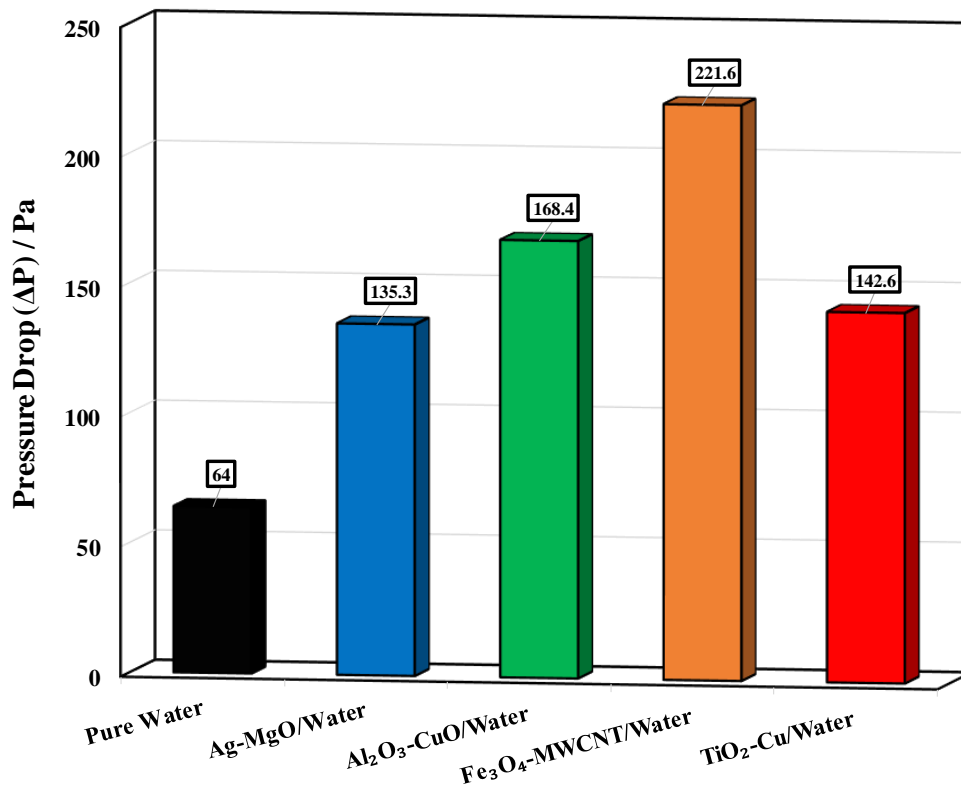
Figure 2-7: Pressure drop for various hybrid nanofluids at $\phi = 0.15$ and Re = 3200.

COP improvement for various hybrid nanofluids at $\phi = 0.15$ and Re = 3200 is presented in Figure 2-8. COP improvement factor is an efficient index that is calculated by Equation (13). In this factor, both the ratios of friction factor (or pressure drop) and average Nusselt number are considered in which higher COP

27

improvement values (more than unity; $\eta > 1$) mean that the proposed method is efficient in terms of pressure drop and heat transfer. From Figure 2-8, it can be seen that all the evaluated hybrid nanofluids present lower COP improvement than unity which means that applying them as working fluid is not economically viable because of having higher pressure drop (or friction factor) than heat transfer enhancement. As a result, it can be concluded that the COP improvement of the evaluated hybrid nanofluids, including Ag-MgO/water, Al_2O_3-CuO/water, Fe_3O_4-MWCNT/water, and TiO_2-Cu/water, is lower than pure water by 32.29, 27.65, 24.8, and 31.04%, respectively. The lowest and the highest COP improvement values belong to the cases with Ag-MgO/water and Fe_3O_4-MWCNT/water hybrid nanofluids, respectively. To see better the heat transfer process in the proposed system, 2D contours of the temperature distribution of the BHE using Ag-MgO/water hybrid nanofluid at various operating hours are illustrated in Figure 2-9 when $\phi = 0.15$ and Re = 3200 (top view at Z = 0). It is worth mentioning that since the contours of various hybrid nanofluids have not demonstrated the differences in various cases appropriately, only the contours of the selected hybrid nanofluid are presented here. As can be seen, the thermal radius around the borehole increases continuously by exchanging heat from the working fluid to the surroundings.
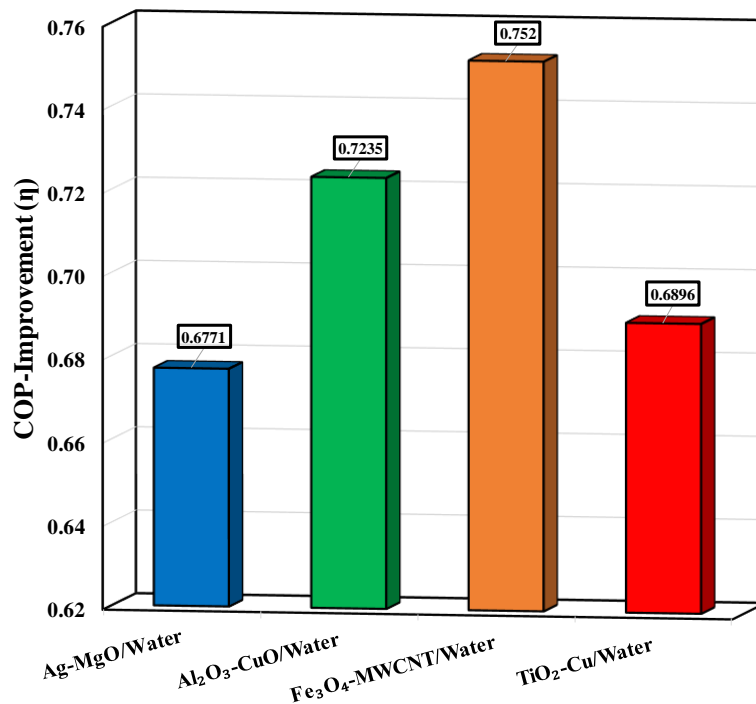
Figure 2-8: Coefficient of performance (COP)-improvement for various hybrid nanofluids at $\phi = 0.15$ and Re = 3200.
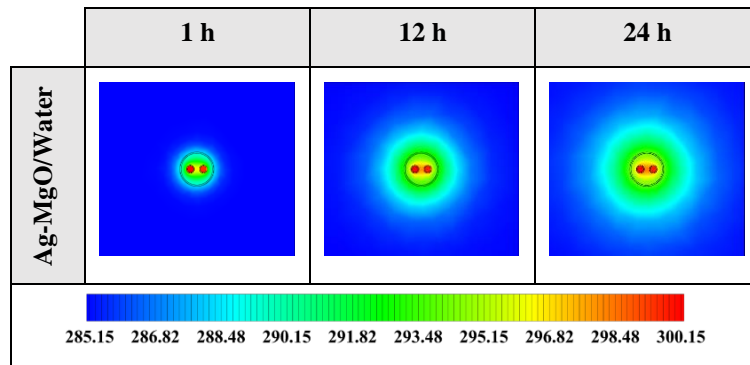
Figure 2-9: Two-dimensional (2D) contours of the temperature distribution of the BHE at various hours of operating using Ag-MgO/water hybrid nanofluid when ϕ = 0.15 and Re = 3200 (Top view at Z = 0).

2.5.2 Impact of volume fraction of hybrid nanofluid

In the second section, the impact of the volume fraction of hybrid nanofluids on the thermal performance of the BHE is performed. It should be noted that the Ag-MgO/water hybrid nanofluid is considered a working fluid, considering its superior effectiveness, minor pressure drop, and appropriate thermal resistance among studied hybrid nanofluids. Therefore, in the present study, the primary criterion for selecting the best hybrid nanofluid is the thermal improvement called effectiveness (see Equation (12)). 4 volume fractions of nanofluids such as 0.05, 0.10, 0.15, and 0.20 are chosen. Also, like Section 2.5.1, the numerical results of Ag-MgO/water hybrid nanofluid with various volume fractions are compared with the case of pure water. Note that the thermo-physical properties of Ag-MgO/water hybrid nanofluid at different volume fractions have been estimated by Equations (4)–(8) (see Table 2-5).

Table 2-5: Thermo-physical properties of Ag-MgO (50:50 vol.%) / Water hybrid nanofluid at various volume fractions.

Property	Volume Fractions			
	ϕ = 0.05	ϕ = 0.10	ϕ = 0.15	ϕ = 0.20
Density (kg/m³)	1602.38	2206.56	2810.74	3414.92
Specific Heat Capacity (J/(kg·K))	2519.2814	1767.1035	1338.2930	1061.2159
Thermal Conductivity (W/(m·K))	1.3313	1.7452	2.2769	2.9852
Viscosity (Pa·s)	0.0013	0.0017	0.0024	0.0035

Figure 2-10 shows the variation of the outlet temperature with operating time using Ag-MgO/water hybrid nanofluid with various volume fractions at Re = 3200. It can be recognized that, first, the differences between the various cases are not noteworthy. Nevertheless, then, the cases with Ag-MgO/water hybrid nanofluids at various volume fractions display lower outlet temperature than the case of pure water. Moreover, the results show that the lowest outlet temperature is achieved by the case containing Ag-MgO/water hybrid nanofluid at ϕ = 0.10, followed by the case at ϕ = 0.15.

29
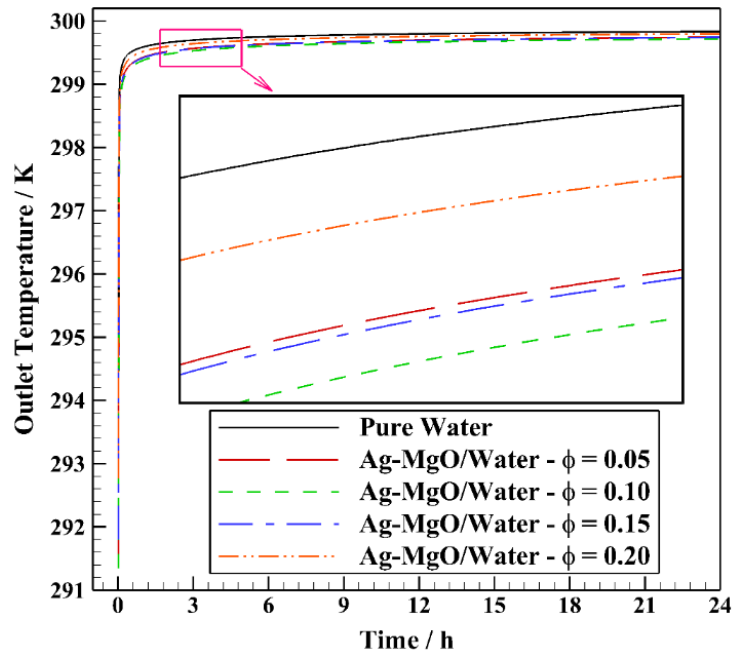
Figure 2-10: The variation of the outlet temperature with operating time using Ag-MgO/water hybrid nanofluid with different volume fractions at Re = 3200.

The effectiveness (E) for Ag-MgO/water hybrid nanofluid with various volume fractions at Re = 3200 is shown in Figure 2-11. It is illustrated that Ag-MgO/water hybrid nanofluid at each value of volume fraction presents more effectiveness than pure water. Also, the effectiveness of cases with ϕ = 0.05, 0.1, 0.15, and 0.2 are more than pure water by 28.36%, 37.02%, 29.81%, and 11.54%, respectively. Accordingly, among the volume fractions under study of Ag-MgO/water hybrid nanofluid, the maximum effectiveness belongs to the case with ϕ = 0.1, and the case with ϕ = 0.15 is positioned at the second level. As indicated in Figure 2-10 and Figure 2-11, Ag-MgO/water hybrid nanofluid's outlet temperature and effectiveness at a volume fraction of 0.20 are found to be higher and lower than that for the other cases, respectively. This matter can be related to a decrease of almost 58% in the specific heat capacity of Ag-MgO/water hybrid nanofluid when the volume fraction changes from 0.05 to 0.20; although the thermal conductivity is improved by 55% (see Table 2-5). Based on Equation (12), the effectiveness is estimated by dividing the real heat exchange rate by the highest heat exchange rate. Because the mass flow rate and the specific heat capacity have been simplified in the numerator and denominator of the fraction, they do not affect the effectiveness obtained. Hence, the most important parameter here is the temperature difference between the inlet and outlet (see Figure 2-10 and Figure 2-11).

The total thermal resistance of the borehole and the surrounding soil and the heat exchange rate per unit BHE depth for Ag-MgO/water hybrid nanofluid with various volume fractions at Re = 3200 are illustrated in Figure 2-12. As shown, Ag-MgO/water hybrid nanofluid at the considered volume fractions achieves lower thermal resistance and higher heat exchange rate per unit BHE depth than pure water. Consequently, the thermal resistances of cases with ϕ = 0.05, 0.1, 0.15, and 0.2 are lower than pure water by 0.88%, 1.14%, 1.35%, and 1.55%, respectively, which are not considerable. However, the lowest one belongs to the case of ϕ = 0.2.
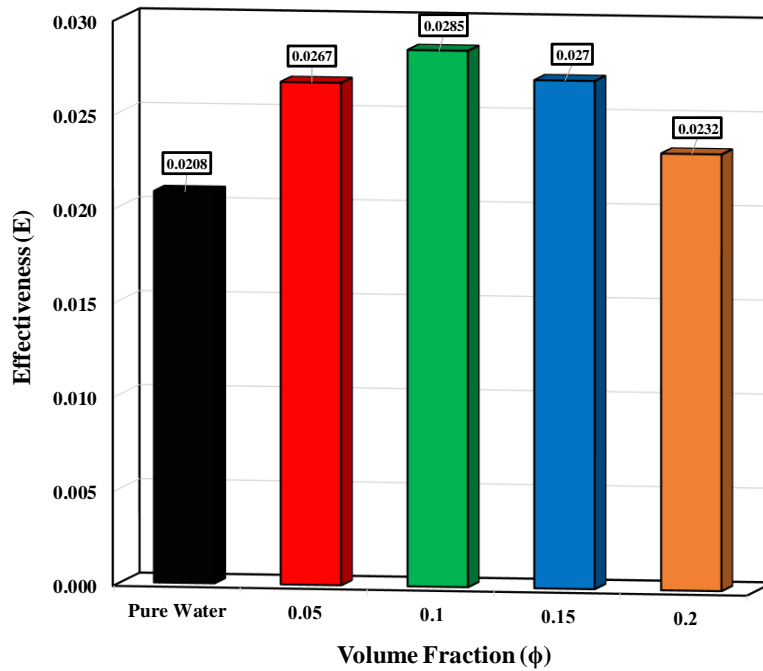
Figure 2-11: Effectiveness when using Ag-MgO/water hybrid nanofluid with different volume fractions at Re = 3200.
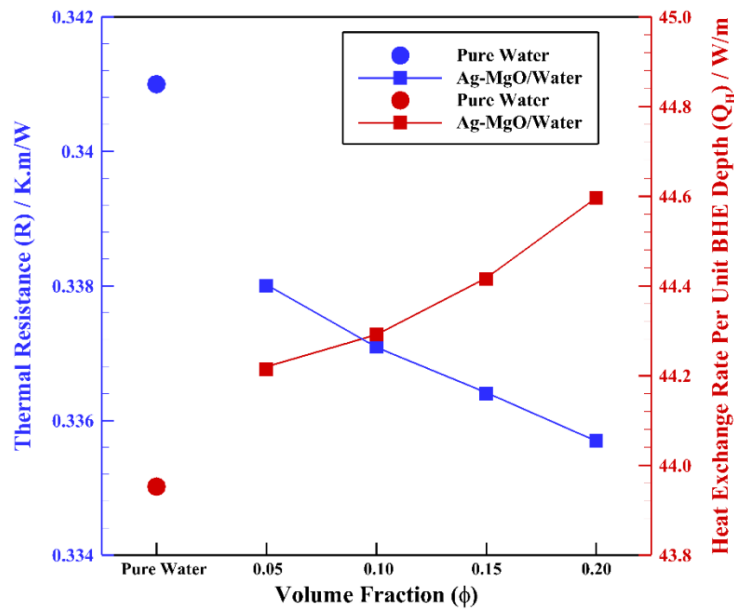
Figure 2-12: The total thermal resistance of the borehole and the surrounding soil and the heat exchange rate per unit BHE depth for Ag-MgO/water hybrid nanofluid with different volume fractions at Re = 3200.

The thermal resistance and the heat exchange rate per unit BHE depth are estimated by Equations (10) and (11). The calculated results have been under the direct influence of the hybrid nanofluids' specific heat capacity and density. Subsequently, the Ag-MgO/water hybrid nanofluid at $\phi = 0.20$ has the lowest effectiveness but the highest heat exchange rate, which can be explained by its higher values of density and thermal conductivity compared to the other cases (see Table 2-5, Figure 2-11 and Figure 2-12). The pressure

drop for Ag-MgO/water hybrid nanofluid with various volume fractions at Re = 3200 is presented in Figure 2-13. This figure indicates that using the Ag-MgO/water hybrid nanofluid at each value of volume fraction instead of pure water causes higher rates of pressure drop. The pressure drops of Ag-MgO/water hybrid nanofluid at ϕ = 0.05, 0.1, 0.15, and 0.2 are higher than the pure water by 5.47%, 37.97%, 111.41%, and 275.94%, respectively. Furthermore, as the volume fraction increases from 0.05 to 0.2 (by 300% growth), the pressure drop rises by 256.44%.
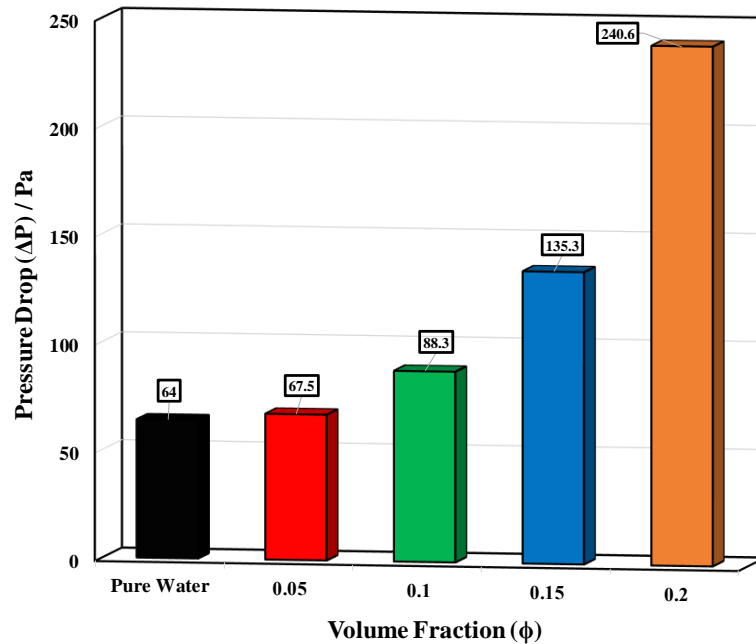
Figure 2-13: Pressure drop when using Ag-MgO/water hybrid nanofluid with different volume fractions at Re = 3200.

Figure 2-14 depicts that Ag-MgO/water hybrid nanofluid with each value of volume fraction shows lower COP improvement than unity, indicating that the studied cases are not economically viable as they cause more pressure drop (or friction factor) than heat transfer augmentation. Consequently, it can be concluded that the COP improvement of the evaluated cases with various volume fractions including ϕ = 0.05, 0.10, 0.15, and 0.20 is lower than pure water by 23.26%, 28.82%, 32.29%, and 34.29%, respectively. In terms of COP improvement, the case with Ag-MgO/water hybrid nanofluid at ϕ = 0.05 could obtain the maximum value of almost 0.77. To see the heat exchange in the BHE containing Ag-MgO/water hybrid nanofluid at ϕ = 0.10 and Re = 3200, 2D contours of the temperature at different hours of operating (top view at Z = 0) are shown in Figure 2-15. This shows that using Ag-MgO/water hybrid nanofluid with the volume fraction fixed at 0.10 results in better temperature distribution and more heat transfer rate.
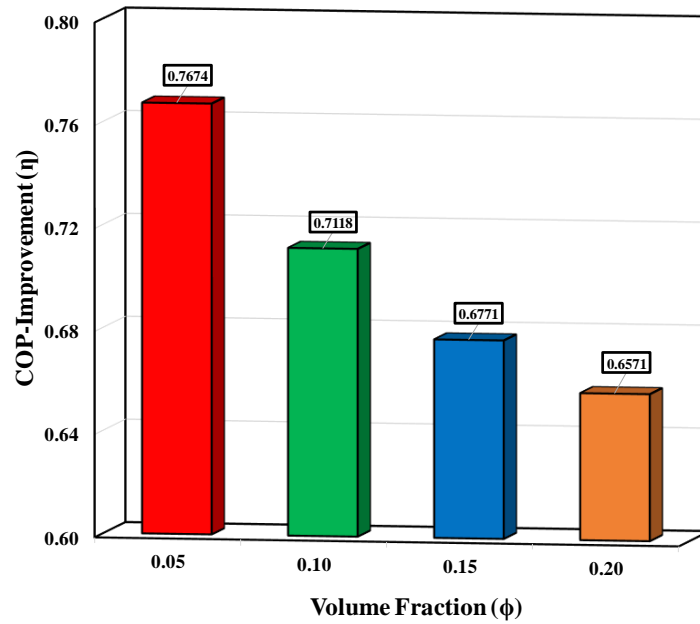
Figure 2-14: COP improvement of Ag–MgO/water hybrid nanofluid with different volume fractions at Re = 3200.
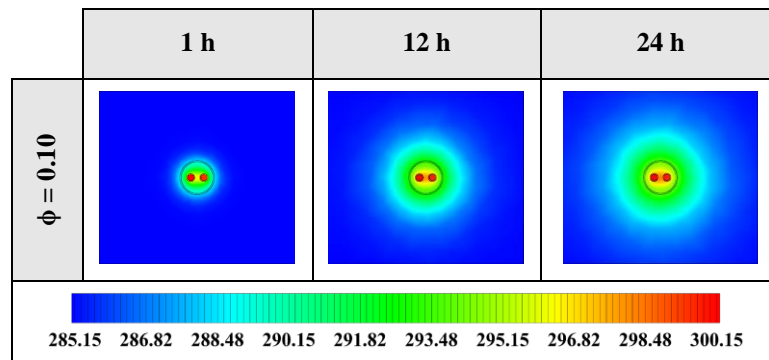

Figure 2-15: Two-dimensional (2D) contours of the temperature distribution of the BHE at various hours of operating using Ag-MgO/water hybrid nanofluid at ϕ = 0.10 and Re = 3200 (Top view at Z = 0).

2.5.3 Impact of Reynolds number of hybrid nanofluid

In the final section, the impact of the Reynolds number (Re) of hybrid nanofluids on the thermal performance of the BHE is investigated. Taking into account the balance between thermal resistance, pressure drop, and effectiveness, the Ag-MgO/water hybrid nanofluid at ϕ = 0.10 is selected as the best working fluid for further studies. Hence, in this research, the primary criterion for choosing the best hybrid nanofluid is the thermal enhancement called effectiveness (see Equation (12)). Four Reynolds numbers of the hybrid nanofluid, including 3200, 4200, 5200, and 6200, are chosen and evaluated. Also, similar to Sections 2.5.1 and 2.5.2, Ag-MgO/water hybrid nanofluid (at ϕ = 0.10) with various Reynolds numbers is compared with the corresponding cases for pure water.

Figure 2-16 displays the outlet temperature variation with operating time using Ag-MgO/water hybrid nanofluid with different Reynolds numbers when ϕ = 0.10. Despite the minor differences between the various

cases initially, all cases with Ag-MgO/water hybrid nanofluids at various Reynolds numbers have reached lower outlet temperatures than the cases of pure water at the corresponding Reynolds numbers. Furthermore, results demonstrate that the minimum outlet temperatures belong to the lowest Reynolds number (Re = 3200). By increasing the Reynolds number, the outlet temperature increases, as the more the fluid flow rate, the less time for heat transfer with the surrounding domain.
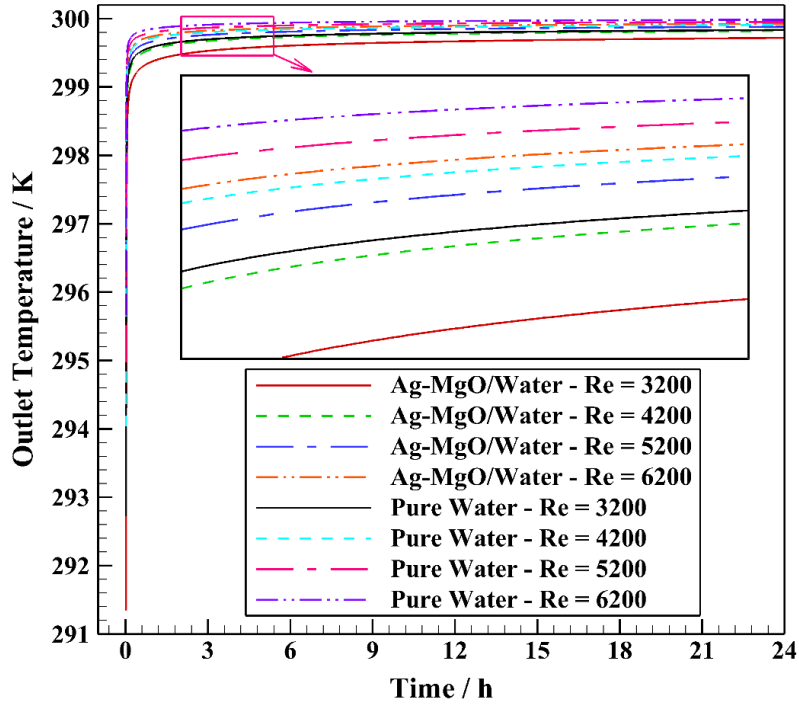

Figure 2-16: The variation of the outlet temperature with operating time using Ag-MgO/water hybrid nanofluid with different Reynolds numbers at $\phi = 0.10$.

The effectiveness (E) for Ag-MgO/water hybrid nanofluid ($\phi = 0.10$) with various Reynolds numbers is shown in Figure 2-17. It can be seen that Ag-MgO/water hybrid nanofluid at each value of Reynolds numbers is more effective than pure water. Also, an increase in the Reynolds number leads to a reduction in the effectiveness of both hybrid nanofluids and pure water. Moreover, Ag-MgO/water hybrid nanofluid's effectiveness at Re = 3200, 4200, 5200, and 6200 are 37.02%, 36.25%, 36.15%, and 36.7%, respectively, compared with the corresponding cases of pure water.

The total thermal resistance of the borehole and the surrounding soil and the heat exchange rate per unit BHE depth for Ag-MgO/water hybrid nanofluid ($\phi = 0.10$) and pure water with various Reynolds numbers are shown in Figure 2-18.
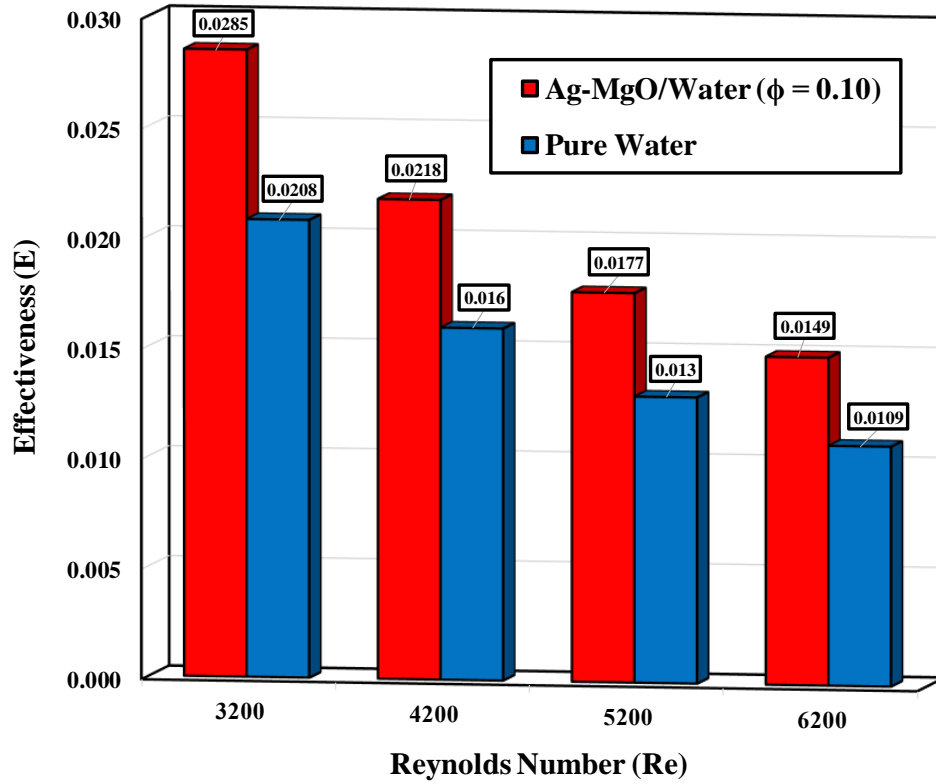
Figure 2-17: Effectiveness when using Ag-MgO/water hybrid nanofluid with different Reynolds numbers at ϕ = 0.10.
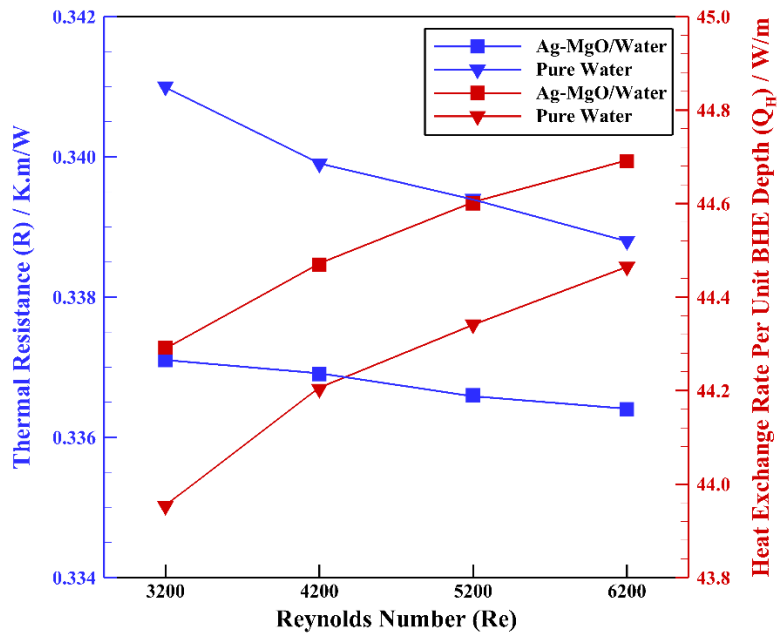

Figure 2-18: The total thermal resistance of the borehole and the surrounding soil and the heat exchange rate per unit BHE depth for Ag-MgO/water hybrid nanofluid with different Reynolds numbers at ϕ = 0.10.

Figure 2-18 displays that Ag-MgO/water hybrid nanofluid ($\phi = 0.10$) at each value of Reynolds number reaches a lower thermal resistance and a higher heat exchange rate than the cases of pure water. From the figure, the thermal resistances of Ag-MgO/water hybrid nanofluid at Re = 3200, 4200, 5200, and 6200 are lower than the corresponding cases of pure water by 1.14%, 0.88%, 0.82%, and 0.71%, respectively. Worth mentioning that augmentation in the Reynolds number leads to a reduction in the thermal resistance difference between the cases of hybrid nanofluid and pure water.

The pressure drop for Ag-MgO/water hybrid nanofluid ($\phi = 0.10$) and pure water with various Reynolds numbers is presented in Figure 2-19. As a result, it can be concluded that employing Ag-MgO/water hybrid nanofluid at each Reynolds number instead of pure water causes higher rates of pressure drop, which can be explained by the Darcy–Weisbach equation. Moreover, the pressure drop of Ag-MgO/water hybrid nanofluid at Re = 3200, 4200, 5200, and 6200 is higher than in the corresponding cases for pure water by 37.97%, 38%, 38.02%, and 38.15%, respectively. Furthermore, as the Reynolds number increases from 3200 to 6200 (a growth of 93.75%), the pressure drop rises by 142.03% for pure water and 142.35% for the Ag-MgO/water hybrid nanofluid.
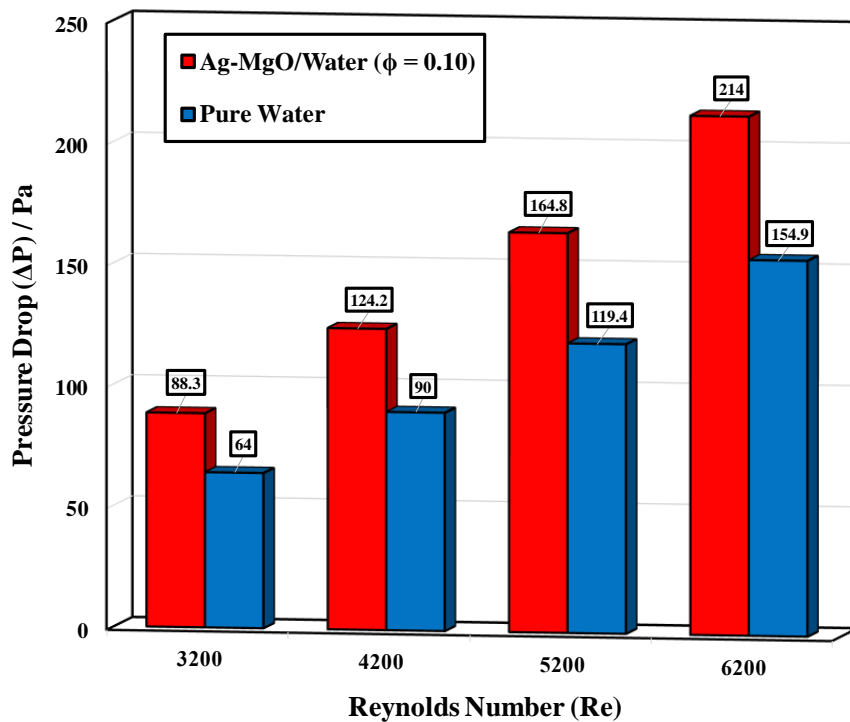
Figure 2-19: Pressure drop when using Ag-MgO/Water hybrid nanofluid with different Reynolds numbers at ϕ = 0.10.

As explained earlier, the COP improvement factor includes both the ratios of friction factor (or pressure drop) and average Nusselt number so that higher COP improvement (more than unity; $\eta > 1$) indicates that the selected working fluid is efficient in terms of pressure drop and heat transfer. COP improvement using Ag-MgO/water hybrid nanofluid ($\phi = 0.10$) with different Reynolds numbers is depicted in Figure 2-20. According to the figure, Ag-MgO/water hybrid nanofluid ($\phi = 0.10$) at each value of Reynolds number has lower COP improvement than unity which means that studied cases are not economically viable because of having more pressure drop (or friction factor) than heat transfer improvement. Accordingly, it can be concluded that the

36

COP improvement of the studied cases with various Reynolds numbers including Re = 3200, 4200, 5200, and 6200 is lower than pure water by 28.82%, 35.62%, 38.39%, and 39.1%, respectively. The maximum COP improvement is achieved by the case with Ag-MgO/water hybrid nanofluid (ϕ = 0.10) at Re = 3200. Figure 2-21 shows 2D contours of the temperature (top view at Z = 0) at different operating hours using Ag-MgO/water hybrid nanofluid at ϕ = 0.10 and Re = 3200. As time passes, the heat transfer from the working fluid to the other regions increases, leading to the better heat exchange of the BHE.
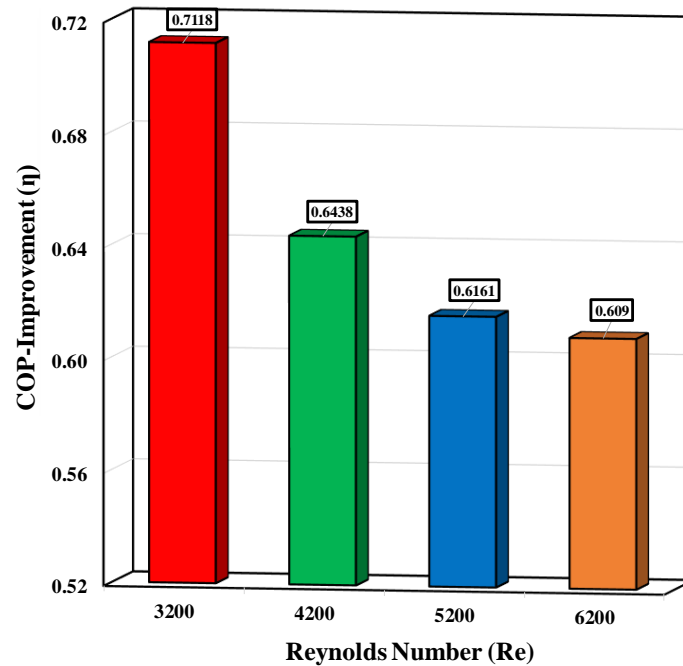
Figure 2-20: COP improvement when using Ag-MgO/water hybrid nanofluid with different Reynolds numbers at ϕ = 0.10.
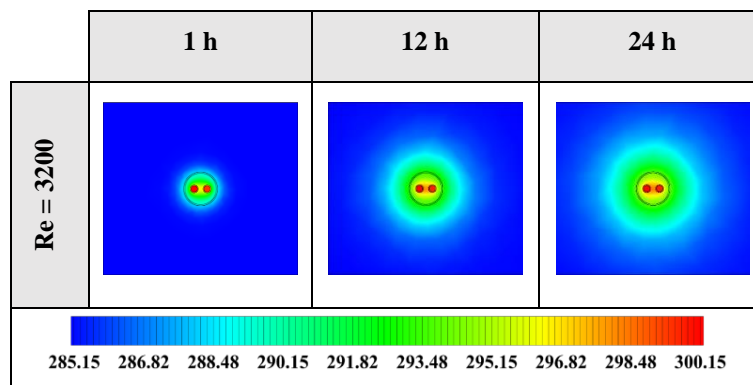
Figure 2-21: Two-dimensional (2D) contours of the temperature distribution of the BHE at various hours of operating using Ag–MgO/water hybrid nanofluid at Re = 3200 and ϕ = 0.10 (Top view at Z = 0).

Using hybrid nanofluids instead of traditional fluids may decrease the size and cost of equipment required in the system. However, some types of hybrid nanofluids preparation techniques cost a lot. The hybrid nanofluids can be synthesized mainly by one-step or two-step methods. In the one-step process, the nanoparticles' preparation and dispersion in the base fluid are parallel. The most important advantage of this technique is the reduction of the possibility of agglomeration of nanoparticles. However, it is difficult to cover

it up for manufacturing purposes on a mass scale for the higher cost, which restricts the implementation of this method [36,58–60].

The two-step technique is initiated by preparing the nanoparticles and then dispersing them in an appropriate liquid. In this technique, nanoparticles' high surface energy leads to aggregation and eventually sedimentation of nanoparticles which deteriorates hybrid nanofluid stability. The two-step approach is used for mass scale processing due to the effortlessness and relatively low cost. Among these two techniques, the two-step method is widely used by researchers and also industrialists [36,58–60].

2.6 Conclusions

A three-dimensional unsteady state numerical model of a single U-tube borehole heat exchanger was investigated by Ansys Fluent commercial software in this study. Four types of hybrid nanofluid, such as Ag-MgO/water, TiO_2-Cu/water, Al_2O_3-CuO/water, and Fe_3O_4-MWCNT/water, were examined numerically to be used as working fluid in a single U-tube borehole heat exchanger. The selected hybrid nanofluid was evaluated at various values of volume fractions and Reynolds numbers.

After comparing the hybrid nanofluids at $\phi = 0.15$ and Re = 3200, Ag-MgO/water hybrid nanofluid was chosen as the most favorable working fluid, considering its superior effectiveness, minor pressure drop, and appropriate thermal resistance amongst studied hybrid nanofluids compared to the pure water.

Hence, the effect of various volume fractions of Ag-MgO/water hybrid nanofluid at Re = 3200 was studied. All cases of Ag-MgO/water hybrid nanofluid with volume fractions of 0.05, 0.10, 0.15, and 0.20 have been able to achieve better effectiveness and lower thermal resistances than pure water except for the pressure drops, which were higher than pure water. Because of this balance between thermal resistance, pressure drop, and effectiveness, Ag-MgO/water hybrid nanofluid at $\phi = 0.10$ is selected as the best working fluid for further studies.

Finally, the influence of different Reynolds numbers of Ag-MgO/water hybrid nanofluid with the volume fraction fixed at $\phi = 0.10$ is analyzed. Ag-MgO/water hybrid nanofluids with Reynolds numbers of 3200, 4200, 5200, and 6200 showed greater effectiveness and lower thermal resistance than the corresponding cases of pure water, while their pressure drops were higher than pure water.

In summary, the effectiveness of a single U-tube borehole heat exchanger can be enhanced by 37.02% when applying the Ag-MgO/water hybrid nanofluid (at $\phi = 0.10$ and Re = 3200) instead of the corresponding case of pure water. Also, the single U-tube borehole heat exchanger's thermal resistance can be decreased by 1.14% when Ag-MgO/water hybrid nanofluid (at $\phi = 0.10$ and Re = 3200) is used instead of the corresponding case of pure water as a heat carrier fluid. Therefore, based on a comparison made, it can be concluded that Ag-MgO/water hybrid nanofluid at a volume fraction of 0.10 and Reynolds number of 3200 is found to be the best working fluid in improving the thermal performance of the single U-tube borehole heat exchanger. Nevertheless, all the studied hybrid nanofluids show lower COP improvement than unity, indicating that using them as working fluid is not economically viable as they cause higher pressure drop than the heat transfer enhancement.

However, it is believed that further investigations such as conducting sensitivity analysis on the present numerical results and performing a numerical simulation of an actual model should be done as this is a new research line in the ground-source heat pump systems.

References

1. Tsagarakis, K.P.; Efthymiou, L.; Michopoulos, A.; Mavragani, A.; Anđelković, A.S.; Antolini, F.; Bacic, M.; Bajare, D.; Baralis, M.; Bogusz, W.; et al. A review of the legal framework in shallow geothermal energy in selected European countries: Need for guidelines. *Renew. Energy* 2020, *147*, 2556–2571.
2. Javadi, H.; Ajarostaghi, S.S.M.; Rosen, M.A.; Pourfallah, M. Performance of ground heat exchangers: A comprehensive review of recent advances. *Energy* 2019, *178*, 207–233.
3. Philippe, M.; Bernier, M.; Marchio, D. Vertical geothermal borefields. *Ashrae J.* 2010, *52*, 20–27.
4. Fossa, M.; Rolando, D. Improving the Ashrae method for vertical geothermal borefield design. *Energy Build.* 2015, *93*, 315–323.
5. Cullin, J.R.; Spitler, J.D.; Montagud, C.; Ruiz-Calvo, F.; Rees, S.J.; Naicker, S.S.; Konečný, P.; Southard, L.E. Validation of vertical ground heat exchanger design methodologies. *Sci. Technol. Built Environ.* 2015, *21*, 137–149.
6. Rolando, D.; José, A.; Marco, F. A web application for geothermal borefield design. In Proceedings of the World Geothermal Congress, Melbourne, Australia, 19–25 April 2015.
7. Spitler, J.D.; Bernier, M. Vertical borehole ground heat exchanger design methods. In *Advances in Ground-Source Heat Pump Systems*; Woodhead Publishing: Cambridge, UK, 2016; pp. 29–61.
8. Fossa, M.; Rolando, D. Improved Ashrae method for BHE field design at 10 year horizon. *Energy Build.* 2016, *116*, 114–121.
9. Staiti, M.; Angelotti, A. Design of Borehole Heat Exchangers for Ground Source Heat Pumps: A Comparison between Two Methods. *Energy Procedia* 2015, *78*, 1147–1152.
10. Fossa, M.; Davide, R.; Antonella, P. Investigation on the effects of different time resolutions in the design and simulation of BHE fields. In Proceedings of the IGSHPA Technical/Research Conference and Expo, Denver, CO, USA, 14–16 March 2017.
11. Capozza, A.; De Carli, M.; Zarrella, A. Design of borehole heat exchangers for ground-source heat pumps: A literature review, methodology comparison and analysis on the penalty temperature. *Energy Build.* 2012, *55*, 369–379.
12. Fossa, M. Correct design of vertical borehole heat exchanger systems through the improvement of the ASHRAE method. *Sci. Technol. Built Environ.* 2017, *23*, 1080–1089.
13. Ahmadfard, M.; Michel, B. Modifications to ASHRAE's sizing method for vertical ground heat exchangers. *Sci. Technol. Built Environ.* 2018, *24*, 803–817.
14. Fossa, M. The temperature penalty approach to the design of borehole heat exchangers for heat pump applications. *Energy Build.* 2011, *43*, 1473–1479.
15. Badenes, B.; Burkhard, S.; Pla, M.Á.M.; Cuevas, J.M.; Bartoli, F.; Ciardelli, F.; González, R.M.; Ghafar, A.N.; Fontana, P.; Zuñiga, L.L.; et al. Development of advanced materials guided by numerical simulations to improve performance and cost-efficiency of borehole heat exchangers (BHEs). *Energy* 2020, *201*, 117628.
16. Garbin, E.; Ludovico, M.; Eloisa, D.S.; Gilberto, A.; Javier, F.U.; Dimitris, M.; David, B.; Jacques, V.; Riccardo, P.; Adriana, B.; et al. Assessing Grouting Mix Thermo-Physical Properties for Shallow Geothermal Systems. In Proceedings of the 22nd EGU General Assembly Conference, Online, 4–8 May 2020.
17. Javadi, H.; Ajarostaghi, S.S.M.; Rosen, M.A.; Pourfallah, M. A Comprehensive Review of Backfill Materials and Their Effects on Ground Heat Exchanger Performance. *Sustainability* 2018, *10*, 4486.

18. Javadi, H.; Ajarostaghi, S.S.M.; Pourfallah, M.; Zaboli, M. Performance analysis of helical ground heat exchangers with different configurations. *Appl. Therm. Eng.* 2019, *154*, 24–36.

19. Javadi, H.; Ajarostaghi, S.S.M.; Mousavi, S.S.; Pourfallah, M. Thermal analysis of a triple helix ground heat exchanger using numerical simulation and multiple linear regression. *Geothermics* 2019, *81*, 53–73.

20. Javadi, H.; Urchueguia, J.F.; Ajarostaghi, S.S.M.; Badenes, B. Numerical Study on the Thermal Performance of a Single U-Tube Borehole Heat Exchanger Using Nano-Enhanced Phase Change Materials. *Energies* 2020, *13*, 5156.

21. Bobbo, S.; Laura, C.; Antonella, B.; Stefano, R.; Laura, F. Characterization of nanofluids formed by fumed Al2O3 in water for geothermal applications. In Proceedings of the 16th International Refrigeration and Air Conditioning Conference, West Lafayette, IN, USA, 11–14 July 2016.

22. Narei, H.; Ghasempour, R.; Noorollahi, Y. The effect of employing nanofluid on reducing the bore length of a vertical ground-source heat pump. *Energy Convers. Manag.* 2016, *123*, 581–591.

23. Daneshipour, M.; Rafee, R. Nanofluids as the circuit fluids of the geothermal borehole heat exchangers. *Int. Commun. Heat Mass Transf.* 2017, *81*, 34–41.

24. Sui, D.; Langåker, V.H.; Yu, Z. Investigation of thermophysical properties of Nanofluids for application in geothermal energy. *Energy Procedia* 2017, *105*, 5055–5060.

25. Diglio, G.; Roselli, C.; Sasso, M.; Channabasappa, U.J. Borehole heat exchanger with nanofluids as heat carrier. *Geothermics* 2018, *72*, 112–123.

26. Sun, X.-H.; Yan, H.; Massoudi, M.; Chen, Z.-H.; Wu, W.-T. Numerical Simulation of Nanofluid Suspensions in a Geothermal Heat Exchanger. *Energies* 2018, *11*, 919.

27. Peng, Y.; Yong, W.; Ruiqing, D. The effect of nanofluid to vertical single U-tube ground heat exchanger. In Proceedings of the 4th Building Simulation and Optimization Conference, Cambridge, UK, 11–12 September 2018.

28. Mishra, S.; Sikata, S.; Das, D.K. Theoretical analysis on application of nanofluids in ground source heat pumps for building cooling. *Int. J. Recent Technol. Mech. Electr. Eng.* 2018, *5*, 28–37.

29. Du, R.; Jiang, D.; Wang, Y.; Shah, K.W. An experimental investigation of CuO/water nanofluid heat transfer in geothermal heat exchanger. *Energy Build.* 2020, *227*, 110402.

30. Du, R.; Jiang, D.; Wang, Y. Numerical Investigation of the Effect of Nanoparticle Diameter and Sphericity on the Thermal Performance of Geothermal Heat Exchanger Using Nanofluid as Heat Transfer Fluid. *Energies* 2020, *13*, 1653.

31. Sarkar, J.; Ghosh, P.; Adil, A. A review on hybrid nanofluids: Recent research, development and applications. *Renew. Sustain. Energy Rev.* 2015, *43*, 164–177.

32. Leong, K.; Ahmad, K.K.; Ong, H.C.; Ghazali, M.; Baharum, A. Synthesis and thermal conductivity characteristic of hybrid nanofluids-A review. *Renew. Sustain. Energy Rev.* 2017, *75*, 868–878.

33. Hamzah, M.H.; Sidik, N.A.C.; Ken, T.L.; Mamat, R.; Najafi, G. Factors affecting the performance of hybrid nanofluids: A comprehensive review. *Int. J. Heat Mass Transf.* 2017, *115*, 630–646.

34. Minea, A.A. Challenges in hybrid nanofluids behavior in turbulent flow: Recent research and numerical comparison. *Renew. Sustain. Energy Rev.* 2017, *71*, 426–434.

35. Gupta, M.; Singh, V.; Kumar, S.; Kumar, S.; Dilbaghi, N.; Said, Z. Up to date review on the synthesis and thermophysical properties of hybrid nanofluids. *J. Clean. Prod.* 2018, *190*, 169–192.

36. Sajid, M.U.; Hafiz, M.A. Thermal conductivity of hybrid nanofluids: A critical review. *Int. J. Heat Mass Transf.* 2018, *126*, 211–234.

37. Kumar, D.D.; Arasu, A.V. A comprehensive review of preparation, characterization, properties and stability of hybrid nanofluids. *Renew. Sustain. Energy Rev.* 2018, *81*, 1669–1689.

38. Suresh, S.; Venkitaraj, K.P.; Selvakumar, P.; Chandrasekar, M. Effect of Al2O3–Cu/water hybrid nanofluid in heat transfer. *Exp. Therm. Fluid Sci.* 2012, *38*, 54–60.

39. Labib, M.N.; Nine, J.; Afrianto, H.; Chung, H.; Jeong, H. Numerical investigation on effect of base fluids and hybrid nanofluid in forced convective heat transfer. *Int. J. Therm. Sci.* 2013, *71*, 163–171.

40. Takabi, B.; Salehi, S. Augmentation of the Heat Transfer Performance of a Sinusoidal Corrugated Enclosure by Employing Hybrid Nanofluid. *Adv. Mech. Eng.* 2014, *6*, 147059.

41. Sundar, L.S.; Singh, M.K.; Sousa, A.C. Enhanced heat transfer and friction factor of MWCNT–Fe3O4/water hybrid nanofluids. *Int. Commun. Heat Mass Transf.* 2014, *52*, 73–83.

42. Madhesh, D.; Parameshwaran, R.; Kalaiselvam, S. Experimental investigation on convective heat transfer and rheological characteristics of Cu–TiO2 hybrid nanofluids. *Exp. Therm. Fluid Sci.* 2014, *52*, 104–115.

43. Yarmand, H.; Gharehkhani, S.; Ahmadi, G.; Shirazi, S.F.S.; Baradaran, S.; Montazer, E.; Zubir, M.N.M.; Alehashem, M.S.; Kazi, S.; Dahari, M. Graphene nanoplatelets–Silver hybrid nanofluids for enhanced heat transfer. *Energy Convers. Manag.* 2015, *100*, 419–428.

44. Esfe, M.H.; Arani, A.A.A.; Rezaie, M.; Yan, W.M.; Karimipour, A. Experimental determination of thermal conductivity and dynamic viscosity of Ag–MgO/water hybrid nanofluid. *Int. Commun. Heat Mass Transf.* 2015, *66*, 189–195.

45. Toghraie, D.; Chaharsoghi, V.A.; Afrand, M. Measurement of thermal conductivity of ZnO–TiO2/EG hybrid nanofluid. *J. Therm. Anal. Calorim.* 2016, *125*, 527–535.

46. Van Trinh, P.; Anh, N.N.; Thang, B.H.; Hong, N.T.; Hong, N.M.; Khoi, P.H.; Minh, P.N.; Hong, P.N. Enhanced thermal conductivity of nanofluid-based ethylene glycol containing Cu nanoparticles decorated on a Gr–MWCNT hybrid material. *R. Soc. Chem. Adv.* 2017, *6*, 318–326.

47. Sundar, L.S.; Singh, M.K.; Ferro, M.; Sousa, A.C. Experimental investigation of the thermal transport properties of graphene oxide/Co 3 O 4 hybrid nanofluids. *Int. Commun. Heat Mass Transf.* 2017, *84*, 1–10.

48. Sahoo, R.R.; Sarkar, J. Heat transfer performance characteristics of hybrid nanofluids as coolant in louvered fin automotive radiator. *Heat Mass Transf.* 2016, *53*, 1923–1931.

49. Ajarostaghi, S.S.M.; Zaboli, M.; Nourbakhsh, M. Numerical evaluation of turbulence heat transfer and fluid flow of hybrid nanofluids in a pipe with innovative vortex generator. *J. Therm. Anal. Calorim.* 2020, *143*, 1–15.

50. Karouei, S.H.H.; Ajarostaghi, S.S.M.; Gorji-Bandpy, M.; Fard, S.R.H. Laminar heat transfer and fluid flow of two various hybrid nanofluids in a helical double-pipe heat exchanger equipped with an innovative curved conical turbulator. *J. Therm. Anal. Calorim.* 2021, *143*, 1455–1466.

51. Ajarostaghi, S.S.M.; Shirzad, M.; Rashidi, S.; Li, L.K.B. Heat transfer performance of a nanofluid-filled tube with wall corrugations and center-cleared twisted-tape inserts. *Energy Sources, Part A Recover. Util. Environ. Eff.* 2020, 1–21.

52. Hamedani, F.A.; Ajarostaghi, S.S.M.; Hosseini, S.A. Numerical evaluation of the effect of geometrical and operational parameters on thermal performance of nanofluid flow in convergent–divergent tube. *J. Therm. Anal. Calorim.* 2020, *140*, 1483–1505.

53. Noorbakhsh, M.; Ajarostaghi, S.S.M.; Zaboli, M.; Kiani, B. Thermal analysis of nanofluids flow in a double pipe heat exchanger with twisted tapes insert in both sides. *J. Therm. Anal. Calorim.* 2021, 1–12. https://doi.org/10.1007/s10973-021-10738-x

54. Khodadadi, J.M.; Fan, L. Expedited freezing of nanoparticle-enhanced phase change materials (NEPCM) exhibited through a simple 1-D stefan problem formulation. In Proceedings of the Heat Transfer Summer Conference, San Francisco, CA, USA, 19–23 July 2009.
55. Hassan, M.; Marin, M.; Ellahi, R.; Alamri. S.Z. Exploration of convective heat transfer and flow characteristics synthesis by Cu–Ag/water hybrid-nanofluids. *Heat Transf. Res*. 2018, *49*, 1837–1848.
56. Jalaluddin; Miyara, A. Thermal performance and pressure drop of spiral-tube ground heat exchangers for ground-source heat pump. *Appl. Therm. Eng.* 2015, *90*, 630–637.
57. Jalaluddin; Miyara, A.; Tsubaki, K.; Inoue, S.; Yoshida, K. Experimental study of several types of ground heat exchanger using a steel pile foundation. *Renew. Energy* 2011, *36*, 764–771.
58. Kadirgama, K.; Anamalai, K.; Ramachandran, K.; Ramasamy, D.; Samykano, M.; Kottasamy, A.; Rahman, M.M. Thermal analysis of SUS 304 stainless steel using ethylene glycol/nanocellulose-based nanofluid coolant. *Int. J. Adv. Manuf. Technol.* 2018, *97*, 2061–2076.
59. Safiei, W.; Rahman, M.M.; Yusoff, A.R.; Radin, M.R. Preparation, stability and wettability of nanofluid: A review. *J. Mech. Eng. Sci.* 2020, *14*, 7244–7257.
60. Urmi, W.T.; Shafiqah, A.; Rahman, M.; Kadirgama, K.; Maleque, A. Preparation Methods and Challenges of Hybrid Nanofluids: A Review. *J. Adv. Res. Fluid Mech. Therm. Sci.* 2020, *78*, 56–66.

Chapter 3

3 Impact of a novel backfill material on a borehole heat exchanger

Numerical Study on the Thermal Performance of a Single U-Tube Borehole Heat Exchanger Using Nano-Enhanced Phase Change Materials

Hossein Javadi [1,*], Javier F. Urchueguia [1], Seyed Soheil Mousavi Ajarostaghi [2] and Borja Badenes [1]

[1] Information and Communication Technologies vs. Climate Change Group, Institute for Information and Communication Technologies, Universitat Politècnica de València, Camino de Vera S/N, 46022 Valencia, Spain; jfurchueguia@fis.upv.es (J.F.U.); borbaba@upv.es (B.B.)

[2] Faculty of Mechanical Engineering, Babol Noshirvani University of Technology, Babol 47148-71167, Iran; s.s.mousavi@stu.nit.ac.ir

[*] Correspondence: hjavadi@doctor.upv.es; Tel.: +98-937-818-5556

Abstract: To investigate the impacts of using nano-enhanced phase change materials on the thermal performance of a borehole heat exchanger in the summer season, a three-dimensional numerical model of a borehole heat exchanger is created in the present work. Seven nanoparticles including Cu, CuO, Al_2O_3, TiO_2, SiO_2, multi-wall carbon nanotube, and graphene are added to the Paraffin. Considering the highest melting rate and lowest outlet temperature, the selected nano-enhanced phase change material is evaluated in terms of volume fraction (0.05, 0.10, 0.15, 0.20) and then the shape (sphere, brick, cylinder, platelet, blade) of its nanoparticles. Based on the results, the Paraffin containing Cu and SiO_2 nanoparticles are found to be the best and worst ones in thermal performance improvement, respectively. Moreover, it is indicated that the increase in the volume fraction of Cu nanoparticles could enhance markedly the melting rate, being 0.20 the most favorable value which increased up to 55% the thermal conductivity of the nano-enhanced phase change material compared to the pure phase change material. Furthermore, the blade shape is by far the most appropriate shape of the Cu nanoparticles by considering about 85% melting of the nano-enhanced phase change material.

Javadi H, Urchueguia Scholzel JF, Ajarostaghi SSM, Badenes B. Numerical study on the thermal performance of a single U-tube borehole heat exchanger using nano-enhanced phase change materials. Energies. Impact Factor: 3.252, Nivel R2.

3.1 Introduction

Presently, due to extreme environmental pollution and energy shortage around the world, the exploitation of renewable energies has become more vital. Geothermal energy is one of the renewable energies that can be used, specifically by means of coupling to ground source heat pump (GSHP) systems. GSHP system provides heating and cooling of buildings through the ground heat exchanger (GHE) which usually appears in horizontal and vertical configurations. Since the vertical GHE, also named borehole heat exchanger (BHE), needs less land for installation and has wide applicability and better performance than the horizontal GHE, it has been comprehensively investigated in recent years [1].

To improve the thermal performance of the BHEs, various approaches have been taken such as geometry improvements [2,3], the use of new materials for pipe, backfill or grout, and working fluid [1,4]. Quaggiotto et al. [5] studied two types of BHEs including coaxial BHE and double U-tube BHE. Based on the comparison made, heat transfer in the coaxial BHE was higher than the double U-tube BHE both in cooling and heating operating modes. Serageldin et al. [6] investigated experimentally and numerically the use of oval cross-section pipes instead of the circular cross-section pipes used in the BHE in the presence of underground water. It was concluded that a BHE with oval cross-section pipes has the potential to decrease the installation costs and increase the thermal performance of the BHE. In a thermal response test (TRT) conducted by Sapinska-Sliwa et al. [7] for three types of BHEs, for instance, single U-tube, double U-tube, and coaxial BHE, the last configuration was found to be the best one in achieving the effective thermal conductivity of the ground. In another study, carried out experimentally and numerically by Janiszewski et al. [8], a single U-tube BHE was used to inject thermal energy into the surroundings. It was proven that a higher thermal conductivity of the pipe and backfill as well as a larger pipe distancing and pipe radius are essential for improving the borehole thermal energy storage (BTES) system efficiency. A review article concerning a variety of nanofluids that can be applied as working fluids in the BHE was conducted by Patil et al. [9]. It was concluded that nanofluids can enhance the thermal performance of the BHE when it operates at higher temperatures, as the higher the temperature the better the thermal conductivity of nanofluids. In an experimental study done by Cao et al. [10], it was shown that a BHE with a steel pipe can have superior thermal performance and lower thermal resistance compared to a BHE with a polyethylene pipe. Li et al. [11] evaluated experimentally single U-tube and double U-tube BHEs at different depths and concluded that increasing the depth of the pipe results in greater thermal performance of BHEs in both summer and winter seasons.

One type of the backfill materials that is applied in the BHE is phase change material (PCM). The PCMs are generally categorized into organic, inorganic, hygroscopic, and solid-solid materials. The organic PCMs such as Paraffin have been widely used in the BTES systems to provide energy for the heat pumps because of their high TES capacity. In addition, organic PCMs are found to be beneficial for GSHP applications. To use such materials as backfill and to improve the thermal performance of the BHEs, their low thermal conductivity must increase, as the higher the thermal conductivity of the backfill the superior the heat transfer from the working fluid to the surrounding ground. Hence, a variety of methods are carried out to tackle this problem [4]. Wang et al. [12] studied numerically the use of a mixture of lauric acid and n-decanoic acid as backfill in a single U-tube BHE. The results showed that the thermal interference radius and the temperature difference between inlet and outlet could decrease and increase by 26% and 67% respectively, compared to the soil as backfill. Lei and Dai [13] investigated theoretically the influence of using a mixture of lauric acid and capric acid as a backfill on the thermal performance of a coaxial BHE. The results indicated that the differences between the inlet and outlet temperatures of the working fluid are 0.24 ℃ when using soil backfill and 0.08 ℃ for the PCM backfill at the end of the cooling operation. A numerical study on applying shape-stabilized PCM

(SSPCM), a mixture of lauric acid and decanoic acid, as backfill in a single U-tube BHE was carried out by Li et al. [14,15]. Based on their results, the heat exchange rate and thermal interference radius for the BHE backfilled with SSPCM could be 1.37 and 0.9 times of that for crushed stone concrete as a backfill. The effects of three types of PCM backfill including acid, enhanced acid, and Paraffin RT27 on the thermal performance of a single U-tube BHE is evaluated numerically by Qi et al. [16]. The results demonstrated that PCM backfills have a smaller thermal interference radius than soil backfill. A numerical investigation of using SSPCM and microencapsulated Paraffin as backfill in a single U-tube BHE was conducted by Chen et al. [17]. It was concluded that SSPCM improves the thermal performance of the BHE compared to microencapsulated Paraffin, thanks to its higher thermal conductivity. It was also found that the use of the SSPCM backfill is beneficial where the effect of underground water is negligible. Besides, Chen et al. [18] examined the impact of different melting temperatures of PCM backfill on the BHE thermal performance and selected 20.4 °C as the best melting temperature which led to improving the cooling operation of the system. A study on the thermal performance of a single U-tube BHE when it is backfilled with salt hydrate PCM was done by Zhang et al. [19]. The numerical results showed that when the PCM was used as a backfill in the BHE, the temperature differences of the working fluid at the inlet and outlet after 6 h of cooling operation increased compared to the corresponding temperature differences in the BHE containing a conventional backfill which led to enhancing the heat transfer rate and system efficiency in the summer. Yang et al. [20] studied both numerically and experimentally the use of a mixture of lauric acid and decyl acid for cooling operating and oleic acid for heating operating as backfill material in a single U-tube BHE. According to the results, PCM backfills reduce almost 88% and 86% of the thermal interference radius for heating operating and cooling operating compared to soil backfill, respectively. An increase of 28% and 9.4% are found in the heat exchange rate per meter of borehole depth for heating and cooling operating, respectively, when using PCM backfills instead of soil backfill.

Please note that there have been also a few articles regarding the use of PCM (microencapsulated PCM) as backfill in the Horizontal GHE [21–23]. Moreover, PCM has had other applications in GSHP systems. Zhang et al. [19] presented a new type of BHE named underground thermal battery in which both BHE and PCM (forming a ring inside the borehole) were immersed in a water tank. In a theoretical study of Rabin and Korin [24], Paraffin was used in the form of a ring as TES inside/outside the borehole. Benli and Durmus [25,26] experimentally investigated the integration of a Horizontal GHE with a TES system containing salt hydrate PCM for heating of a greenhouse. A mixture of microencapsulated Paraffin and soil was examined as TES combined with a Horizontal GHE both experimentally and numerically [27]. Eslami-Nejad and Bernier [28] evaluated numerically the use of a PCM-sand mixture as a ring inside the borehole. In a numerical investigation conducted by Zhu et al. [29], hydrate sodium sulfate was applied as TES which was integrated with a BHE. Jeon et al. [30] studied numerically the incorporation of a panel form of PCM as TES with a Horizontal GHE. In a numerical study carried out by Alkhwildi et al. [31], a BHE combined with a TES system containing salt hydrate PCM. The application of microencapsulated PCM slurry as a working fluid in a tree-shaped BHE was evaluated numerically by Pu et al. [32].

Furthermore, there is another type of PCM called nano-enhanced PCM (NEPCM) that is created by dispersing the nanoparticle into a pure PCM. Khodadadi and Hosseinizadeh [33] were the first scholars who investigated the addition of nanoparticles into PCM and proved that the created NEPCM has better thermal conductivity and higher TES capacity than the conventional PCMs. NEPCM has brought many benefits to buildings [34], heat exchangers [35], TES [36], solar systems [37], and electronic devices [38]. Kalaiselvam et al. [34] dispersed experimentally Al_2O_3 and Al nanoparticles to a PCM comprised of n-hexadecane and n-tetradecane which were applied in an advanced building for cooling operation. Their results indicated 4.97% and 12.97% reductions in the solidification time when using Al and Al2O3 nanoparticles, respectively, in

46

comparison with the pure PCM. The impact of adding CuO nanoparticles to RT50 PCM placed inside a shell and tube heat exchanger was carried out numerically by Pahamli et al. [35]. It was concluded that the melting time decreases by 11.6% and 4.56% provided that the volume fractions of the nanoparticles are 4% and 2%, respectively, resulting in superior thermal performance of the heat exchanger. Ramakrishnan et al. [36] added experimentally graphene nanoparticles to a PCM consisted of expanded perlite and RT27 which were used as TES. According to the results, both melting and solidification time decrease by 33% compared to the pure PCM, due to an increase of 49% in the thermal conductivity of the PCM when applying graphene with 1% by weight. An experimental investigation of adding graphene oxide, TiO_2, and CuO nanoparticles to the Paraffin used in a solar still was conducted by Rufuss et al. [37]. The results showed the increments of 101%, 25%, and 29% in the thermal conductivity of the PCM at the presence of graphene oxide, TiO_2, and CuO nanoparticles, respectively, which led to the higher production of freshwater. In another study, the use of NEPCM made of Paraffin wax as PCM and multi-wall carbon nanotube (MWCNT) as nanoparticles in an electronic chipset was examined experimentally by Farzanehnia et al. [38]. The studied NEPCM was found to extend the time of electronic board operation and decrease the time of the cooling process by 6%.

However, based on the previous works concerning NEPCMs [39–41] and to the best of the authors' knowledge, to this day, no scholar has studied the application of NEPCMs as backfill in the BHE which indicates the significance of this study. Therefore, the novelty of the present article is the numerical simulation of NEPCMs in a single U-tube BHE. Accordingly, in the first section of the present study, seven types of NEPCMs are considered and numerical results are compared. Afterward, the selected NEPCM (from the first section) is evaluated in terms of volume fraction and shape of its nanoparticles.

3.2   Computational fluid dynamics model and simulation conditions

In this work, an unsteady 3D model of a BHE is simulated numerically by ANSYS Fluent 18.2 software (see Figure 3-1). The BHE comprises a single U-tube (copper tube), working fluid (water), backfill (NEPCM), and the surrounding ground. The whole domain is considered to be a cube with a side length of 1.2 m while the length of the U-tube is 1.1 m. The borehole depth and borehole diameter are 1.2 m and 0.06 m, respectively. The distance between centers of two legs of U-tube is 0.0365 m and the outer and inner diameters of U-tube are 0.0065 m and 0.005 m, respectively. The thermo-physical properties of the BHE components are shown in Table 3-1 and Table 3-2. Based on a review article conducted by Yang et al. [39], mostly dispersed nanoparticles into the PCMs, such as Cu, CuO, Al_2O_3, TiO_2, SiO_2, MWCNT, and graphene, are used as nanoparticles in this study to be added to the Paraffin (n-Octadecane) as the base fluid.

As illustrated in Figure 3-2, the meshing of the model is provided with high accuracy, especially in the regions near the center of the model as in view of their great influence in the performance of the BHE. Table 3-3 indicates the grid independence test performed by analyzing four different numbers of elements in terms of outlet temperature of working fluid and liquid fraction after 10 h of BHE operation. Taking into account the balance between precision and calculation speed, a total number of 2,244,671 elements with maximum skewness of 0.79 and minimum orthogonal quality of 0.25 is selected for the numerical simulations. We have applied structured meshing methods for the fluid and the U-tube, and unstructured methods for the backfill and the ground. The BHE works in the summer season for 12 h daily and the inlet temperature of working fluid is considered to be 308.15 K. At the inlet of the model (see Figure 3-1b), we used a Velocity Inlet boundary condition with a constant value of 0.6 m/s and at the outlet, a Pressure Outlet boundary condition is chosen which can minimize the reverse flows when a backflow condition occurs. The interfaces between the regions are supposed to be temperature-coupled walls and the BHE components are homogeneous, isotropic, and temperature independent. Since the heat transfer fluid inside U-tube is in turbulent regime, we

47

implemented the standard k-epsilon as a turbulence model and the SIMPLE scheme for the velocity-pressure condition. The energy and momentum equations that are discretized spatially by Second-Order Upwind have the Under Relaxation Factors of 1 and 0.7, respectively. The numerical simulation converged once the residuals for momentum, continuity, k, and epsilon were less than 10^{-3} while the corresponding value for energy was 10^{-6} (see Table 3-4).

(**a**)

(**b**)
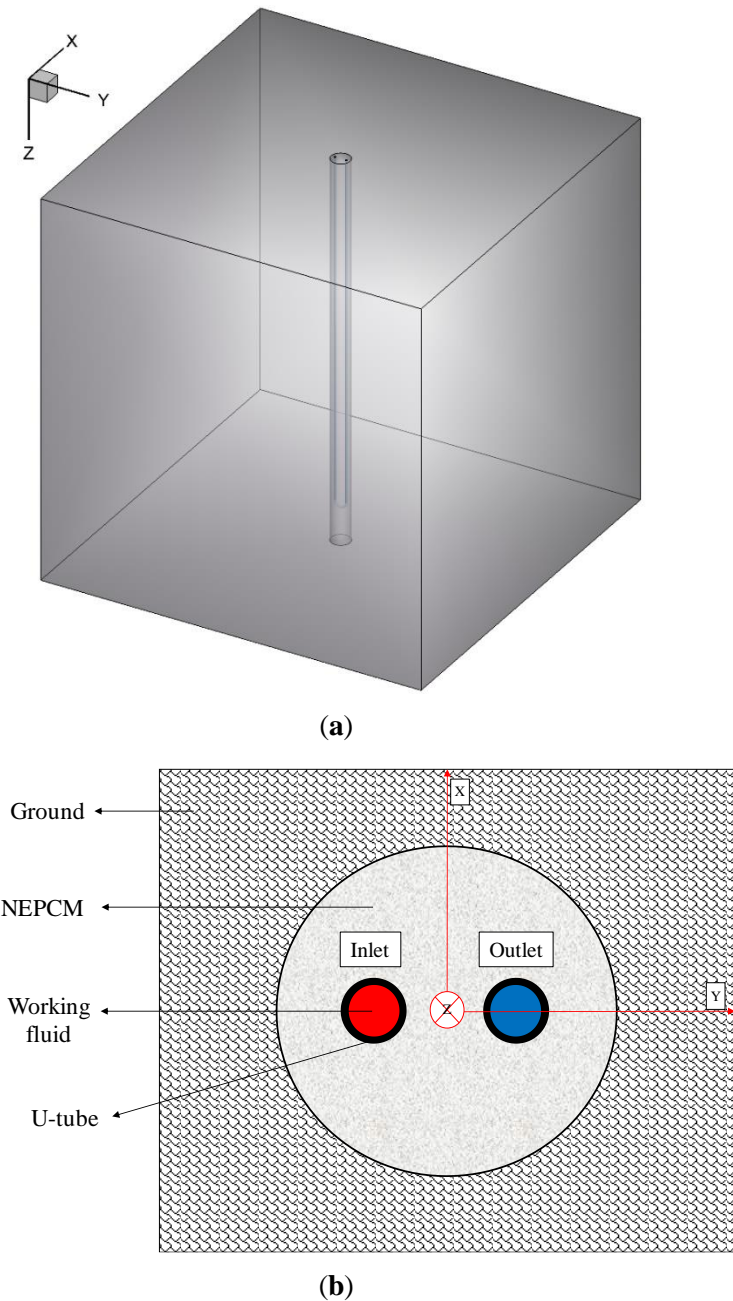
Figure 3-1: Schematic of the studied BHE: (a) 3D view, and (b) 2D view (Ground surface).

(a)   **(b)**
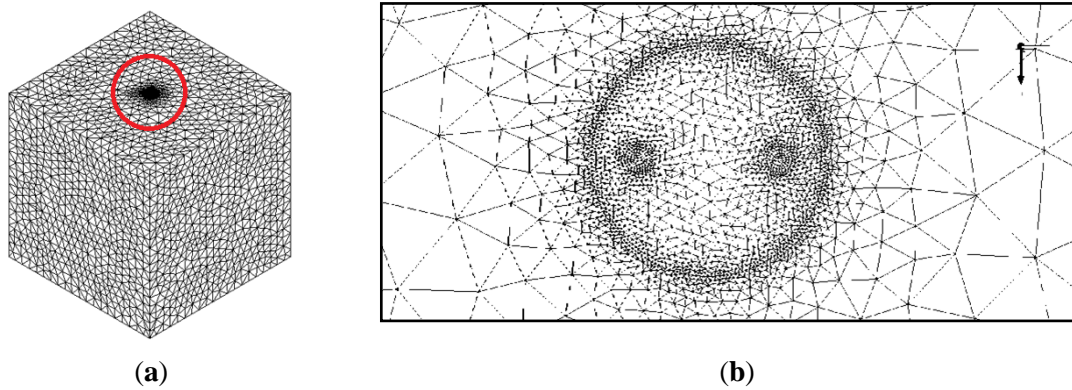
Figure 3-2: The meshing of the studied BHE: (a) 3D view, and (b) 2D view (Ground surface).

Table 3-1: Thermo-physical properties of working fluid, pipe, and ground.

Property	Working Fluid	Pipe	Ground
ρ [kg/m^3]	998.2	8978	1600
C_p [J/(kg·K)]	4182	381	1640
k [W/(m·K)]	0.6	387.6	0.69
μ [Pa·s]	0.001003	-	-

Table 3-2: Thermo-physical properties of different types of NEPCM as backfill.

Property	PCM Paraffin (n-Octadecane) [42]	Nanoparticles						
		Cu [43]	CuO [43]	Al$_2$O$_3$ [43]	TiO$_2$ [43]	SiO$_2$ [44]	MWCNT [45]	Graphene [46]
ρ [kg/m^3]	770	8933	6510	3880	4175	2200	1600	2200
C_p [J/(kg·K)]	2196	385	540	792	692	775	796	790.1
k [W/(m·K)]	0.148	401	18	42.34	8.4	1.38	3000	5000
L [J/kg]	243500	-	-	-	-	-	-	-
μ [Pa·s]	0.00385	-	-	-	-	-	-	-
T_m [K]	301.15	-	-	-	-	-	-	-

Table 3-3: Grid independence test.

Elements Numbers	571,924	1,328,873	2,244,671	3,476,561
Outlet temperature of working fluid [K]	307.41	307.55	307.63	307.60
Liquid fraction	0.67	0.69	0.72	0.71

Table 3-4: Geometry details, simulation conditions, and considered variables.

Parameters	Value
Calculation domain	$1.2 \times 1.2 \times 1.2$ m^3
U-tube length	1.1 m
Borehole depth	1.2 m

49

Borehole diameter	0.06 m
Pipe spacing of U-tube (between centers)	0.0365 m
Outer diameter of pipe	0.0065 m
Inner diameter of pipe	0.005 m
Inlet temperature	308.15 K
Inlet velocity	0.6 m/s
Operating time	12 h
NEPCMs	Addition of seven nanoparticles including Cu, CuO, Al$_2$O$_3$, TiO$_2$, SiO$_2$, MWCNT, and graphene to the Paraffin
Volume concentration of nanoparticles	0.05, 0.10, 0.15, 0.20
Shape of nanoparticles	sphere, brick, cylinder, platelet, blade

3.3 Mathematical formulation

The nanoparticles and PCM that form NEPCM are in thermal equilibrium and the no-slip condition is considered between them. Other key assumption for this study is to consider the thermo-physical properties of the NEPCM as temperature independent. The density of NEPCM (ρ_{NEPCM}) is written as [33]:

$$\rho_{NEPCM} = \phi \rho_{Nanoparticle} + (1-\phi)\rho_{PCM} \tag{1}$$

where ϕ is the volume fraction of the nanoparticles. The specific heat of NEPCM ((C_p)$_{NEPCM}$) is given by [33]:

$$(C_p)_{NEPCM} = \frac{\phi(\rho C_p)_{Nanoparticle} + (1-\phi)(\rho C_p)_{PCM}}{\rho_{NEPCM}} \tag{2}$$

The latent heat of NEPCM (L_{NEPCM}) can be expressed as [33]:

$$L_{NEPCM} = \frac{(1-\phi)(\rho L)_{PCM}}{\rho_{NEPCM}} \tag{3}$$

The dynamic viscosity of NEPCM (μ_{NEPCM}) is defined as [33]:

$$\mu_{NEPCM} = \frac{\mu_{PCM}}{(1-\phi)^{2.5}} \tag{4}$$

The thermal conductivity of NEPCM (k_{NEPCM}) can be calculated by means of the Hamilton–Crosser formula [47], in which in addition to including the thermal conductivities of nanoparticles and PCM as well as the nanoparticle volume fraction, the shape of nanoparticles has also been taken into account, which is as follows:

$$k_{NEPCM} = k_{PCM}\left[\frac{k_{PCM} + k_{Nanoparticle} + nk_{PCM} + \phi(k_{Nanoparticle} - k_{PCM}) - n\phi(k_{PCM} - k_{Nanoparticle})}{k_{PCM} + k_{Nanoparticle} + nk_{PCM} + \phi(k_{PCM} - k_{Nanoparticle})}\right] \tag{5}$$

where n represents the shape factor of the nanoparticles as shown in Table 3-5.

n	Nanoparticle Shape
3	Sphere
3.7	Brick
4.9	Cylinder
5.7	Platelet
8.6	Blade
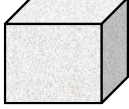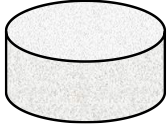
To model the phase change process of NEPCM, we used the Enthalpy-Porosity method. The Boussinesq approximation is applied to account for buoyancy effects [33]:

$$\beta_{NEPCM} = \frac{\phi(\rho\beta)_{Nanoparticle} + (1-\phi)(\rho\beta)_{PCM}}{\rho_{NEPCM}} \tag{6}$$

The continuity, momentum, and energy equations are as follows [50–52]:

$$\nabla . \vec{V} = 0 \tag{7}$$

$$\frac{\partial \vec{V}}{\partial t} + \vec{V} . \nabla \vec{V} = \frac{1}{\rho_{NEPCM}}(-\nabla P + \mu_{NEPCM} \nabla^2 \vec{V} + (\rho\beta)_{NEPCM} \vec{g}(T - T_{ref})) + \vec{S} \tag{8}$$

$$\frac{\partial h_{sens}}{\partial t} + \frac{\partial h_{lat}}{\partial t} + \nabla . (\vec{V} h_{sens}) = \nabla . (\frac{k_{NEPCM}}{(\rho C_p)_{NEPCM}} \nabla h_{sens}) \tag{9}$$

where h_{sens} and h_{lat} are the sensible heat enthalpy and latent heat enthalpy, respectively. The total enthalpy is obtained by summation of the enthalpies:

$$h_{tot} = h_{sens} + h_{lat} \tag{10}$$

The sensible heat and latent heat enthalpies can be obtained by Equations (11) and (12) [53–55]:

$$h_{sens} = h_{ref} + \int_{T_{ref}}^{T} C_p dT = h_{ref} + C_p \int_{T_{ref}}^{T} dT \tag{11}$$

$$h_{lat} = \sum_{i=1}^{N} \lambda_i L \tag{12}$$

where λ is the liquid fraction which varies from 0 to 1. λ = 0 indicates that the material is in solid phase, while for λ = 1, the NEPCM is full of liquid. The region where $0 < \lambda < 1$ is considered to be the mushy zone, which acts as a porous region. This parameter is defined as:

$$\lambda = \begin{cases} \dfrac{h_{lat}}{L} = 0 & if \ \ T \leq T_{solidus} \\[2ex] \dfrac{h_{lat}}{L} = 1 & if \ \ T \geq T_{liquidus} \\[2ex] \dfrac{h_{lat}}{L} = \dfrac{T - T_{solidus}}{T_{liquidus} - T_{solidus}} & if \ \ T_{solidus} < T < T_{liquidus} \end{cases} \tag{13}$$

In Equation (8), $\vec{S}$ which is a source term named Darcy's law damping term is added to the momentum equation:

$$\vec{S} = A(\lambda)\vec{V} \tag{14}$$

where $A(\lambda) = C_{mush}(1-\lambda)^2 / (\lambda^3 + \varepsilon)$ indicates the slow increase of the velocities from zero value in the full solid phase to a finite value in the liquid phase throughout the computational cells at the phase transition occurrence. C_{mush} is the mushy zone constant fixed at 10^5 and ε is a small positive quantity (here 0.001) called computational constant which prevents a division by zero [53–55].

3.4 Verification

The verification of the numerical results to the experimental data of Yang et al. [20] is done by comparing the backfill and soil temperatures at different radiuses. The three radiuses of r_1, r_2, r_3 are 0.03 m, 0.19 m, and 0.27 m, respectively, at a depth of 0.3 m (see Figure 3-3). The BHE works 10 h a day for cooling operation to release the heat to the ground. In the validation, just a mixed acid PCM used as backfill which consists of decyl acid and lauric acid with a mass proportion of 66:34. The other conditions are the same as stated in Section 3.2 of the present study. As shown in Figure 3-4, the numerical and experimental results display an excellent agreement with the percent errors of less than 5%.
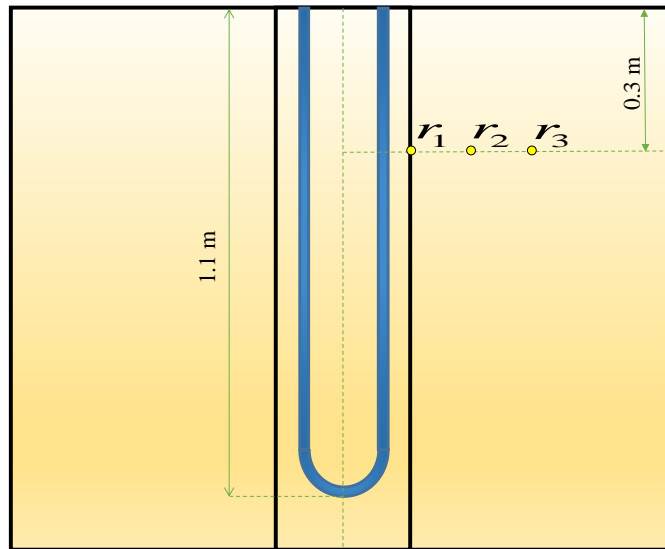
Figure 3-3: Three different radiuses selected for validation.
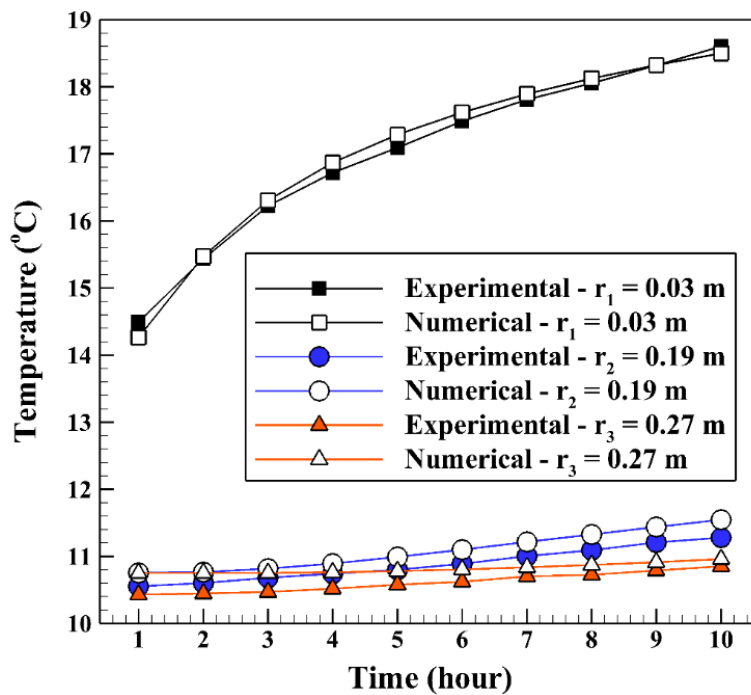
Figure 3-4: Validation of the numerical backfill and soil temperatures at different radiuses to the experimental results of Yang et al. [20].

3.5 Results and discussion

In the present work, a single U-tube BHE is evaluated numerically by computational fluid dynamics (CFD) software. The aim is to compare different types of NEPCM which are used as backfill in the BHE to allow an optimal selection. Moreover, the chosen NEPCM is analyzed in terms of the volume fraction and shape factor of its nanoparticles.

3.5.1 Impact of nano-enhanced phase change material type

In the first step, comparing various NEPCMs, the nanoparticles are dispersed to the base fluid with volume fraction and shape factor of 20% and 3, respectively. Figure 3-5 shows the variation of the liquid fraction with operating time when using different NEPCMs. We used Paraffin as the base fluid and added seven kinds of nanoparticles to it to conform the NEPCMs. From this figure, it can be seen that the NEPCM containing Cu nanoparticles is melted better than the other NEPCMs (with the liquid fraction of almost 0.55) and the worst one is found to be the NEPCM containing SiO_2 nanoparticles with the liquid fraction close to 0.45. At the end of cooling operation, we can observe the small differences between the liquid fractions of NEPCMs with Cu, graphene, MWCNT, and Al_2O_3 nanoparticles compared to that for the NEPCMs with CuO, TiO_2 and SiO_2 nanoparticles. It is worth mentioning that all of the NEPCMs have a significantly higher rate of melting than the pure Paraffin, thanks to the presence of nanoparticles which improve the thermal conductivity of the PCM.
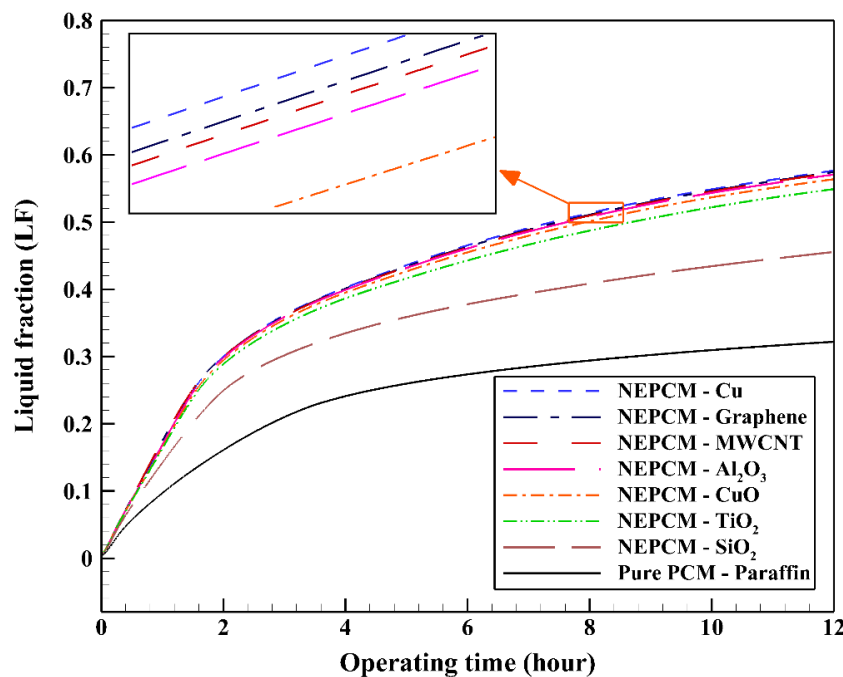
Figure 3-5: Variation of the liquid fraction with operating time using different NEPCMs at $\phi = 0.20$ and n = 3.

The contours of liquid fraction for various cases at four different times including 3, 6, 9, and 12 h are illustrated in Figure 3-6. The impact of using NEPCMs instead of pure Paraffin on the melting rate can be realized clearly. Compared to the other materials, in the case with pure Paraffin, the evolution of the contour lines after 6 h from the start of the process is significantly more restricted. In contrast, all NEPCMs present much higher melting rates. Among the studied NEPCMs, the SiO_2 nanoparticle material shows the smallest melting rate, although the differences between the rest of compounds are not as marked. The compound using Cu nanoparticle shows a better melting rate with a small difference compared to the others after 12 h.
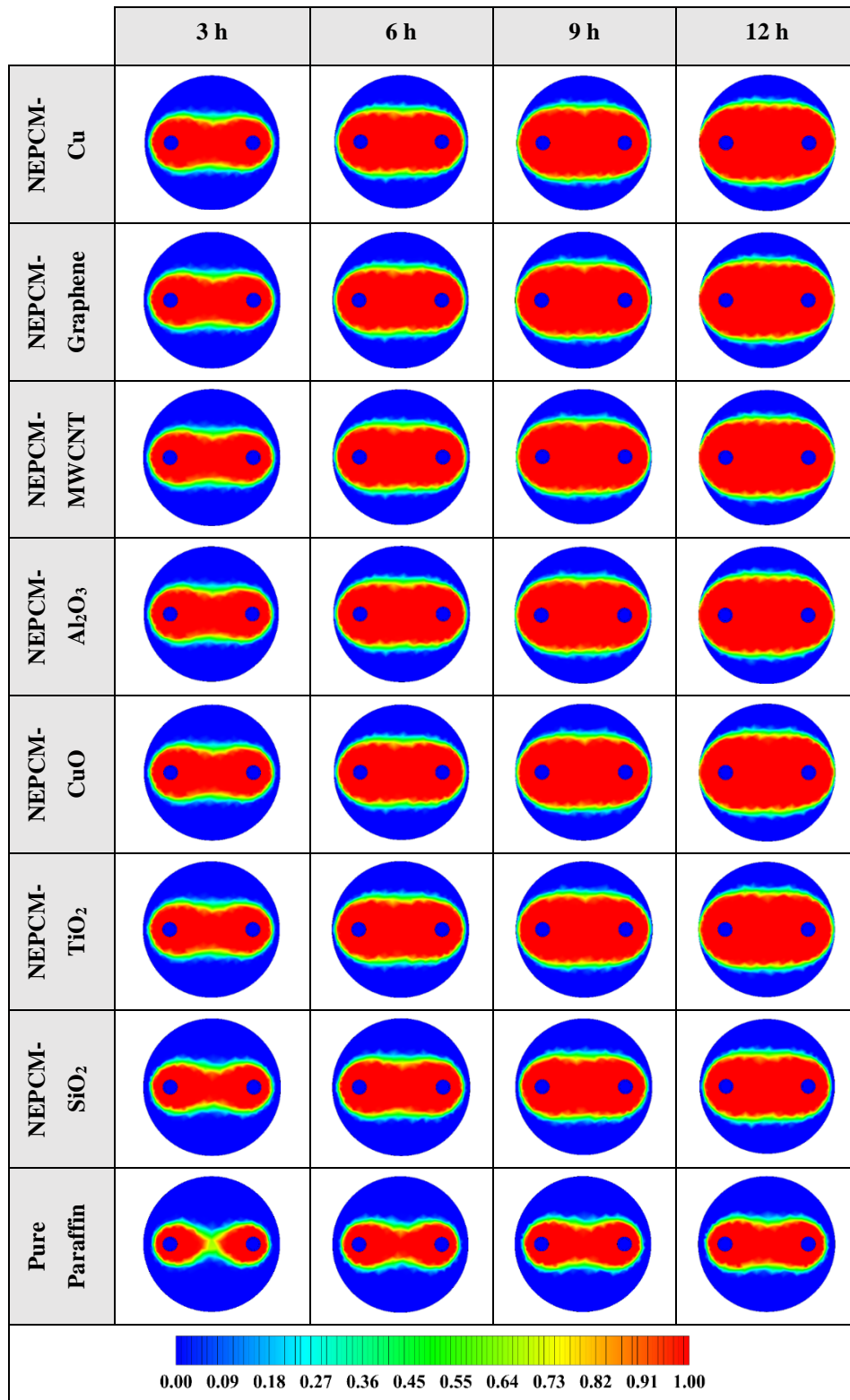
Figure 3-6: 2D contours of the liquid fraction of different NEPCMs at various hours of operating when φ = 0.20 and n = 3 (Top view at Z = 0).

Considering NEPCM with Cu nanoparticles, the BHE can release more heat to the ground which leads to its superior thermal performance (see Figure 3-7). As illustrated, after approximately two hours of BHE

operation start, the outlet temperatures of all NEPCMs showed a constant increase which can be explained by the fact that during this time, the temperature difference between the working fluid and other BHE components decreases. Consequently, it prevents the BHE to exchange more heat to the surrounding regions. According to the comparison conducted between seven types of NEPCM, Figure 3-5 and Figure 3-7, the addition of Cu nanoparticles to the Paraffin leads to enhancing considerably the thermal performance of the BHE. 2D contours of the temperature distribution of the BHE at various hours of operating using different NEPCMs when ϕ = 0.20, n = 3, and Z = 0 are illustrated in Figure 3-8.
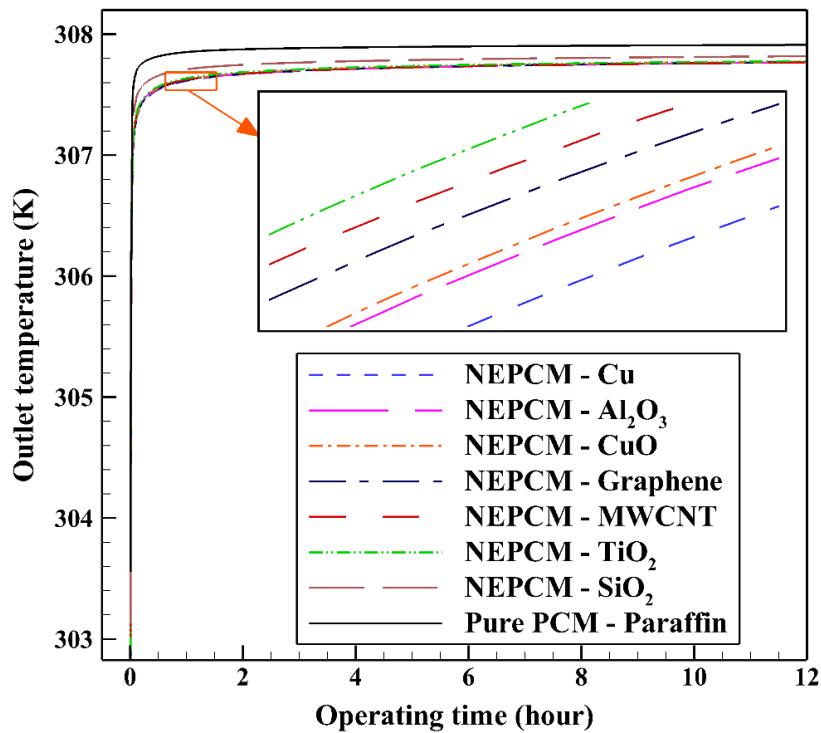
Figure 3-7: Variation of the outlet temperature with operating time when using different NEPCMs at ϕ = 0.20 and n = 3.

56

	3 h	6 h	9 h	12 h
NEPCM-Cu				
NEPCM-Graphene				
NEPCM-MWCNT				
NEPCM-Al$_2$O$_3$				
NEPCM-CuO				
NEPCM-TiO$_2$				
NEPCM-SiO$_2$				
Pure Paraffin				

283.90 286.59 289.29 291.98 294.68 297.37 300.07 302.76 305.46 308.15
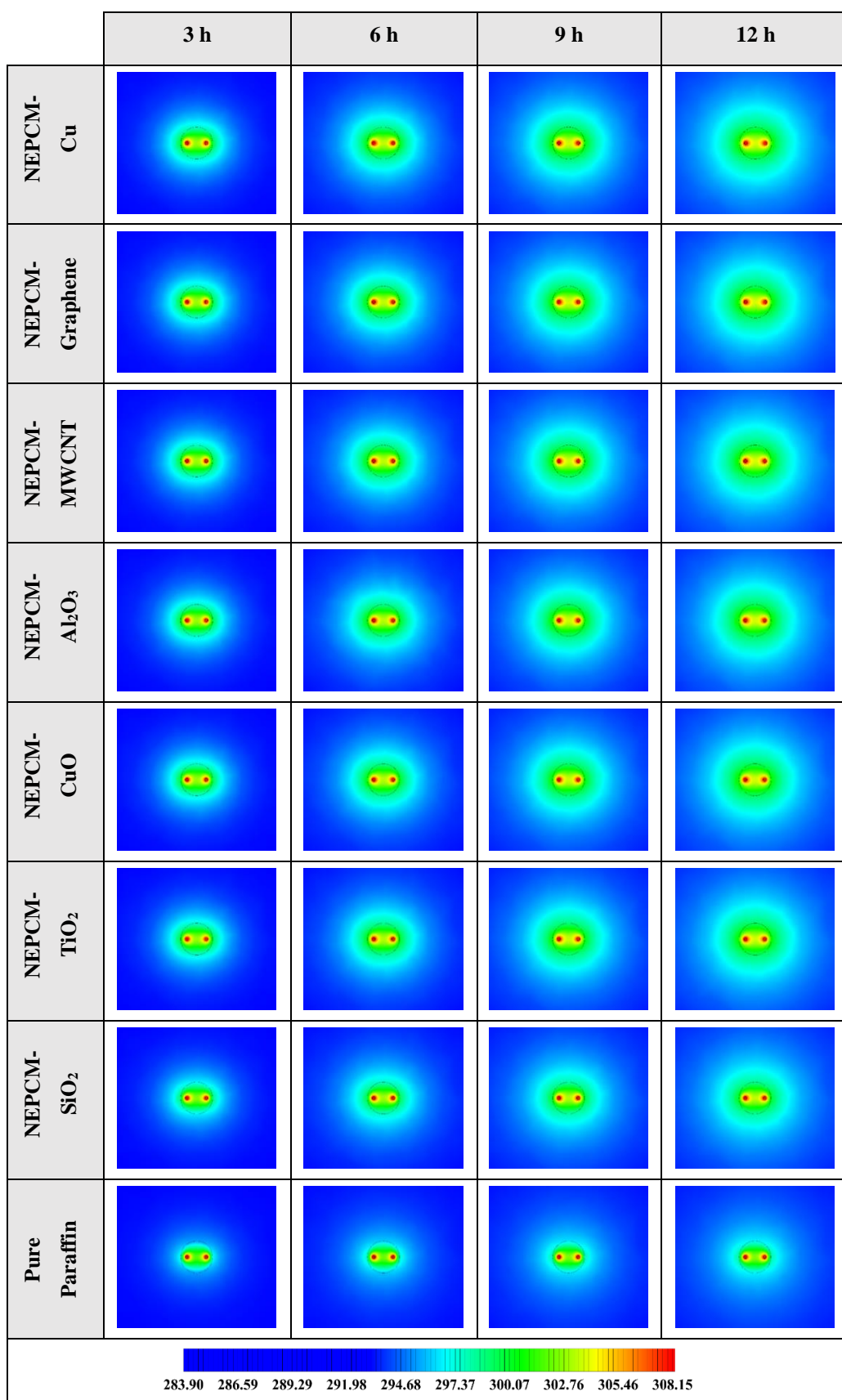
Figure 3-8: 2D contours of the temperature distribution of the BHE at various hours of operating using different NEPCMs when ϕ = 0.20 and n = 3. (Top view at Z = 0).

Figure 3-8 shows that by using pure Paraffin as PCM, the heat transfer rate between the fluid in the U-tube and the PCM and consequently between PCM and soil is very low. Instead, by using NEPCMs instead of pure PCM, the heat transfer rate increases significantly. Also, among the evaluated NEPCMs, PCM with SiO_2 nanoparticle displays the lower heat transfer rate, and based on Figure 3-8, the differences between the other models are not significant. To realize better the melting process and heat transfer between different BHE components, 3D contours of temperature distribution and 2D contours of temperature distribution (front view, middle plane) of the BHE are presented in Figure 8-1 and Figure 8-4 (Appendix A), respectively. Based on the abovementioned explanations, the NEPCM containing Cu nanoparticles is chosen for further investigation.

3.5.2 Impact of nano-enhanced phase change material volume fraction (ϕ)

In the second step of the study, the volume fraction of Cu nanoparticles was varied from 0.05 to 0.2 while the shape factor is fixed at 3. The range of volume fraction of nanoparticles (0–20%) is chosen based on the past NEPCM published articles, e.g., [33–41]. Twenty percent is the maximum percentage of nanoparticles' volume fraction that has been dispersed into the base fluid to prepare a NEPCM thus far [39–41]. The variation of the liquid fraction with operating time at various volume fractions of the NEPCM containing Cu nanoparticles is represented in Figure 3-9. Based on this figure, the increase in the volume fraction of Cu nanoparticles improves markedly the melting rate of NEPCM, being 0.2 the most favorable volume fraction. The maximum and the minimum values of liquid fraction, 0.57 and 0.36, are obtained by 0.2 and 0.05 of Cu nanoparticles' volume fractions, respectively. The thermal conductivity of the NEPCM, which is calculated by Equation (5), can increase up to 55% when using Cu nanoparticles at 20% of volume fraction compared to the pure PCM. The differences between the curves are noticeable, highlighting the great influence of nanoparticles' volume fraction on the cooling operation of the studied BHE.
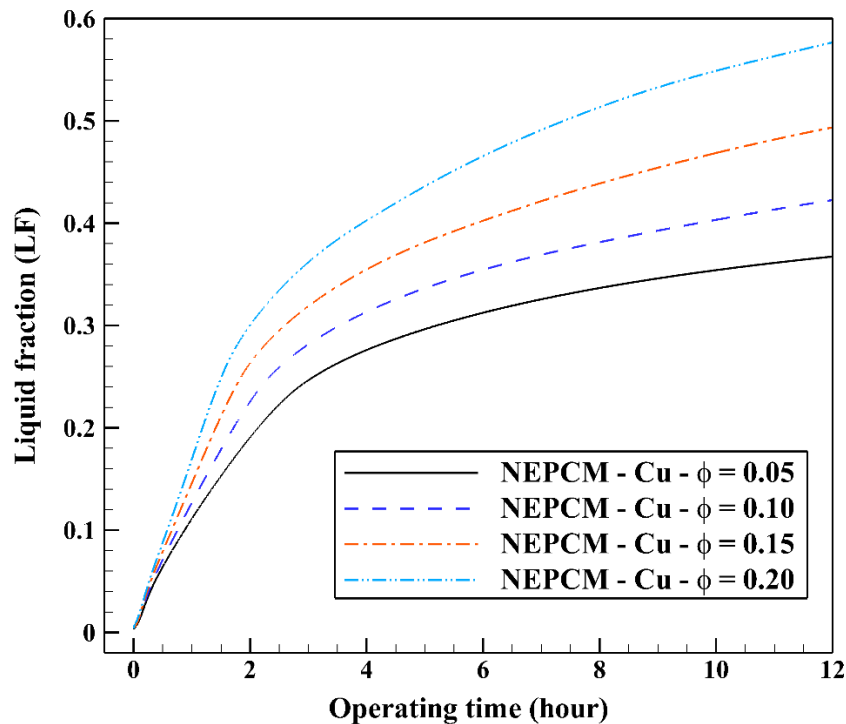
Figure 3-9: Variation of the liquid fraction with operating time at various volume fractions of the NEPCM containing Cu nanoparticles when n = 3.

The contours of liquid fraction for various volume fractions at four different operating times including 3, 6, 9, and 12 h are illustrated in Figure 3-10. It should be noted that as the volume concentration of the nanoparticle in the NEPCM increases, the thermal conductivity of the NEPCM rises which leads to higher heat transferring and melting rate. This fact is shown clearly in Figure 3-10. Accordingly, at higher volume concentrations of the Cu nanoparticles in the NEPCM, the melted PCM (red region) is more than the lower volume fractions.

Also, Figure 3-11 shows the variation of the outlet temperature with operating time at various volume fractions of the NEPCM containing Cu nanoparticles. It is observed that the inlet temperature can be reduced by 0.39 K when adding 20% of the volume fraction of Cu nanoparticles to the PCM. Considering Figure 3-9 and Figure 3-11, we select the Cu nanoparticles with the volume fraction of 0.2 as an additive to the PCM for the next part of the evaluation. 2D contours of the temperature distribution of the BHE at various hours of operating using different NEPCMs when $n = 3$ and Z = 0 are illustrated in Figure 3-12.

Figure 3-12 shows that by using NEPCM with a higher volume concentration of nanoparticle, the heat transfer rate between the fluid in the U-tube and the PCM and consequently between PCM and soil can be considerable. Because as noted previously, a higher volume concentration of the nanoparticle leads to increasing the thermal conductivity of the NEPCM. Therefore, it causes more heat exchanging and better melting of the NEPCM. To realize better the melting process and heat transfer of the BHE, 3D contours of temperature distribution and 2D contours of temperature distribution (front view, middle plane) of the BHE are presented in Figure 8-2 and Figure 8-5 (Appendix A), respectively.
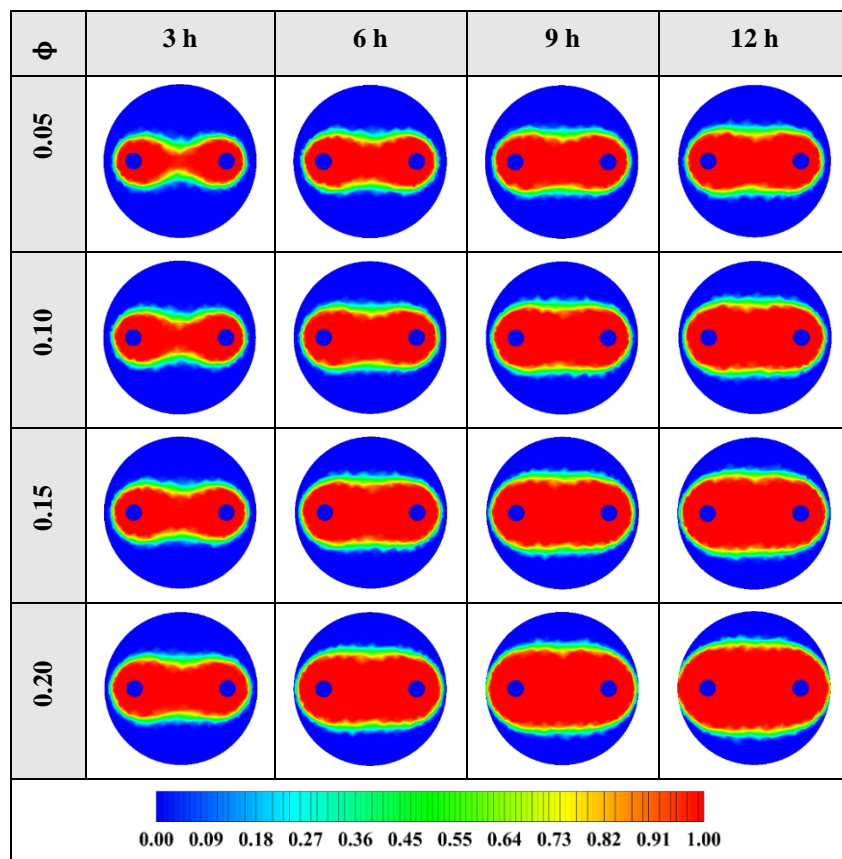
Figure 3-10: 2D contours of the liquid fraction of NEPCM containing Cu nanoparticles with different volume fractions at various hours of operating when n = 3 (Top view at Z = 0).
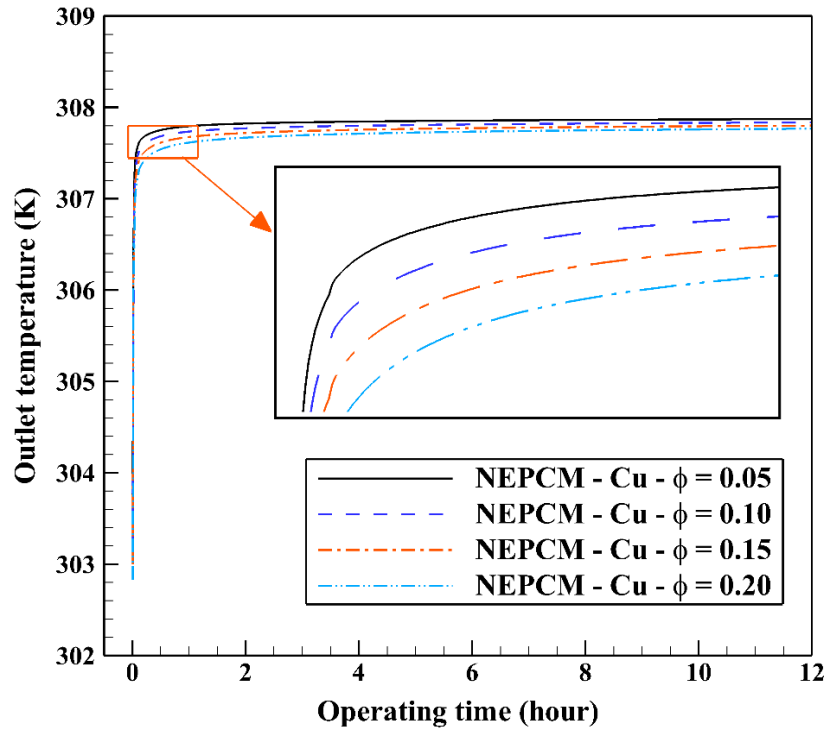
Figure 3-11: Variation of the outlet temperature with operating time at various volume fractions of the NEPCM containing Cu nanoparticles when n = 3.
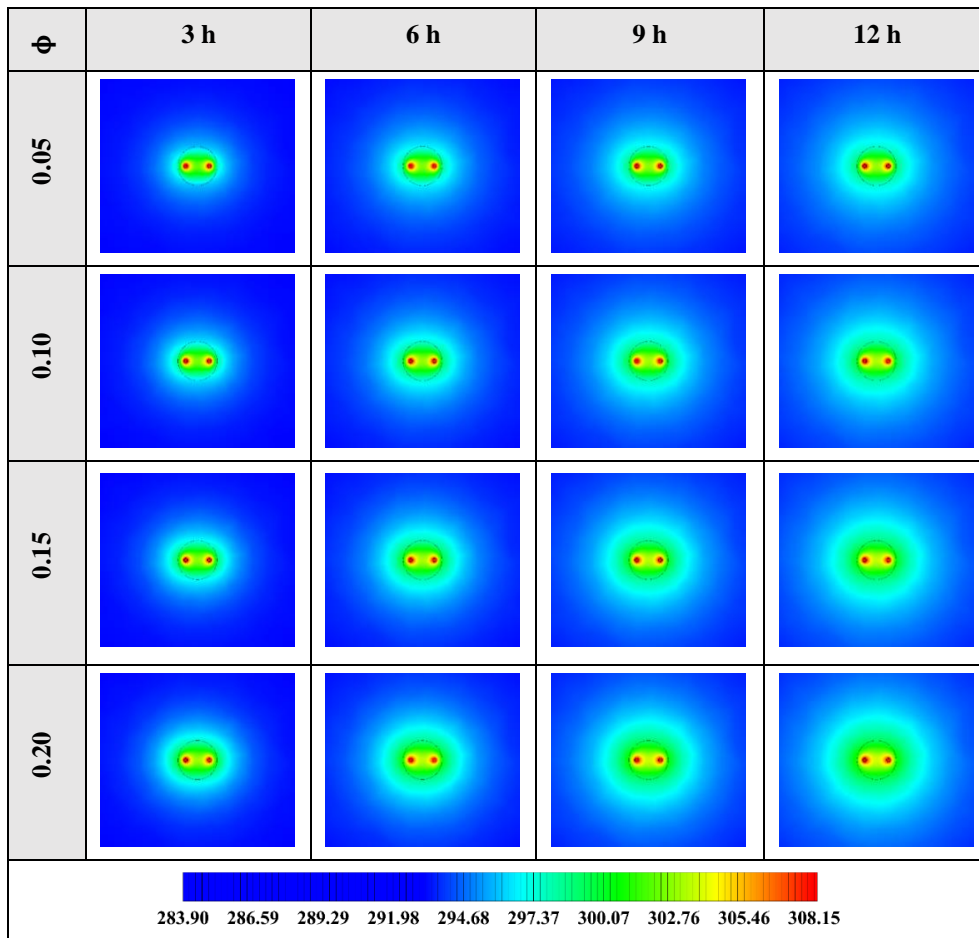
Figure 3-12: 2D contours of the temperature distribution of the BHE at various hours of operating when using NEPCM containing Cu nanoparticles with different volume fractions at n = 3 (Top view at Z = 0).

3.5.3 Impact of nano-enhanced phase change material shape factor (n)

The variation of the liquid fraction with operating time at various shape factors of Cu nanoparticles is presented in Figure 3-13. The considered shape factors are 3, 3.7, 4.9, 5.7, and 8.6, as provided in Table 3-5, which have impacts on the thermal conductivity of the NEPCM (see Equation (5)). According to Figure 3-13, $n = 8.6$ is by far the most appropriate shape factor of the Cu nanoparticles which results in the melting of about 85% of the NEPCM. This means that the blade shape of Cu nanoparticles should be dispersed to the pure Paraffin to enhance remarkably the heat storage capacity of the NEPCM. By changing the shape factor from 8.6 to 3, the liquid fraction of the NEPCM decreases almost 27%. The contours of liquid fraction for various volume fractions at four different operating times such as 3, 6, 9, and 12 h are depicted in Figure 3-14.
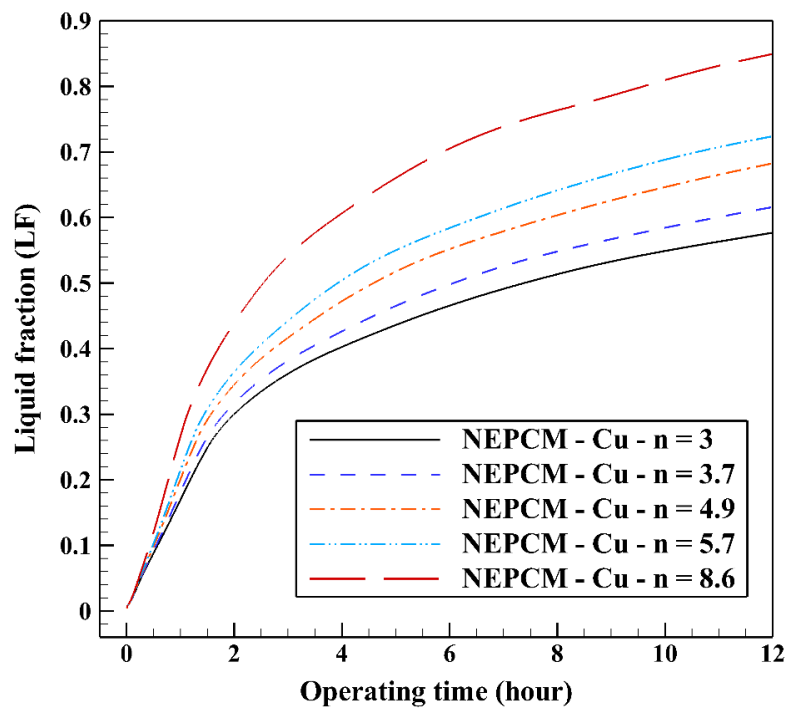
Figure 3-13: Variation of the liquid fraction with operating time at various shape factors of Cu nanoparticles when $\phi = 0.20$.
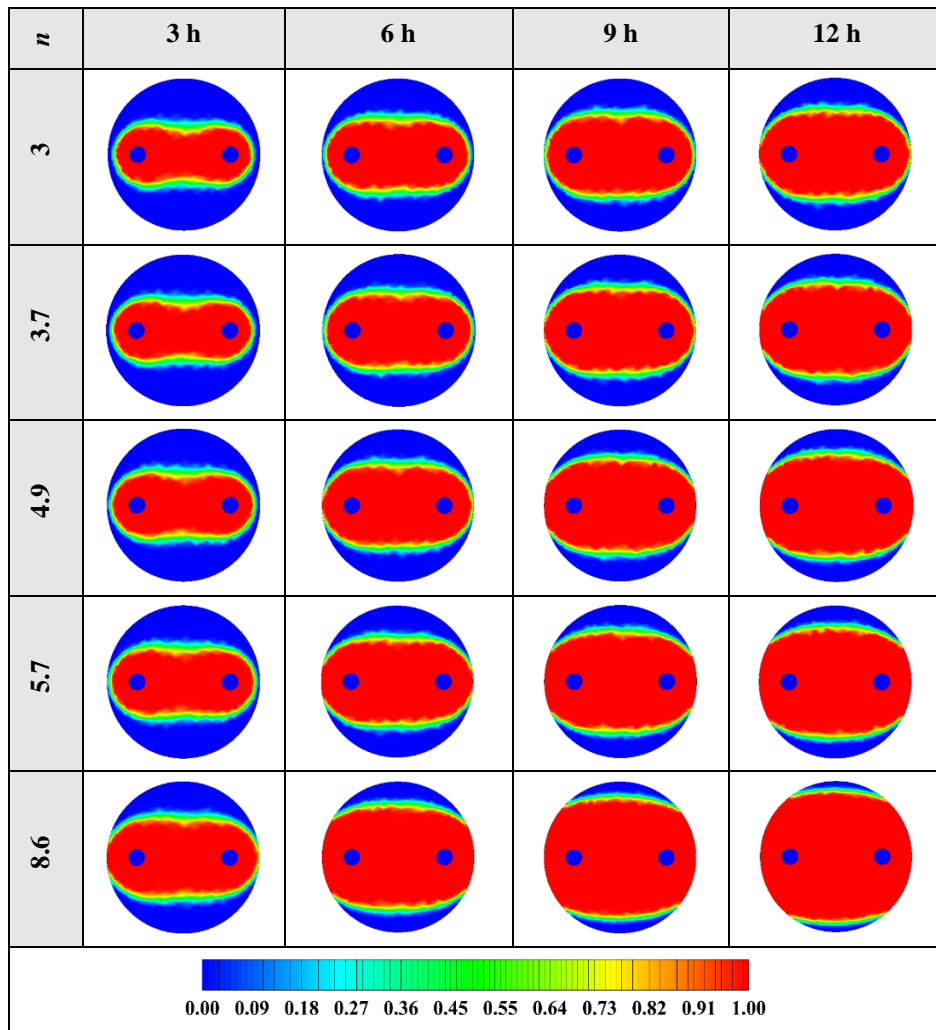
Figure 3-14: 2D contours of the liquid fraction of NEPCM containing Cu nanoparticles with different shape factors at various hours of operating when $\phi = 0.20$ (Top view at $Z = 0$).

Figure 3-14 illustrates that as the nanoparticle shape factor rises, the heat transfer and melting rate increase which proves the results presented in Figure 3-13. Figure 3-15 demonstrates the variation of the outlet temperature with operating time at various shape factors of Cu nanoparticles. The NEPCM containing the blade shape of Cu nanoparticles ($n = 8.6$) has better potential to absorb thermal energy from the working fluid and subsequently could reduce noticeably the outlet water temperature (almost 0.48 K) in comparison with the other shapes of Cu nanoparticles dispersed into the pure PCM.
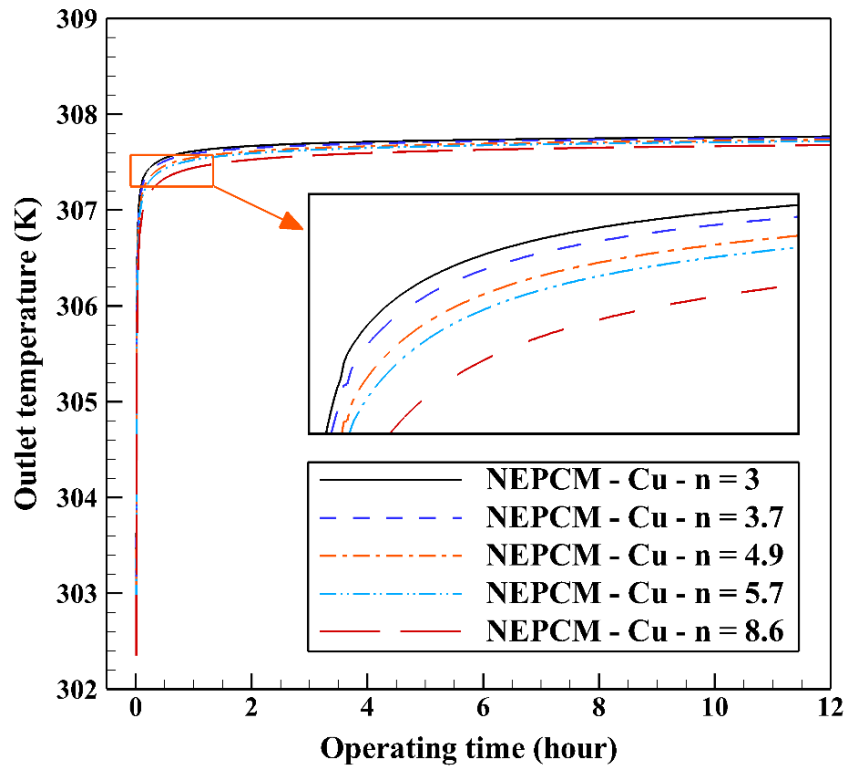
Figure 3-15: Variation of the outlet temperature with operating time at various shape factors of Cu nanoparticles when ϕ = 0.20.

2D contours of the temperature distribution of the BHE at various hours of operating using NEPCM containing Cu nanoparticles with different shape factors when ϕ = 0.20 are illustrated in Figure 3-16. It is shown that by using NEPCMs with a higher value of nanoparticle shape factor, the heat transfer rate between the fluid in the U-tube and the NEPCM and consequently between the NEPCM and surrounding ground can be improved markedly. For a better understanding of the melting process and heat exchange of BHE components, 3D contours of temperature distribution and 2D contours of temperature distribution (front view, middle plane) of the BHE are presented in Figure 8-3 and Figure 8-6 (Appendix A), respectively.
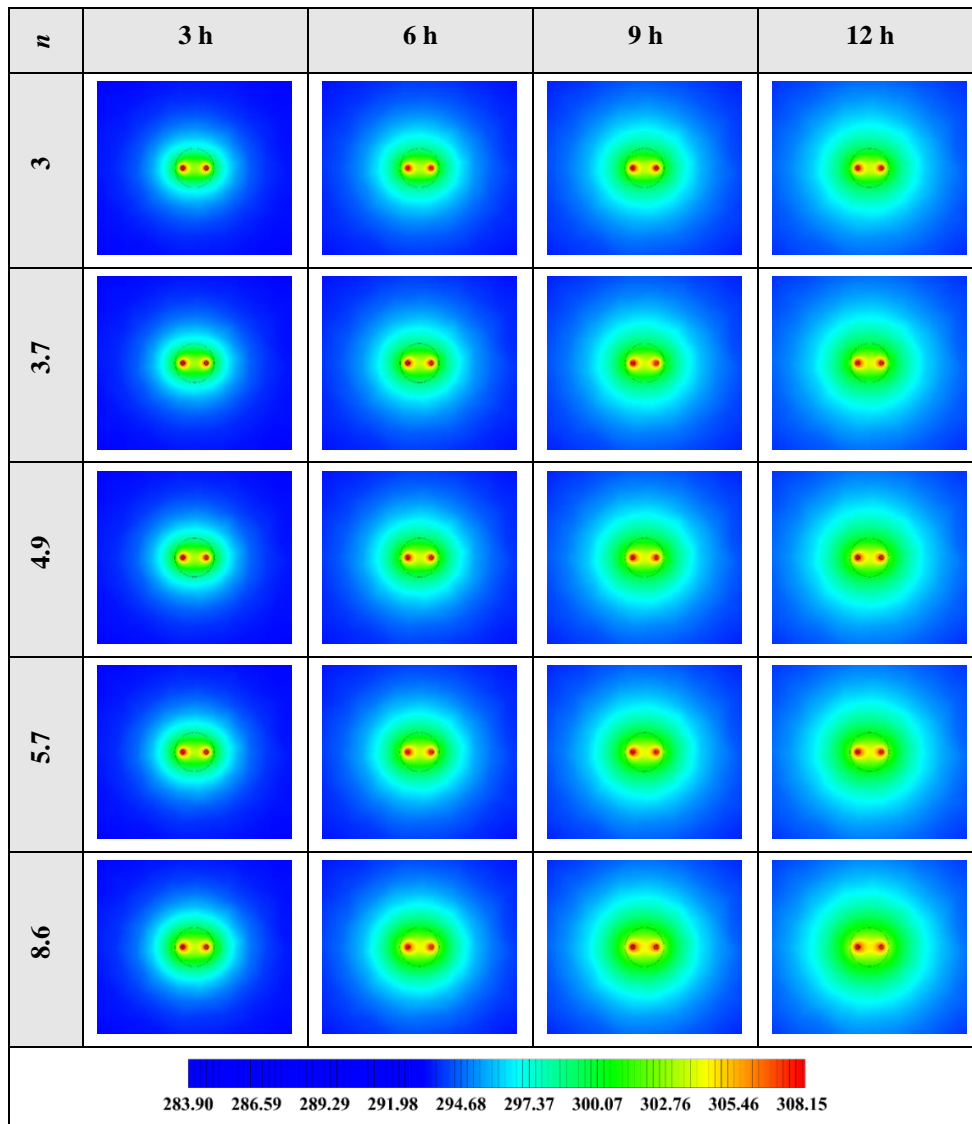
Figure 3-16: 2D contours of the temperature distribution of the BHE at various hours of operating using NEPCM containing Cu nanoparticles with different shape factors when $\phi = 0.20$. (Top view at $Z = 0$).

3.6 Conclusions and future scope

In this study, a 3D numerical model of a single U-tube borehole heat exchanger is investigated by means of commercial computational fluid dynamics code, ANSYS Fluent 18.2, to simulate ground source heat pump cooling operation. The objectives of the research are first to analyze the application of seven kinds of nano-enhanced phase change material made from the addition of Cu, CuO, Al_2O_3, TiO_2, SiO_2, multi-wall carbon nanotube, and graphene nanoparticles to the Paraffin as backfill in the borehole heat exchanger; then, to study the effects of volume fraction of nanoparticles which varies from 0.05 to 0.20 on the thermal performance of the borehole heat exchanger; and finally, to evaluate the role of nanoparticles' shape such as the sphere, brick, cylinder, platelet, and the blade on the melting rate of nano-enhanced phase change material. The obtained results are as follows:

- The nano-enhanced phase change materials with Cu and SiO_2 nanoparticles demonstrated to be the best and worst nanoparticles in improving the thermal performance of the single U-tube borehole heat exchanger, respectively. Therefore, Cu nano-enhanced phase change material was selected for further investigation.

- In terms of volume fraction, it was founded that the increase in the volume fraction of Cu nanoparticles enhanced considerably the melting rate of nano-enhanced phase change material, being 0.20 the most suitable volume fraction which increased up to 55% the thermal conductivity of the nano-enhanced phase change material in comparison with the pure phase change material.

- Concerning the shape of nanoparticles, the blade shape was by far the best shape of the Cu nanoparticles which resulted in about 85% melting of the nano-enhanced phase change material.

To sum up, the nano-enhanced phase change material with Cu nanoparticles in the blade shape at 20% of volume fraction showed to have notable potential to absorb thermal energy from the heat transfer fluid and decrease the outlet water temperature compared to the other nanoparticles which were used as the addition to the Paraffin.

It is worth mentioning that this is the first time that a nano-enhanced phase change material is implemented in a borehole heat exchanger; therefore, more numerical studies are necessary to extend the flow solver to model the melting and solidification processes in the proposed borehole heat exchanger. Also, performing experimental tests for both the charging/discharging process are required to see how the borehole heat exchanger equipped with nano-enhanced phase change material works in a real project.

References

1. Javadi, H.; Ajarostaghi, S.S.M.; Rosen, M.A.; Pourfallah, M. Performance of ground heat exchangers: A comprehensive review of recent advances. *Energy* 2019, *178*, 207–233, doi:10.1016/j.energy.2019.04.094.
2. Javadi, H.; Ajarostaghi, S.S.M.; Pourfallah, M.; Zaboli, M. Performance analysis of helical ground heat exchangers with different configurations. *Appl. Therm. Eng.* 2019, *154*, 24–36, doi:10.1016/j.applthermaleng.2019.03.021.
3. Javadi, H.; Ajarostaghi, S.S.M.; Ajarostaghi, S.S.M.; Pourfallah, M. Thermal analysis of a triple helix ground heat exchanger using numerical simulation and multiple linear regression. *Geothermics* 2019, *81*, 53–73, doi:10.1016/j.geothermics.2019.04.005.
4. Javadi, H.; Ajarostaghi, S.S.M.; Rosen, M.A.; Pourfallah, M. A Comprehensive Review of Backfill Materials and Their Effects on Ground Heat Exchanger Performance. *Sustainability* 2018, *10*, 4486, doi:10.3390/su10124486.
5. Quaggiotto, D.; Zarrella, A.; Emmi, G.; De Carli, M.; Pockelé, L.; Vercruysse, J.; Psyk, M.; Righini, D.; Galgaro, A.; Mendrinos, D.; et al. Simulation-Based Comparison Between the Thermal Behavior of Coaxial and Double U-Tube Borehole Heat Exchangers. *Energies* 2019, *12*, 2321, doi:10.3390/en12122321.
6. Serageldin, A.A.; Radwan, A.; Sakata, Y.; Katsura, T.; Nagano, K. The Effect of Groundwater Flow on the Thermal Performance of a Novel Borehole Heat Exchanger for Ground Source Heat Pump Systems: Small Scale Experiments and Numerical Simulation. *Energies* 2020, *13*, 1418, doi:10.3390/en13061418.
7. Sapińska-Śliwa, A.; Sliwa, T.; Twardowski, K.; Szymski, K.; Gonet, A.; Żuk, P. Method of Averaging the Effective Thermal Conductivity Based on Thermal Response Tests of Borehole Heat Exchangers. *Energies* 2020, *13*, 3737, doi:10.3390/en13143737.
8. Janiszewski, M.; Hernández, E.C.; Siren, T.; Uotinen, L.; Kukkonen, I.T.; Rinne, M. In Situ Experiment and Numerical Model Validation of a Borehole Heat Exchanger in Shallow Hard Crystalline Rock. *Energies* 2018, *11*, 963, doi:10.3390/en11040963.
9. Patil, M.S.; Seo, J.-H.; Kang, S.-J.; Lee, M.-Y. Review on Synthesis, Thermo-Physical Property, and Heat Transfer Mechanism of Nanofluids. *Energies* 2016, *9*, 840, doi:10.3390/en9100840.
10. Cao, S.-J.; Kong, X.-R.; Deng, Y.; Zhang, W.; Yang, L.; Ye, Z.-P. Investigation on thermal performance of steel heat exchanger for ground source heat pump systems using full-scale experiments and numerical simulations. *Appl. Therm. Eng.* 2017, *115*, 91–98, doi:10.1016/j.applthermaleng.2016.12.098.
11. Li, B.; Zheng, M.; Shahrestani, M.; Zhang, S. Driving factors of the thermal efficiency of ground source heat pump systems with vertical boreholes in Chongqing by experiments. *J. Build. Eng.* 2020, *28*, 101049, doi:10.1016/j.jobe.2019.101049.
12. Wang, J.L.; De Zhao, J.; Liu, N. Numerical Simulation of Borehole Heat Transfer with Phase Change Material as Grout. *Appl. Mech. Mater.* 2014, *577*, 44–47, doi:10.4028/www.scientific.net/amm.577.44.
13. Lei, H.Y.; Dai, C.S. Heat transfer analysis of centric borehole heat exchanger with different backfill materials. In Proceedings of the World Geothermal Congress, Melbourne, Australia, 19–25 April 2015.

14. Li, X.; Tong, C.; Duanmu, L.; Liu, L. Research on U-tube Heat Exchanger with Shape-stabilized Phase Change Backfill Material. *Procedia Eng.* 2016, *146*, 640–647, doi:10.1016/j.proeng.2016.06.420.

15. Li, X.; Tong, C.; Duanmu, L.; Liu, L. Study of a U-tube heat exchanger using a shape-stabilized phase change backfill material. *Sci. Technol. Built Environ.* 2017, *23*, 1–11, doi:10.1080/23744731.2016.1243409.

16. Qi, D.; Pu, L.; Sun, F.; Li, Y. Numerical investigation on thermal performance of ground heat exchangers using phase change materials as grout for ground source heat pump system. *Appl. Therm. Eng.* 2016, *106*, 1023–1032, doi:10.1016/j.applthermaleng.2016.06.048.

17. Chen, F.; Mao, J.; Chen, S.; Li, C.; Hou, P.; Liao, L. Efficiency analysis of utilizing phase change materials as grout for a vertical U-tube heat exchanger coupled ground source heat pump system. *Appl. Therm. Eng.* 2018, *130*, 698–709, doi:10.1016/j.applthermaleng.2017.11.062.

18. Chen, F.; Mao, J.; Li, C.; Hou, P.; Li, Y.; Xing, Z.; Chen, S. Restoration performance and operation characteristics of a vertical U-tube ground source heat pump system with phase change grouts under different running modes. *Appl. Therm. Eng.* 2018, *141*, 467–482, doi:10.1016/j.applthermaleng.2018.06.009.

19. Zhang, M.; Liu, X.; Biswas, K.; Warner, J. A three-dimensional numerical investigation of a novel shallow bore ground heat exchanger integrated with phase change material. *Appl. Therm. Eng.* 2019, *162*, 114297, doi:10.1016/j.applthermaleng.2019.114297.

20. Yang, W.; Xu, R.; Yang, B.; Yang, J. Experimental and numerical investigations on the thermal performance of a borehole ground heat exchanger with PCM backfill. *Energy* 2019, *174*, 216–235, doi:10.1016/j.energy.2019.02.172.

21. Bottarelli, M.; Georgiev, A.; Aydin, A.A.; Su, Y.; Yousif, C. Ground-source heat pumps using phase change materials. In Proceedings of the European Geothermal Congress, Pisa, Italy, 3–7 June 2013.

22. Michele, B.; Bortoloni, M.; Su, Y.; Yousif, C.; Aydın, A.A.; Georgiev, A. Numerical analysis of a novel ground heat exchanger coupled with phase change materials. *Appl. Therm. Eng.* 2015, *88*, 369–375, doi:10.1016/j.applthermaleng.2014.10.016.

23. Michele, B.; Bortoloni, M.; Su, Y. Heat transfer analysis of underground thermal energy storage in shallow trenches filled with encapsulated phase change materials. *Appl. Therm. Eng.* 2015, *90*, 1044–1051, doi:10.1016/j.applthermaleng.2015.04.002.

24. Rabin, Y.; Korin, E. Incorporation of phase-change materials into a ground thermal energy storage system: Theoretical study. *J. Energy Resour. Technol.* 1996, *118*, 237–241, doi:10.1115/1.2793868.

25. Hüseyin, B.; Durmuş, A. Evaluation of ground-source heat pump combined latent heat storage system performance in greenhouse heating. *Energy Build.* 2009, *41*, 220–228, doi:10.1016/j.enbuild.2008.09.004.

26. Hüseyin, B. Energetic performance analysis of a ground-source heat pump system with latent heat storage for a greenhouse heating. *Energy Convers. Manag.* 2011, *52*, 581–589, doi:10.1016/j.enconman.2010.07.033.

27. Dehdezi, P.K.; Hall, M.R.; Dawson, A.R. Enhancement of soil thermo-physical properties using microencapsulated phase change materials for ground source heat pump applications. *Appl. Mech. Mater.* 2011, *110*, 1191–1198, doi:10.4028/www.scientific.net/amm.110-116.1191.

28. Eslami-nejad, P.; Bernier, M. A preliminary assessment on the use of phase change materials around geothermal boreholes. *ASHRAE Trans.* 2013, *119*, 312–321.

29. Na, Z.; Hu, P.; Lei, Y.; Jiang, Z.; Lei, F. Numerical study on ground source heat pump integrated with phase change material cooling storage system in office building. *Appl. Therm. Eng.* 2015, *87*, 615–623.

30. Jun-Seo, J.; Lee, S.R.; Kim, M.J. Benefit of phase change material on the performance of horizontal ground heat exchanger: A numerical study. In Proceedings of the World Congress on Advances in Civil, Environmental, and Materials Research, Jeju Island, Korea, 28 August–1 September 2016.

31. Alkhwildi, A.; Elhashmi, R.; Chiasson, A. Parametric modeling and simulation of Low temperature energy storage for cold-climate multi-family residences using a geothermal heat pump system with integrated phase change material storage tank. *Geothermics* 2020, *86*, 101864, doi:10.1016/j.geothermics.2020.101864.

32. Pu, L.; Xu, L.; Zhang, S.; Li, Y. Optimization of ground heat exchanger using microencapsulated phase change material slurry based on tree-shaped structure. *Appl. Energy* 2019, *240*, 860–869, doi:10.1016/j.apenergy.2019.02.088.

33. Khodadadi, J.M.; Hosseinizadeh, S.F. Nanoparticle-enhanced phase change materials (NEPCM) with great potential for improved thermal energy storage. *Int. Commun. Heat Mass Transf.* 2007, *34*, 534–543, doi:10.1016/j.icheatmasstransfer.2007.02.005.

34. Kalaiselvam, S.; Parameshwaran, R.; Harikrishnan, S. Analytical and experimental investigations of nanoparticles embedded phase change materials for cooling application in modern buildings. *Renew. Energy* 2012, *39*, 375–387, doi:10.1016/j.renene.2011.08.034.

35. Pahamli, Y.; Hosseini, M.J.; Ranjbar, A.; Bahrampoury, R. Effect of nanoparticle dispersion and inclination angle on melting of PCM in a shell and tube heat exchanger. *J. Taiwan Inst. Chem. Eng.* 2017, *81*, 316–334, doi:10.1016/j.jtice.2017.09.044.

36. Ramakrishnan, S.; Wang, X.; Sanjayan, J.; Wilson, J. Heat transfer performance enhancement of paraffin/expanded perlite phase change composites with graphene nano-platelets. *Energy Procedia* 2017, *105*, 4866–4871, doi:10.1016/j.egypro.2017.03.964.

37. Rufuss, D.; Winfred, D.; Suganthi, L.; Iniyan, S.; Davies, P.A. Effects of nanoparticle-enhanced phase change material (NPCM) on solar still productivity. *J. Clean. Prod.* 2018, *192*, 9–29, doi:10.1016/j.jclepro.2018.04.201.

38. Farzanehnia, A.; Khatibi, M.; Sardarabadi, M.; Passandideh-Fard, M. Experimental investigation of multiwall carbon nanotube/paraffin based heat sink for electronic device thermal management. *Energy Convers. Manag.* 2019, *179*, 314–325, doi:10.1016/j.enconman.2018.10.037.

39. Yang, L.; Huang, J.-N.; Zhou, F. Thermophysical properties and applications of nano-enhanced PCMs: An update review. *Energy Convers. Manag.* 2020, *214*, 112876, doi:10.1016/j.enconman.2020.112876.

40. Tariq, S.L.; Ali, H.M.; Akram, M.A.; Janjua, M.M.; Ahmadlouydarab, M. Nanoparticles enhanced phase change materials (NePCMs)-A recent review. *Appl. Therm. Eng.* 2020, *176*, 115305, doi:10.1016/j.applthermaleng.2020.115305.

41. Leong, K.Y.; Rahman, M.R.A.; Gurunathan, B. Nano-enhanced phase change materials: A review of thermo-physical properties, applications and challenges. *J. Energy Storage* 2019, *21*, 18–31, doi:10.1016/j.est.2018.11.008.

42. Dhaidan, N.S.; Khodadadi, J.; Al-Hattab, T.; Al-Mashat, S.M. Experimental and numerical investigation of melting of NePCM inside an annular container under a constant heat flux including the effect of eccentricity. *Int. J. Heat Mass Transf.* 2013, *67*, 455–468, doi:10.1016/j.ijheatmasstransfer.2013.08.002.

43. Khodadadi, J.M.; Fan, L. Expedited freezing of nanoparticle-enhanced phase change materials (NEPCM) exhibited through a simple 1-D stefan problem formulation. In Proceedings of the Heat Transfer Summer Conference, San Francisco, CA, USA, 19–23 July 2009.

44. Babapoor, A.; Karimi, G. Thermal properties measurement and heat storage analysis of paraffinnanoparticles composites phase change material: Comparison and optimization. *Appl. Therm. Eng.* 2015, *90*, 945–951, doi:10.1016/j.applthermaleng.2015.07.083.

45. Shadab, S.; Lafdi, K.; Hallinan, K. Carbon nanoadditives to enhance latent energy storage of phase change materials. *J. Appl. Phys.* 2008, *103*, 94302, doi:10.1063/1.2903538.

46. Karunesh, K.; Shukla, A.; Sharma, A.; Biwole, P.H. Heat transfer study of phase change materials with graphene nano particle for thermal energy storage. *Sol. Energy* 2017, *146*, 453–463, doi:10.1016/j.solener.2017.03.013.

47. Hamilton, R.L.; Crosser, O.K. Thermal conductivity of heterogeneous two-component systems. *Ind. Eng. Chem. Fundam.* 1962, *1*, 187–191, doi:10.1021/i160003a005.

48. Timofeeva, E.V.; Routbort, J.L.; Singh, D. Particle shape effects on thermophysical properties of alumina nanofluids. *J. Appl. Phys.* 2009, *106*, 014304, doi:10.1063/1.3155999.

49. Shi, X.; Jaryani, P.; Amiri, A.; Rahimi, A.; Malekshah, E.H. Heat transfer and nanofluid flow of free convection in a quarter cylinder channel considering nanoparticle shape effect. *Powder Technol.* 2019, *346*, 160–170, doi:10.1016/j.powtec.2018.12.071..

50. Ajarostaghi, M.; Soheil, S.; Poncet, S.; Sedighi, K.; Delavar, M.A. Numerical modeling of the melting process in a shell and coil tube ice storage system for air-conditioning application. *Appl. Sci.* 2019, *9*, 2726, doi:10.3390/app9132726.

51. Afsharpanah, F.; Ajarostaghi, S.S.M.; Sedighi, K. The influence of geometrical parameters on the ice formation enhancement in a shell and double coil ice storage system. *SN Appl. Sci.* 2019, *1*, 1264, doi:10.1007/s42452-019-1317-3.

52. Khashayar, P.; Ajarostaghi, S.S.M.; Sedighi, K. Numerical simulation of solidification process in an ice-on-coil ice storage system with serpentine tubes. *SN Appl. Sci.* 2019, *1*, 1258, doi:10.1007/s42452-019-1316-4.

53. Ajarostaghi, M.; Soheil, S.; Sedighi, K.; Delavar, M.A.; Poncet, S. Numerical study of a horizontal and vertical shell and tube ice storage systems considering three types of tube. *Appl. Sci.* 2020, *10*, 1059, doi:10.3390/app10031059..

54. Ajarostaghi, M.; Soheil, S.; Sedighi, K.; Delavar, M.A.; Poncet, S. Influence of geometrical parameters arrangement on solidification process of ice-on-coil storage system. *SN Appl. Sci.* 2019, *2*, 109, doi:10.1007/s42452-019-1912-3.

55. Ajarostaghi, M.; Soheil, S.; Delavar, M.A.; Dolati, A. Numerical investigation of melting process in phase change material (PCM) cylindrical storage considering different geometries. *Heat Transf. Res.* 2017, *48*, 1515–1529.

Chapter 4

4 Innovative research methodology for borehole heat exchangers

Innovative research methodology of borehole heat exchangers incorporating advanced materials for use as thermal energy storage (BTES)

Hossein Javadi[1*], Javier Fermín Urchueguía Schölzel[1], Borja Badenes[1], Ali Nejad Ghafar[2], Lenin Guillermo Lemus Zúñiga[1], Miguel Ángel Mateo Pla[1], Ojas Arun Chaudhari[2]

[1]*Institute of Information and Communication Technologies, Universitat Politècnica de València, Spain, hjavadi@upv.es*
[2]*RISE Research Institutes of Sweden, Sweden*

Nowadays, the benefits of combining phase change materials with borehole heat exchangers aiming at thermal energy storage have attracted a great deal of interest. Drilling costs, heat pump electricity consumption, and borehole thermal resistance can be reduced using backfill/grout materials with appropriate thermo-physical properties. The borehole's capability in storing thermal energy is likely to be enhanced by using the phase change materials, which decreases the temperature variation in the surrounding environment, reduces the required borehole depth, and improves the thermal performance of the whole system.

Keywords: Shallow geothermal energy, borehole thermal energy storage, phase change material, thermal performance

Fourth International Scientific Conference
"Alternative Energy Sources, Materials and Technologies (AESMT'21)"
14th June - 15th June 2021, Ruse, Bulgaria

Certificate of Participation

This is to certify that

Hossein Javadi

presented orally at AESMT'21 the paper

Hossein Javadi, Javier Fermín Urchueguía Schölzel, Borja Badenes, Ali Nejad Ghafar, Lenin Guillermo Lemus Zúñiga, Miguel Ángel Mateo Pla, Ojas Arun Chaudhari. Innovative research methodology of borehole heat exchangers incorporating advanced materials for use as thermal energy storage (BTES)

June 23 2021

Prof. Aleksandar Georgiev, PhD
Conference Chair

Javadi H, Urchueguia Scholzel JF, Badenes B, Nejad Ghafar A, Lemus Zúñiga LG, Mateo Pla MA, Arun Chaudhari O. Innovative research methodology of borehole heat exchangers incorporating advanced materials for use as thermal energy storage (BTES). ***Proceedings of 4th International Scientific Conference Alternative Energy Sources, Materials and Technologies (AESMT'21);*** *2021 June 14-15; Ruse, Bulgaria. (Presented orally).* ***Nivel C4.***

4.1 Introduction

Phase change materials (PCM) are useful for high-density energy storage as they can store thermal energy in the form of latent heat and have a good energy density. The thermal performance of the borehole thermal energy storage (BTES) can be enhanced considering that phase change materials' temperature is nearly fixed during the melting and solidification processes. Besides, the thermal radius around the borehole is likely to be decreased, which can minimize the required borehole field area [1-3]. The impact of applying paraffin as thermal energy storage inside/outside the borehole was studied theoretically [4]. The use of a mixture of lauric acid and n-decanoic acid as a backfill/grout in the single U-tube borehole heat exchanger was evaluated numerically [5]. Hydrate sodium sulfate was used numerically as thermal energy storage coupled to a borehole heat exchanger [6]. The application of shape-stabilized and microencapsulated phase change materials as backfill/grout materials in the single U-tube borehole heat exchanger was studied numerically [7-9]. The influences of using oleic acid for space heating and a mixture of lauric acid and decyl acid for space cooling as backfill/grout materials in the single U-tube borehole heat exchanger were examined experimentally and numerically [10]. The numerical simulation of using salt hydrate phase change material as thermal energy storage integrated with a borehole heat exchanger was conducted [11]. However, according to the background described above, it is quite clear that there have been just a few numerical studies on applying phase change materials in the borehole heat exchangers and that thermal energy storage application of borehole heat exchangers has not yet been explicitly investigated. In this work, the objective is to propose an advanced research methodology including experimental and numerical studies to comprehensively evaluate the borehole heat exchanger's potential as thermal energy storage.

4.2 Methodology

Two different types of studies will be carried out to analyze the borehole heat exchangers as thermal energy storage systems incorporating the phase change materials. In the numerical approach, the unsteady state three-dimensional numerical models of the borehole thermal energy storage system will be simulated numerically by commercial computational fluid dynamics (CFD) software. The models will be meshed by structured and unstructured meshing methods depending on each part of the system's geometry. The grid independence test will be performed, and the most suitable model will be selected based on the balance between accuracy and calculation speed. Since the numerical simulations are pressure-velocity coupling, the proper scheme and spatial discretization settings will be implemented for the solution methods. The conservation equations of continuity, energy, and momentum will also be taken into account. Based on the heat transfer fluid regime, a compatible viscous model will be chosen, and one of the best solidification/melting methods will be conducted to simulate the phase change process of the phase change materials. Moreover, influential variables, e.g., inlet flow and inlet temperature of the heat transfer fluid, volumetric heat capacity, latent heat, phase transition temperature, and thermal conductivity of phase change material, running time, that affect the thermal performance of the borehole thermal energy storage system will be assessed in detail to see how the system's efficiency can be enhanced.

Besides, experimental tests will be carried out to verify the outcomes achieved from the numerical study explained above. To accomplish this objective, at first, different kinds of materials will be tested in the laboratory to create two mixtures with good thermo-physical properties beneficial for the borehole thermal energy storage systems named improved grout and improved grout plus the phase change material. These mixtures will then be applied independently in two borehole thermal energy storage systems located at the field test site, comprised of the heat transfer fluid, U-tube pipe, backfill/grout, casing, and the soil, to study their influences on the thermal efficiency of the system. Thermal heat injection will be controlled by the use

of a proportional integral derivative (PID) controller, which leads to more accurate data compared to the conventional way, in which the power injection cannot be controlled, and the thermal effects of outdoor temperature and thermal dissipation through the pipes are not considered. Advanced electronic systems, temperature sensors, and measurement systems will be applied in the geothermal laboratory to better analyze the system operating.

4.3 Conclusions

In this research, a methodology is presented to examine the borehole heat exchanger's ability to store thermal energy when coupled to the phase change material. The need for field area and the deeper depth of drilling, and the electrical power consumption of the heat pump, will decrease by using the considered borehole thermal energy storage. Furthermore, the suggested design can improve the system's thermal efficiency and reduces the borehole's thermal resistance.

References

1. Javadi, H., S.S.M. Ajarostaghi, M.A. Rosen, M. Pourfallah. A comprehensive review of backfill materials and their effects on ground heat exchanger performance. *Sustainability* 10, 4486 (2018).

2. Javadi, H., S.S.M. Ajarostaghi, M.A. Rosen, M. Pourfallah. Performance of ground heat exchangers: A comprehensive review of recent advances. *Energy* 178, 207-233 (2019).

3. Tsagarakis, K.P., L. Efthymiou, A. Michopoulos, A. Mavragani, A.S. Anđelković, F. Antolini, M. Bacic, D. Bajare, M. Baralis, W. Bogusz, and S. Burlon, J. Figueira, M.S. Genç, S. Javed, A. Jurelionis, K. Koca, J. Ryżyński, J.F. Urchueguia, B. Žlender. A review of the legal framework in shallow geothermal energy in selected European countries: Need for guidelines. *Renewable Energy* 147, 2556-2571 (2020).

4. Rabin, Y., E. Korin. Incorporation of phase-change materials into a ground thermal energy storage system: theoretical study. *Energy Resources Technology* 118, 237-241 (1996).

5. Wang, J.L., J.D. Zhao, N. Liu. Numerical simulation of borehole heat transfer with phase change material as grout. *Applied Mechanics and Materials* 577, 44-47 (2014).

6. Zhu, N., P. Hu, Y. Lei, Z. Jiang, F. Lei. Numerical study on ground source heat pump integrated with phase change material cooling storage system in office building. *Applied Thermal Engineering* 87, 615-623 (2015).

7. Li, X., C. Tong, L. Duanmu, L. Liu. Research on U-tube heat exchanger with shape-stabilized phase change backfill material. *Procedia Engineering* 146, 640-647 (2016).

8. Li, X., C. Tong, L. Duanmu, L. Liu. Study of a U-tube heat exchanger using a shape-stabilized phase change backfill material. *Science and Technology for the Built Environment* 23, 430-440 (2017).

9. Chen, F., J. Mao, S. Chen, C. Li, P. Hou, L. Liao. Efficiency analysis of utilizing phase change materials as grout for a vertical U-tube heat exchanger coupled ground source heat pump system. *Applied Thermal Engineering* 130, 698-709 (2018).

10. Yang, W., R. Xu, B. Yang, J. Yang. Experimental and numerical investigations on the thermal performance of a borehole ground heat exchanger with PCM backfill. *Energy* 174, 216-235 (2019).

11. Alkhwildi, A., R. Elhashmi, A. Chiasson. Parametric modeling and simulation of Low temperature energy storage for cold-climate multi-family residences using a geothermal heat pump system with integrated phase change material storage tank. *Geothermics* 86, 101864 (2020).

Chapter 5

5 Investigation on developed grouting materials for borehole heat exchangers (BHE) and borehole thermal energy storage (BTES) systems

Laboratory and numerical study on innovative grouting materials applicable to borehole heat exchangers (BHE) and borehole thermal energy storage (BTES) systems

Hossein Javadi [a, *], Javier F. Urchueguía [a], Borja Badenes [a], Miguel Á. Mateo [a], Ali Nejad Ghafar [b], Ojas Arun Chaudhari [c], Giedrius Zirgulis [c], Lenin G. Lemus [a]

[a] Information and Communication Technologies versus Climate Change (ICTvsCC), Institute of Information and Communication Technologies (ITACA), Universitat Politècnica de València (UPV), Camino de Vera S/N, 46022, Valencia, Spain
[b] Implenia Sverige AB, Liljeholmsstranden 5, 117 43, Stockholm, Sweden
[c] RISE Research Institutes of Sweden, Department Instrastructure and Concrete Construction, Drottning Kristinas väg 26, 114 28, Stockholm, Sweden

ARTICLE INFO

ABSTRACT

In this study, a laboratory-scale prototype of a borehole field has been designed and built to assess various innovative grouting products in a fully controlled environment. Three novel grout formulations are developed and evaluated: enhanced grout, a mixture of enhanced grout and microencapsulated phase change material, and a mixture of enhanced grout and shape stabilized phase change material. The objective is to evaluate the enhancement in their thermal properties (i.e., thermal conductivity and thermal energy storage capacity) compared to those using a commercial reference grout. Besides, three-dimensional numerical modeling is performed to provide a better understanding of the heat transfer and phase transition inside and outside the grout columns and to study the capability of the developed grouts to be used in a borehole heat exchanger or as borehole thermal energy storage system. To the best of the authors' knowledge, there have been just a few numerical studies on using phase change materials inside borehole heat exchangers to assess thermal energy storage applications. The experimental and numerical results showed much higher efficiency of the grout developed with a high thermal conductivity than the reference grout in terms of heat transfer in both the grout column and the surrounding sand. Furthermore, the results indicated the noticeable influence of the microencapsulated phase change material's presence in the grout formulation in terms of heat absorption/storage during the phase transition (from solid to liquid). However, it is concluded that reengineering shape stabilized phase change material should be conducted to make it more appropriate for thermal energy storage applications.

Javadi H, *Urchueguia Scholzel JF, Badenes B, Mateo Pla MA, Nejad Ghafar A, Arun Chaudhari O, Zirgulis G, Lemus Zúñiga LG. Laboratory and numerical study on innovative grouting materials applicable to borehole heat exchangers (BHE) and borehole thermal energy storage (BTES) systems.* **Renewable Energy**. **Impact Factor: 8.634**. *Nivel R2*.

5.1 Introduction

Shallow geothermal energy (SGE) is becoming a key driver in the energy transition to a future without fossil fuels and promoting renewable energies. SGE can play a vital role in the reduction of CO_2 emissions from the building air-conditioning sector. The ground source heat pump (GSHP) falls into the SGE division, in which a borehole heat exchanger (BHE) is considered one of the main components [1–5]. The most widely developed underground thermal energy storage (UTES) systems are based on boreholes (borehole thermal energy storage (BTES)) or aquifers (aquifer thermal energy storage (ATES)) and are mainly applied for seasonal energy storage. Energy storage by ATES systems requires a suitable aquifer, where at least two thermal wells are installed. ATES systems extract groundwater from a well, exploit it energetically, and then re-inject it into the aquifer through another well. Furthermore, thermal energy can be stored underground employing BTES systems. BTES systems use the underground for storing thermal energy and are adaptable to almost any ground conditions. These systems consist of one or several boreholes to store energy underground for later use, in general seasonally, with several typologies, from single buildings to large-scale commercial buildings or district heating network systems coupled to a GSHP. BTES allows heat to be injected into the ground during the summer and extracted to satisfy the heating needs in the winter or vice versa [6,7].

To improve such systems and make them more cost-competitive for consumers, materials that enhance thermal storage in BHEs are currently being studied. Numerical analyses have been conducted to verify the impact of the use of phase change materials (PCMs) in geothermal borehole grouting, e. g. using a mixture of n-decanoic acid and lauric acid (DLC) [8], and found that the use of PCM has certain advantages over the use of standard grouting [9,10]. Thermal energy partial storage and release from changes in the PCM structure reduce the sensible heat exchange in the soil. [11]. The use of microencapsulated PCM (MPCM) could decrease the required BHE length (about 7%) when the thermal conductivities of the PCM and grout are close to each other for a given PCM melt temperature [12]. The use of PCM grouts with a thermal conductivity comparable to an ordinary grout has been observed to improve the efficiency and operational stability of a GSHP system [13,14], validated by experimental results [15]. Enhanced thermal performance is observed with the addition of PCM to the grout in different borehole configurations: coaxial ground heat exchangers (GHEs) [16], U-tube GHEs [17–19], horizontal GHEs [20–22], experimental GHEs [23–25], novel vertical air-soil heat exchangers (VASHEs) [26] or earth-to-air heat exchangers (EAHEs) ventilation systems [27]. The performance analysis of cascade PCM heat exchangers in geothermal district heating systems has also been carried out [28].

The use of thermal storage enhancers in BTES has also been generally analyzed, noting that the performance of the energy storage system can be significantly improved by incorporating PCM storage units [29] and its effect on the electric load shifting in building demand-side management [30]. The effect of the energy capacity of PCM during the charge–discharge phases with latent heat storage has also been analyzed [31,32], but the high-frequency intermittent mode might not be suitable for BHE with PCM backfilling [33]. Some examples of numerical modeling and energy simulations of GHEs are BHEs integrated with hydrated sodium sulfate as thermal energy storage (TES) [34], PCM-Sand mixture ring around the borehole wall of a BHE [35], PCM containers implemented in building foundation piles as a BHE [36,37]. Additionally, family residences using a GSHP system integrated with a PCM storage tank [38], MPCM slurry as the working fluid in a tree-shaped BHE [39], and partially charging and discharging a PCM TES tank in a commercial building [40]. Also, two examples of PCM usage in the horizontal GHE include horizontal GHE integrated with the panel form of PCM as TES [41] and horizontal GHE integrated with microencapsulated paraffin and soil as TES [42]. Also, two kinds of PCMs have been evaluated for latent heat thermal energy storage (LHTES) applications [43].

Nevertheless, considering the past articles being studied, there have been only a few numerical studies on implementing PCM in the BHEs, and the TES application of BHEs has not yet been explicitly examined. Therefore, in this research, two laboratory tests, including single-column and four-column tests, have been conducted to evaluate various grouting materials that can be used in the BHE or BTES systems. In the first test, a single grout column containing a reference grout (commercial grout) is examined to learn more about the system's behavior, the potential defects, solutions, and verification of the numerical modeling. In the second test, four grout columns backfilled with different materials such as reference grout, enhanced grout, enhanced grout with MPCM, and enhanced grout with shape stabilized PCM (SSPCM) were simultaneously tested to provide the same conditions for all grout columns. Moreover, 3D numerical simulation of the two laboratory tests is conducted to understand better the heat transfer and phase transition occurrence inside the sandbox.

5.2   Laboratory test

The laboratory test was principally based on the circulation of a heat carrier fluid with the constant temperature inside a pipe centrally located in a sandbox's grout column. The grout thermal conductivity variation used in the grout column are reflected in different temperature field changes inside and outside the column, which were measured using different sets of thermocouples. Each grout column was placed in the sand which was compacted using water and then completely drained out to simulate soil conditions like a BHE/BTES system. The sand was chosen due to simplicity in handling (the box was filled and unloaded using shovels) and economic reasons [44,45]. Also, the compaction with water procedure assumingly created the same soil density, water saturation, and thermal properties around columns. Thermo-physical properties were measured once based on the same assumption. The grout columns used in the experiments are 190 mm in diameter and 1000 mm in height. A single Polyethylene (PE) pipe with 20 mm in diameter was located in the center of each column for heat injection through water circulation. Although the test setup is larger than bench laboratory tests, the grout columns' heights are still small compared to the real borehole. This test did not reflect reality fully; instead, it created controlled conditions focused on grout thermal performance and temperature distribution around the heat source (pipe). The single pipe was chosen for the sake of simplicity as a heat injector. The circulation fluid temperature was varied between 20 °C to 50 °C to trigger the temperature field change. The temperature range was chosen on the basis of the PCMs' melting and crystallization temperatures (sufficiently high and low than the phase transition temperatures), which was planned to be used in the laboratory test.

5.2.1   Description of the laboratory test

In this study, the sandbox was used in the test rig was built on two wooden pallets to provide a flat and firm basis for safe transportation (Figure 5-1a). The sandbox walls were made of 12 mm laminated water-resistant plywood sheets, which are widely used to prepare concrete molds in the building industry. The supporting frames were made of 100×50 mm wood boards to prevent any potential deflection in the walls. The sandbox was then completely insulated (from all sides) with 100 mm styrofoam thermal panels (see Figure 5-1a). A circulation pump was used to circulate the heat carrier fluid (i.e., water) within the system. An open surface water tank (60-liter plastic container) with a heater was employed in the test setup to provide the designated constant temperature in circulating water along with the experiments. The temperature of water in the heating phase (heat from 20 °C to 50 °C and maintain a constant level) was controlled by a digital thermostat and a 2 kW heater. To provide the possibility of heating and cooling for the circulating water (without changing the test setup), the water tank, with the installed heating system, was placed in a cooling chamber. To allow cool-down in the cooling phase, as shown in Figure 5-1b, (reduce the water temperature from 50 °C to 20 °C and

maintain in constant level), the water tank was placed in a cooling chamber with a temperature set to 0 °C (work in continuous mode). The water tank's heating system (including a heater, a digital thermostat, and a temperature sensor) was kept operational during the cooling phase to prevent water from overcooling. Moreover, the molds used for casting the grout columns are cardboard molds, which could be used for casting concrete foundations. The cardboard molds' inner walls were covered with plastic tape to prevent moisture loss from the fresh grout mix (Figure 5-2a). The PE pipe was placed in the mold's center and secured with two metal lids (Figure 5-2b). Besides, a metal bar was placed inside the pipe during the setting time to support the PE pipe and keep it straight while the grout was still in fluid form.

(a)   (b)

Figure 5-1: The single-column test rig: (a) The sandbox, cooling chamber, and data acquisition system, and (b) Water tank with a mounted heating system inside the cooling chamber.
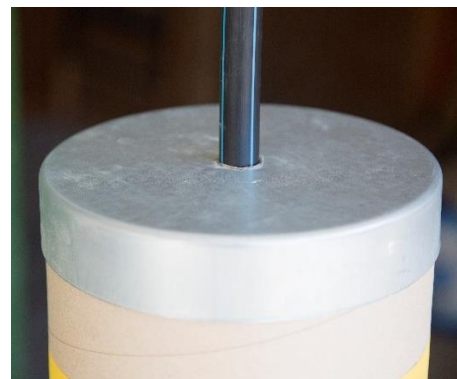
(a)   (b)

Figure 5-2: Grout column used in the tests: (a) Cardboard mold fixed on a wooden pallet and the inner mold surface covered by plastic tape, and (b) Metal lid used to center the PE pipe.

5.2.2 Mixing, casting, and curing of the developed grouting materials

A twin shaft handheld mixer was used in this study to obtain a proper dispersion of the solid particles in the grout suspension during the mixing process. A mixer with a maximum rotation speed of 950 rpm was applied in all mixing processes. The dual propellers rotating in opposite directions apply sufficient shear to provide the required dispersion. The mixing procedure was kept the same for all five grout columns (single- and four-column tests) as follows:

- The dry component was poured in a plastic container and premixed in dry conditions with the same mixer (with low speed).

- The required water (the amount of water needed for one gout column) was poured into another plastic container.

- The dry mixed components were slowly added to the water while mixing at a low speed for about 2 min.

- The primary mixing was then continued for about four more minutes, resulting in 6 min of the mixing process in total.

The casting process of each grout column was performed manually by filling the mold (Figure 5-3a) through a funnel with an attached hose. The end of the hose reached the bottom of the mold to provide the possibility of bottom-up filling. After demolding, the grout columns were wrapped in plastics and filled with water for curing for up to 28 days (Figure 5-3b). Two grout formulations were used to prepare the grout columns in this research, with and without PCM. All the quality control tests were performed on fresh grout, e.g., wet density test, marsh cone test, the flow table test, and bleeding test. Furthermore, quality control tests were also conducted for the hardened grout, including a compressive strength test, thermal conductivity test, and latent heat test (only on the grout with PCM).

(a)

(b)

Figure 5-3: Casting and curing of the grout columns: (a) Filling the grout through the funnel, and (b) Curing the grout columns.

5.2.3 Single-column test

2D schematics, the geometrical parameters, and a picture of the sandbox in the single-column test are shown in Figure 5-4. The sandbox was a thermally insulated cubic box with a 1000 mm edge length, comprising one column with 190 mm in diameter placed in the center of the box. The column consisted of circulation fluid, single pipe, reference grout, and silica sand, which was previously fully saturated with water to provide sufficient compaction and then drained out. The circulation fluid entered at the top of the PE pipe with 1000 mm length and exited from the bottom. In this test, a flow rate of 1800 liter/h was considered for the circulating fluid to assure turbulent flow conditions. Thermo-physical properties of the sandbox and geometry details, simulation conditions, and thermocouple positions for the first test are presented in Table 5-1 and Table 5-2, respectively.

(a)

(b)

(c)
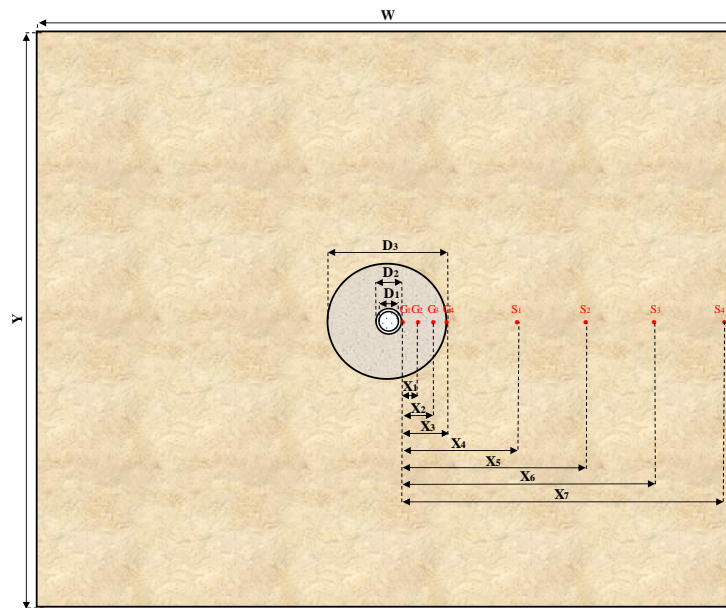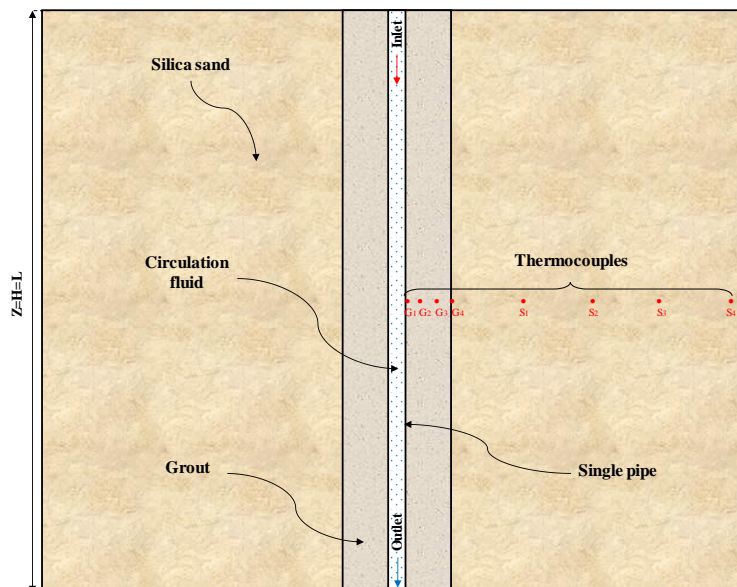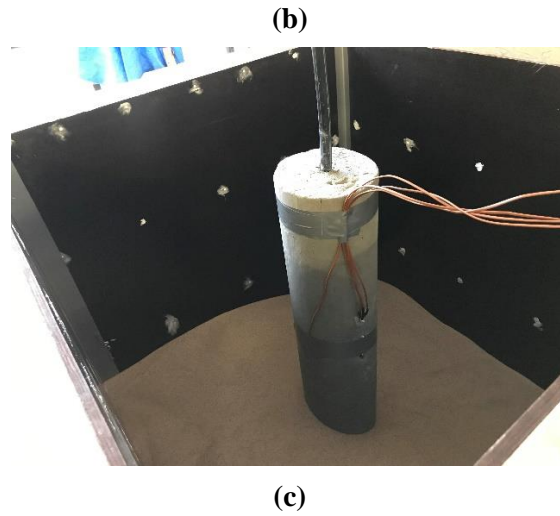
Figure 5-4: 2D schematics, the geometrical parameters, and the picture of the sandbox in the single-column test: (a) Top view, (b) Front view, and (c) The grout column installed in the box filled with silica sand.

Table 5-1: Thermo-physical properties of the sandbox.

Material		Thermal conductivity (W/(m·K))	Density (kg/m³)	Specific heat capacity (J/(kg·K))	Latent heat (kJ/kg)	Phase transition temperature (℃)
Circulation fluid (Pure water)		0.6	998	4260	-	-
Pipe (Standard PE 100)		0.421	960	2600	-	-
Grout	Reference grout	2	1520	750	-	-
	Enhanced grout	2.7	2000	800	-	-
	Enhanced grout + MPCM	1.025	1510.00	1593.15	24.36	23.5–28.8
	Enhanced grout + SSPCM	2.17	1760.00	1959.12	25.00	20-30
Silica sand		2.65	2647	830	-	-

Table 5-2: Geometry details, simulation conditions, and thermocouple positions.

Parameters	Value	Unit
Sandbox, W×Y×Z	1000×1000×1000	mm³
Pipe length, L	1000	mm
Pipe inner diameter, D_1	16	mm
Pipe outer diameter, D_2	20	mm
Grout column diameter, D_3	190	mm

Grout column depth, H				1000	mm
Insulation wall thickness, I_1				40	mm
The initial temperature of the circulation fluid				20	°C
Flow rate				1800	liter/h
Thermocouples distance from the surface of the pipe (G_1 at the surface)	X_1	28	X_8	28	mm
	X_2	56	X_9	56	mm
	X_3	86	X_{10}	84	mm
	X_4	185	X_{11}	159	mm
	X_5	285	X_{12}	234	mm
	X_6	385			mm
	X_7	485			mm
Thermocouples distance from the bottom of the sandbox, I_2				500	mm

In the test setup, the temperature field in the sandbox (inside and around the grout column) was measured using several thermocouples located at various distances from the center of the grout column (Figure 5-4a,b). As illustrated in the figures, in the single-column test, eight temperature sensors (G_1, G_2, G_3, G_4, S_1, S_2, S_3, and S_4) were installed inside the sandbox to measure the temperature at various distances at a depth of 500 mm. The first thermocouple was attached to the surface of the centrally located pipe. The thermocouples in each grout column were secured in position along with a wooden stick using cable ties so that the heat transfer in the grout column was not significantly affected (Figure 5-5).

Figure 5-5: Thermocouples with waterproof covers and a wiring system were fixed in position along with a wooden stick.

5.2.4 Four-column test

In the four-column test, the test setup is slightly modified to perform the test with the four grout columns simultaneously as described below:

- Grout column 1 made of a commercially available grout as a reference

- Grout column 2 made of grout with high thermal conductivity

- Grout column 3 made of grout with high thermal conductivity and high thermal storage capacity by incorporation of MPCM

- Grout column 4 made of grout with high thermal conductivity and high thermal storage capacity by incorporation of SSPCM

Figure 5-6 depicts 2D schematics and the geometrical parameters of the sandbox in the four-column test. The sandbox was divided into four sections using 40 mm extruded polystyrene insulation plates to accommodate all four grout columns in the set. Accordingly, two of the four thermocouples installed in the sand around the grout column in the single-column test must be discarded, applying two thermocouples with smaller distances. Therefore, as shown in Figure 5-6a,b, six temperature sensors of G_1, G_2, G_3, G_4, S_1, and S_2 were installed inside each section of the sandbox to obtain the temperature data at various distances at a fixed depth of 500 mm. Thermo-physical properties of the sandbox and geometry details, simulation conditions, and thermocouple positions for the second test are given in Table 5-1 and Table 5-2, respectively. Note that there was a relative error of up to 10% in the thermo-physical properties of the developed grouting materials measured in the laboratory. In this setup, similar PE pipes (with the same diameter) were applied in four grout columns as used in the previous test. The flow rate of 1800 liter/h is calculated based on circulation pump technical data and divided between four pipes/columns; nevertheless, the fluid flow regime is still turbulent in all four columns. To reduce the possibility of moisture loss in the sand (and consequently the possibility of change in the sand thermal conductivity in time during the test), the inner walls of the test box were covered with plastic. As in the previous test, the box was filled with silica sand after installing the grout columns. Afterward, the sand was compacted using water and then completely drained out (Figure 5-7a). The centrally located PE pipes in the grout columns were symmetrically connected with the brass fittings to connect the grout columns to the circulation pump, ensuring similar flow rates in all four grout columns (Figure 5-7b). Also, all pipes and hoses were thermally insulated.
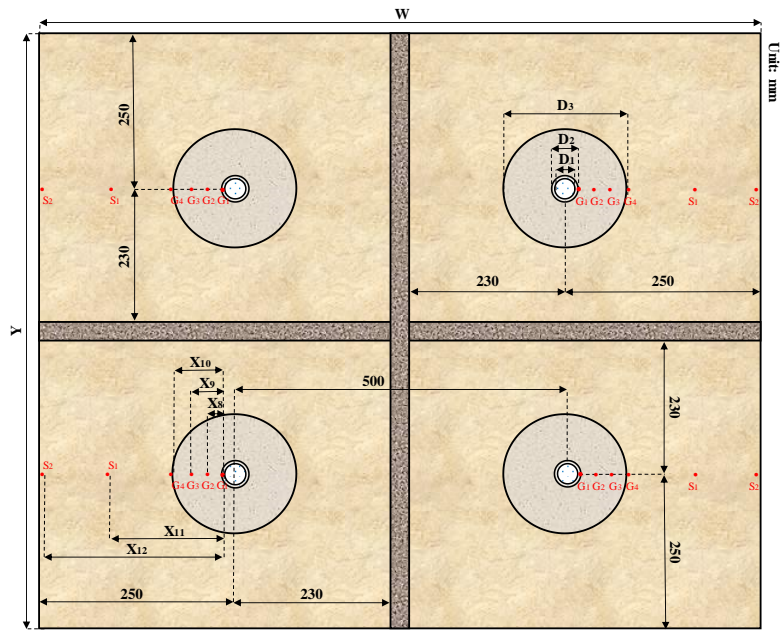
(a)
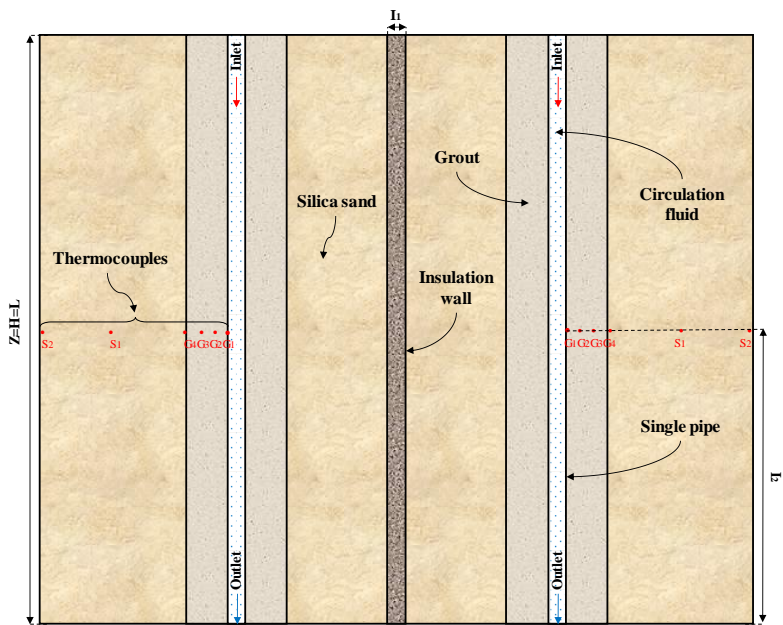
(b)

Figure 5-6: 2D schematics and the geometrical parameters of the sandbox in the four-column test: (a) Top view, and (b) Front view.

<div align="center">(a)   (b)</div>

Figure 5-7: The four-column test setup: (a) Four separated columns filled with sand and saturated with water, and (b) Connection of the grout columns to the circulation pump.

5.3 Numerical simulation

In the numerical approach, a 3D unsteady numerical model of the sandbox is simulated by using Ansys Fluent 18 software. The most common commercially available CFD programs technique is the finite volume method (FVM) applied in this numerical modeling. FVM is efficient in conserving the continuity, momentum, and energy equations, even in coarse grids. Besides, FVM benefits memory usage and speed in turbulent flow computation, higher speed flows, vast geometries, etc. Since the sandbox was thermally insulated in both tests, including the single-column and four-column tests, the insulation walls (outer walls) were considered adiabatic in the numerical simulation. Additionally, in the four-column test, where the sandbox was divided into four sections by the insulation plates, these walls were also selected as adiabatic walls. Moreover, the contact thermal resistance of different interfaces is insignificant, and all joints of the components were considered temperature-coupled walls when modeling the tests numerically. A velocity-inlet condition with a constant velocity and variable temperature is set for the inlet boundary, and a pressure-outlet condition is chosen for the outlet boundary. The circulation fluid flow inside the pipe is incompressible and forced. The circulation fluid and sand are assumed to be temperature independent, isotropic, and homogeneous. Given that the Reynolds number of the fluid circulating inside the pipe for both tests is in the turbulent regime range, a standard k-epsilon turbulence model is selected. Moreover, the velocity-pressure condition is fulfilled using the SIMPLE scheme. Worth mentioning that the numerical outcomes have been achieved using a desktop computer equipped with a 3.20 GHz seven-core processor (Intel® Core™ i7-8700 CPU) and 16.0 GB RAM with a time step of 30 s. The residuals for the energy, continuity, momentum, epsilon, and k equations are less than 10^{-6} when the convergence occurred.

5.3.1 Governing equations

In this numerical simulation, the enthalpy-porosity method [19] is applied to simulate and solve the heat transfer process of columns backfilled with PCM. The conservation equations are presented below:

Continuity equation:

$$\nabla \cdot (\rho_{CF} \, \vec{v}) + \frac{\partial \rho_{CF}}{\partial t} = 0 \tag{1}$$

Momentum equation:

$$\nabla \cdot (\rho_{PCM} v_i \vec{v}) + \frac{\partial(\rho_{PCM} \vec{v})}{\partial t} = \rho_{PCM} g_i - \frac{\partial \rho_{PCM}}{\partial x_i} + \nabla \cdot (\mu_{PCM} \nabla v_i) + S_i \tag{2}$$

$$S_i = C_{mush} (v - v_p) \frac{(1-\beta)^2}{(\beta^3 + \varepsilon)} \tag{3}$$

where $\vec{v}$ is the velocity vector, v_i is the velocity component in the i direction, v is the circulation fluid velocity, and v_p is the velocity of the solidified material moving throughout the computational cells during the phase transition. ρ_{CF} and ρ_{PCM} show the densities of circulation fluid and PCM, respectively. S_i is the source term, which shows the relevance of the momentum and porosity in the mushy zone and considers the pressure drop created from the existence of solid material. C_{mush} and ε are known as the constants of mushy zone and computation, respectively [19].

Energy equation:

$$\nabla \cdot (\rho_{PCM} h_t v) + \frac{\partial(\rho_{PCM} h_t)}{\partial t} = \nabla \cdot (\lambda_{PCM} \nabla T) + S_e \tag{4}$$

where λ_{PCM} is the thermal conductivity of PCM, S_e is the source term, and h_t is the total enthalpy of PCM calculated by summating latent heat enthalpy (h_{lat}) and sensible heat enthalpy (h_{sens}), as given below:

$$h_t = h_{lat} + h_{sens} \tag{5}$$

$$h_{lat} = \sum_{i=1}^{n} \beta_i L_f \tag{6}$$

$$h_{sens} = h_{ref} + \int_{T_{ref}}^{T} C_p dT \tag{7}$$

where L_f is the latent heat of PCM and β is the liquid fraction that presents the liquefaction level of PCM, which can be expressed as

$$\beta = \begin{cases} 0 & T \leq T_{solidus} \\ \dfrac{T - T_{solidus}}{T_{liquidus} - T_{solidus}} & T_{solidus} < T < T_{liquidus} \\ 1 & T \geq T_{liquidus} \end{cases} \tag{8}$$

5.3.2 Grid independence test

In the numerical approach, two types of grids have been applied to perform the numerical model's meshing, including hexagonal structured and tetrahedral unstructured grids. In the structured meshing, the points of an elemental cell are marked by triple indices (i, j, k) in a 3D simulation, where the central cell is joined by six adjacent cells. Hence, the connectivity is straightforward when using a structured method, leading to easy data management and programming, high-quality solutions, and better convergence with fewer elements than unstructured meshing. Alternatively, in the unstructured meshing, the cells are placed freely inside the computational domain. Consequently, unstructured meshes are efficient for modeling more complex geometries. To evaluate these alternatives, both methods have been used to generate the most suitable grids of

the model. The schematic of the meshed model is illustrated in Figure 5-8. As can be seen, the volumes near the grout column center have been meshed with finer elements compared to the other volumes, as they are of high importance in the heat transfer process. Moreover, the interfaces between each circulation fluid and pipe, pipe and grout, and grout and sand, were meshed with a four-layer boundary mesh with a transition ratio of 0.15 (see Figure 5-8a). The maximum skewness and minimum orthogonal quality values achieved were 0.39 and 0.8, respectively. Table 5-3 shows the grid independence test conducted for the column containing the reference grout by generating four cases ranging from a coarse mesh to a fine mesh. The created models have been compared in terms of heat exchange rate per meter of grout column depth at the pipe radius after 96 h of operation. By considering the computational speed and accuracy, the third mesh (case 3) is selected for further numerical investigations.

Table 5-3: Grid independence test.

	Case 1	Case 2	Case 3	Case 4
Elements' total number	428,437	795,169	1,129,328	1,564,718
Heat exchange rate per meter of grout column depth at the pipe radius after 96 h of operating [W/m]	212.72	213.39	213.84	213.81

(a)

(b)   **(c)**
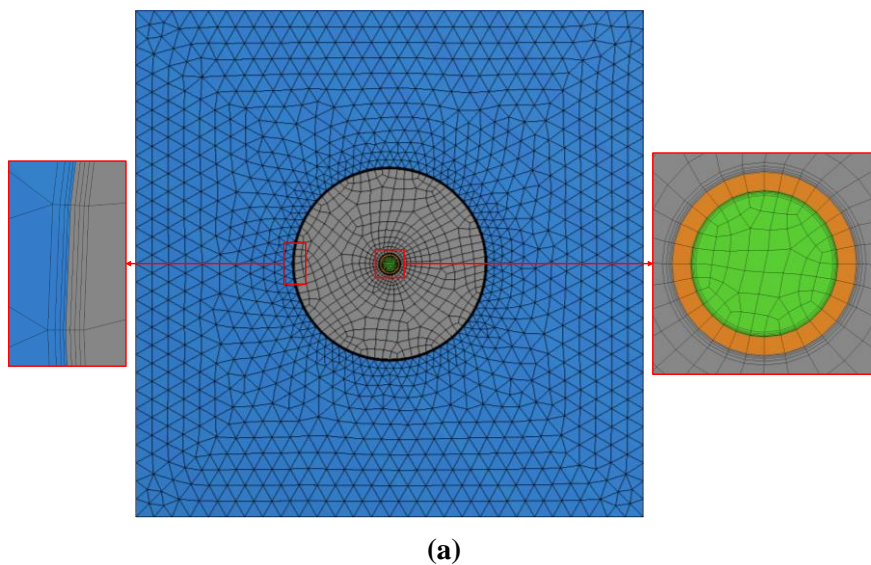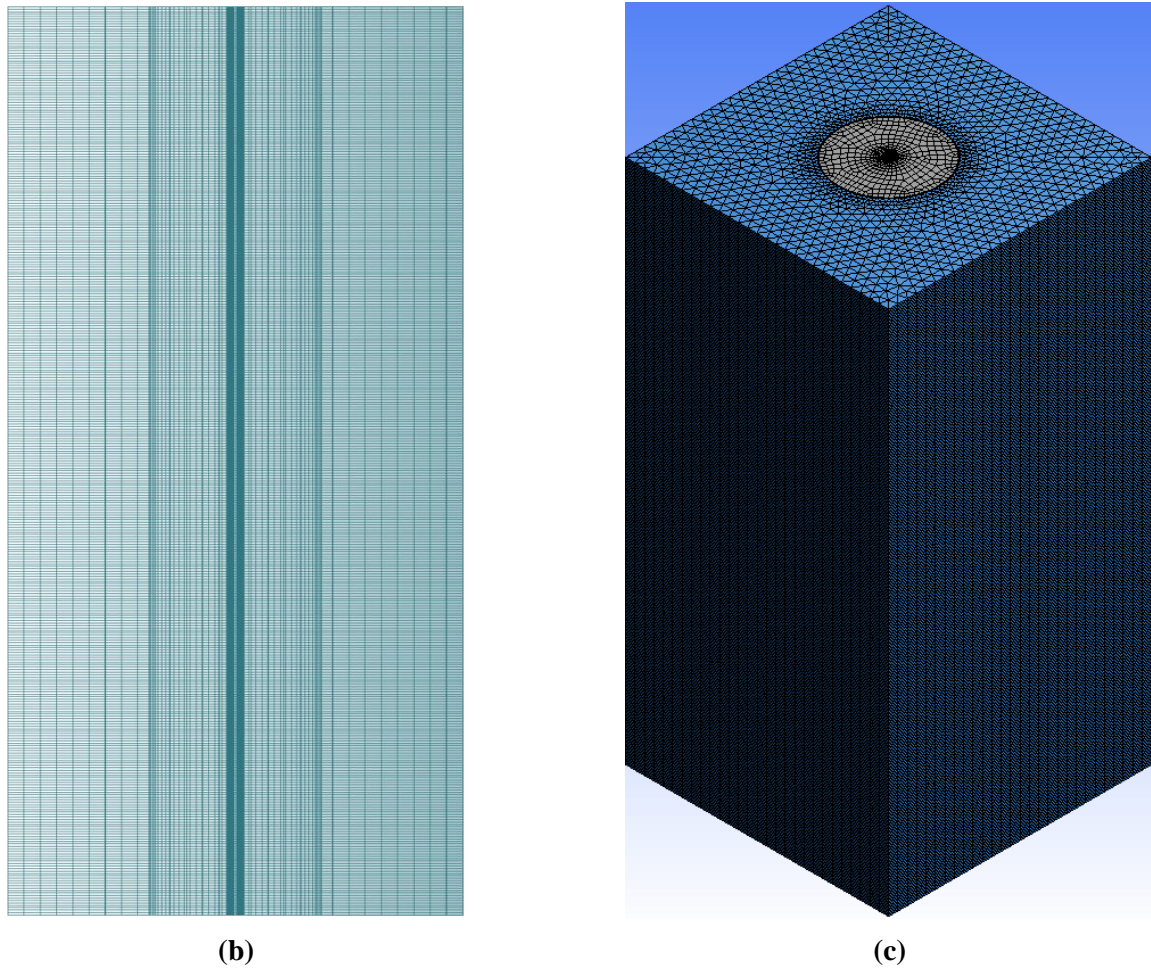
Figure 5-8: The meshing of the model: (a) Top view, (b) Front view, and (c) 3D view.

5.4   Results and discussion

5.4.1   Single-column test (Verification)

The variation of the temperature versus time for the measurement points in the single-column test using experimental and numerical approaches is presented in Figure 5-9. The figure shows the temperature response of the grout column and the surrounding sand to the heating of circulating fluid from 20 °C to 40 °C and 50 °C and then cooling down to 20 °C. It can be seen that there is an appropriate agreement between the measured and simulated results, which shows the accuracy and reliability of numerical modeling. As illustrated in Figure 5-9, in the temperature variation of G_1 to G_4 during the first 5 h, the temperature difference between G_1 and inlet temperature (approximately 4 °C) can be related to the low heat transfer efficiency between the circulation fluid and the outer surface of the pipe, where the first temperature sensor (G_1) is located. Considering that this temperature loss is not as high as other temperature losses in the figure (in the same period), one can infer to what extent a pipe with higher thermal conductivity can improve the system's thermal behavior. Alternatively, the high-temperature difference between G_1 and G_2 in the first 5 h (approximately 8 °C) and in only 28 mm distance in the grout, compared to the lower differences between G_2-G_3 and G_3-G_4 (approximately 2.5 °C) can be related to the significant influence of the grout-pipe interface. Similar behavior (but with lower intensity)

90

can be seen at the grout-sand interface, highlighting the importance of interfaces, especially the grout-pipe interface, on the system's overall thermal behavior.
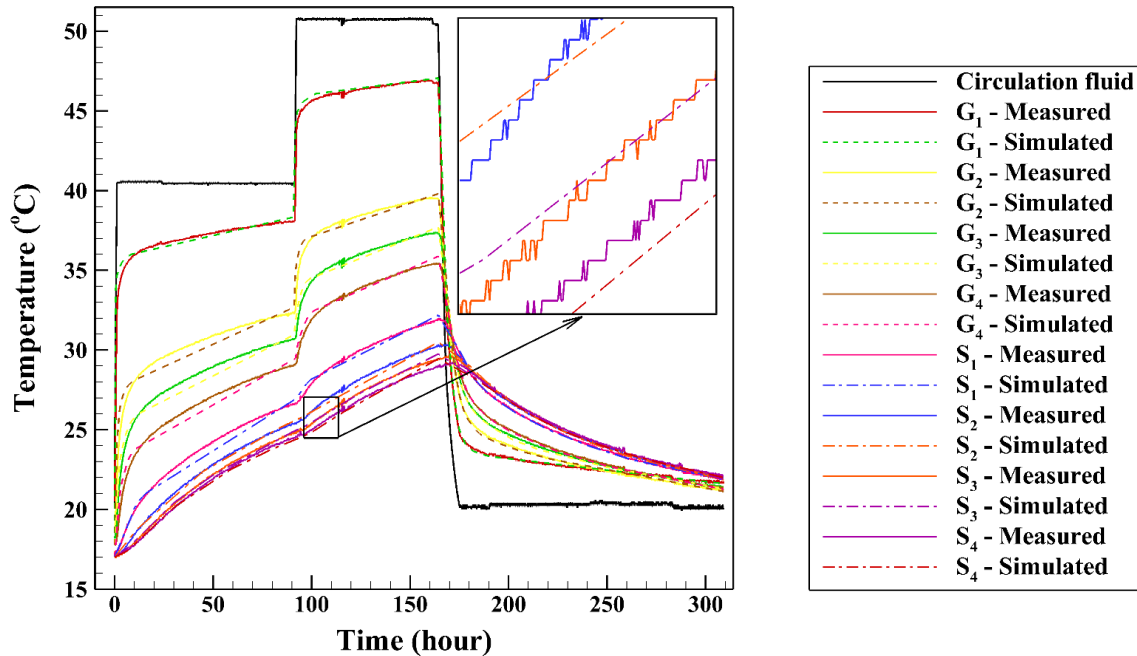
**Figure 5-9: Variation of the temperature versus time for the measurement points in the single-column test using experimental and numerical approaches.**

5.4.2   Four-column test (Comparison)

One complete cycle of heating and cooling with temperature variations from 20 °C to 50 °C and then back to 20 °C have been applied to the circulating fluid during the test. The four grout columns used in the setup include a reference grout (commercial grout) and three newly enhanced grouts with high thermal conductivity (using graphite-based materials) and high TES capacity (using MPCM and SSPCM). The idea is to ensure as similar test conditions as possible for the four grout columns to allow a proper comparison between their thermal behavior to show the newly developed grouts' efficiency.

Figure 5-10 illustrates the time - dependent temperature field distribution in the four-column test during one complete cycle. The column containing enhanced grout reaches the temperature levels faster than the other grout columns in the heating operation, thanks to its high thermal conductivity. This time difference between the enhanced grout and the others is quite significant at the temperature level of 45 °C almost after 60 h of heat injection. Similarly, in the cooling operation, when decreasing the circulation fluid temperature from 50 °C to 20 °C, thermally enhanced grout cooled down earlier than the other grouting materials. In contrast, the mixture of enhanced grout and MPCM reached the temperature levels later than the others, specifically at the temperature level of around 30 °C, near the range of phase transition temperature of MPCM. This effect can be explained by the presence of MPCM in the enhanced grout mixture and the corresponding increase in its heat capacity. However, after the complete melting of the MPCM particles, which occurs around 20 h after the start of heat injection, the mixture cannot store more thermal energy, and accordingly, it dissipates the heat to the surroundings. In cooling operation, like in heating mode, it takes longer for the mixture of MPCM and enhanced grout to reach lower temperature levels compared to the rest of grout materials, especially at the

91

temperature level of 23 °C. The reason that no such behavior is observed in the grout column with SSPCM can be related to the broader range of phase transition temperatures of the SSPCM compared to the MPCM.

Figure 5-11 shows the comparison of the thermocouples' thermal responses during the full duration of heat injection between the different grout columns. Each plot corresponds to a given sensor location. In the first measurement point (G_1), which is located on the PE pipe's surface, no significant difference is observed between the temperatures registered during the 30 h in the four grout columns. However, sensor located farther away (i.e., at G_2, G_3, and G_4), show increasingly larger temperature differences. At the same measurement points (G_2, G_3, and G_4), the highest temperature registered is usually in the grout column with high thermal conductivity (enhanced grout), whereas the lowest temperature is in the one with MPCM. This issue is once again related to the heat absorption of the PCM particles during the phase change (solid to liquid) that hindered the temperature increase. However, after approximately 17 h, when the temperature at G_4 increased to 28.8 °C (the peak transition temperature of MPCM), all the MPCM particles incorporated in the grout column are already subjected to phase transition. Accordingly, there is no further hindrance against the increase in temperature, and thus the temperature gradient registered at G_4 increases afterward. Similar behavior is observed in the grout column with SSPCM after approximately 6 h when the temperature at G_4 reached 24 °C (to the peak transition temperature of SSPCM). This matter suggests that most of the SSPCM incorporated in the grout column are subjected to the phase change (solid to liquid) at nearly 24 °C. Following that, the temperature gradient registered at G_4 is considerably increased. The intersection points of the horizontal line (chosen as 24 °C and 28.8 °C, i.e., the melting points of SSPCM and MPCM, respectively) and the graphs of the temperature variation registered at each measurement point in different grout columns indicate the time difference needed to reach the same temperature at a certain distance from the circulating pipe when various grouting materials are applied. As shown in the same figure, the longer the distance from the pipe in the grout column, the longer the time needed to reach the same temperature in different grout columns. At G_4, the time difference to reach 28.8 °C between the grout column with enhanced grout and the grout with MPCM is more than 10 h. This issue can be related to the faster heat transfer in the grout column with enhanced grout compared to the combined delays caused by the phase change and the lower thermal conductivity of the MPCM. Figure 5-12 shows the time needed for various thermocouples in different grout columns to reach the same temperatures of 21 °C, 28.3 °C, 35 °C, and 40 °C during the heating process. In all cases, the shortest time for reaching the desired temperature was seen in the column with enhanced grout and the longest time in the grout column containing MPCM with enhanced grout. This issue supports the observations previously presented in Figure 5-11.

Worth mentioning that these time differences created in four grout columns can bring advantages or disadvantages to the GSHP system, depending on the system's goal. Thermally enhanced grout in a BHE will benefit the GSHP performance aimed at conventional heating and cooling by increasing the heat transfer at the shortest time to or from the surrounding ground during heat dissipation or extraction, respectively. However, the use of enhanced grout will not be a good idea when the system is targeted at storing energy. Here is when the MPCM grout can play a vital role in the BTES system because of its higher heat capacity and lower thermal conductivity than reference and thermally enhanced grouts. Therefore, the MPCM particles will not be suitable for typical heating and cooling operation, as they are practical for storing the thermal energy and reusing it daily or seasonally, not thermal exchanging with the surroundings.
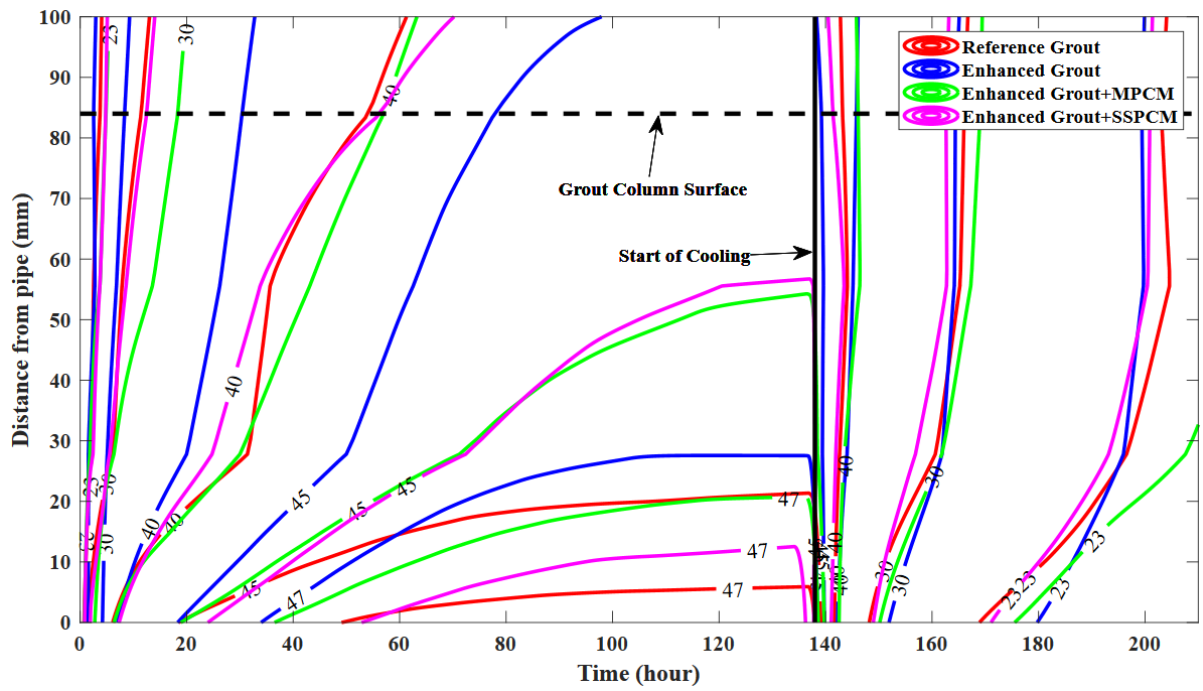
Figure 5-10: Temperature field distribution in the four-column test at different operation hours during one complete cycle.
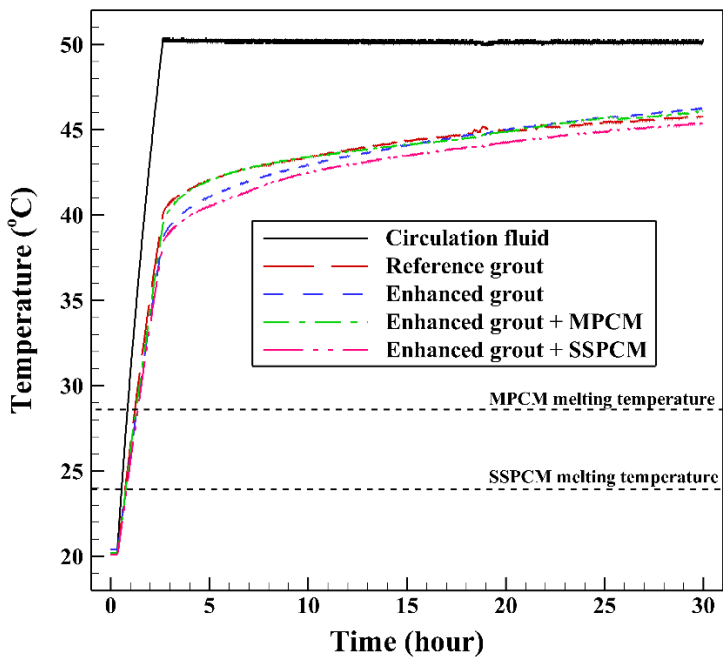

(a)
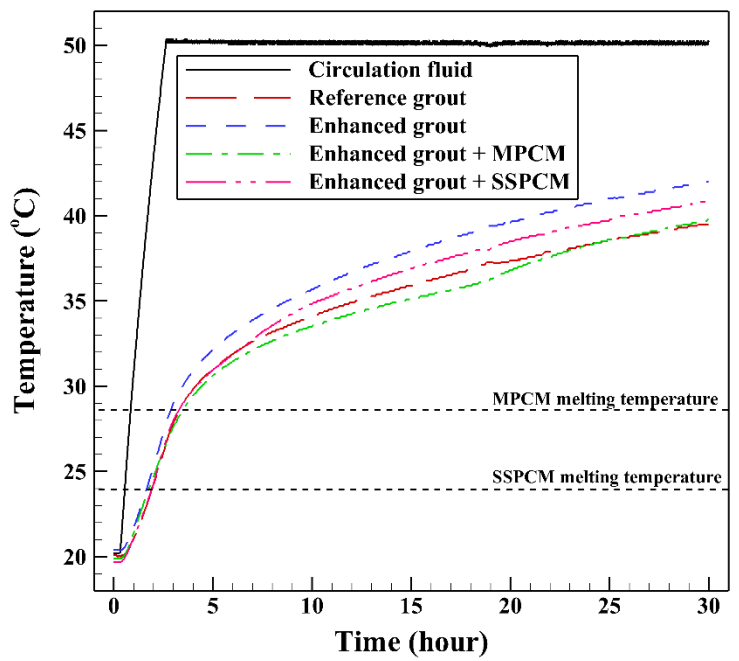
(b)
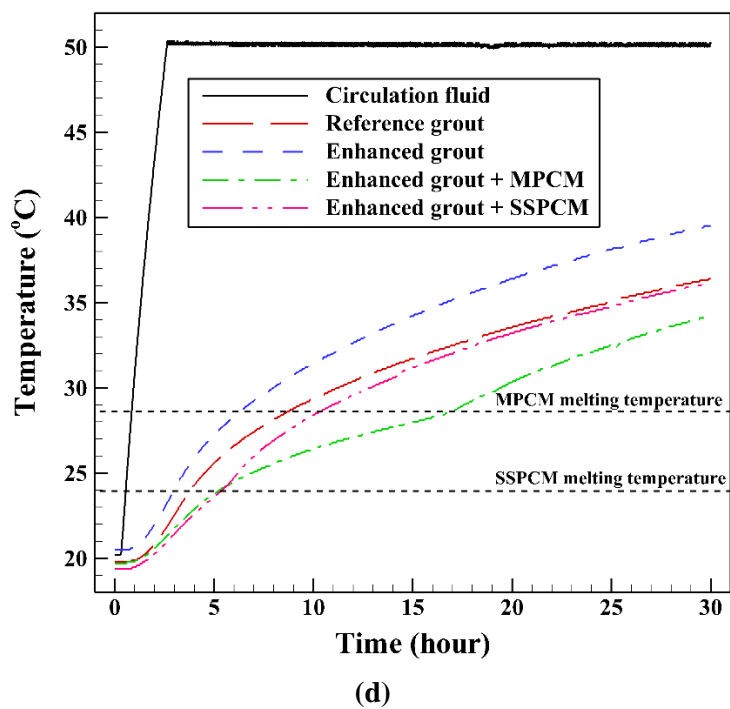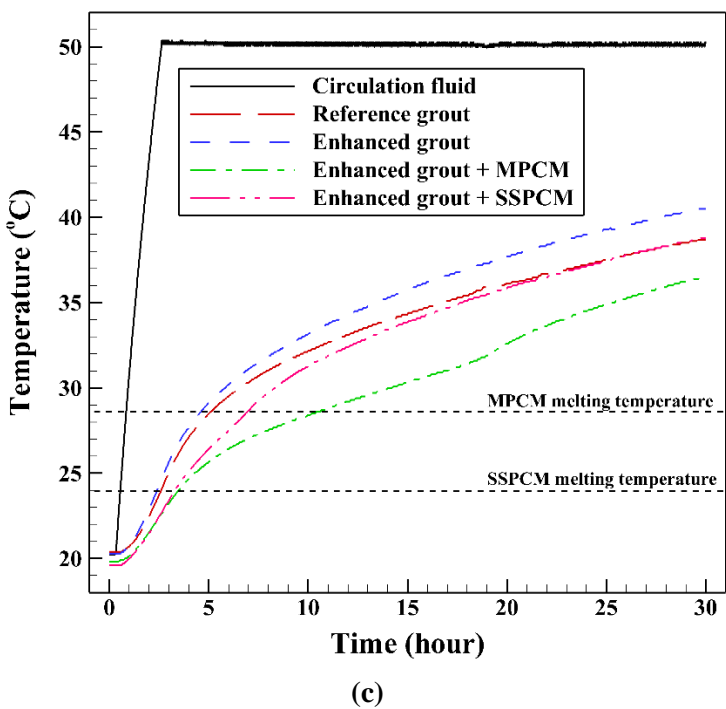
Figure 5-11: Comparison of the thermocouples' thermal responses during the 30 hours of the heat injection from 20 °C to 50 °C to different grout columns: (a) G$_1$, (b) G$_2$, (c) G$_3$, and (d) G$_4$.
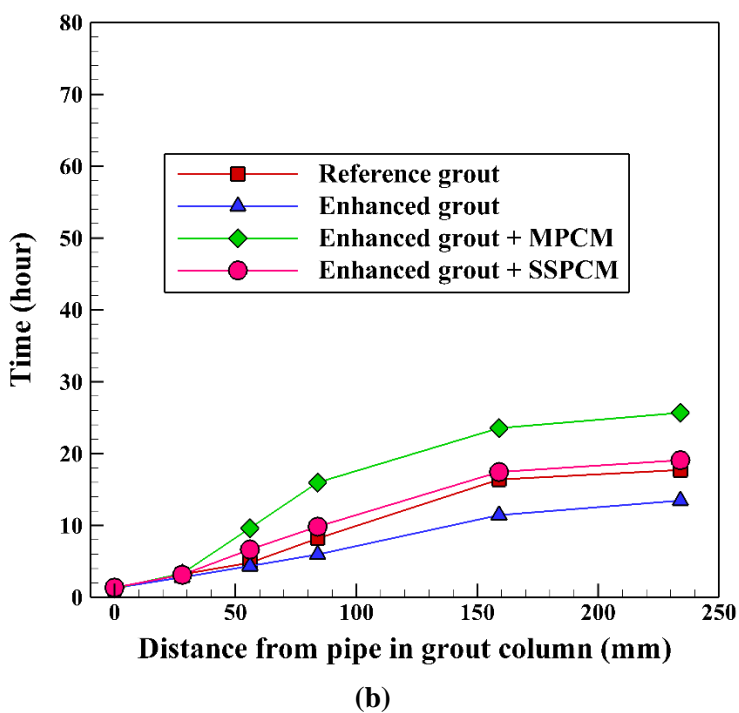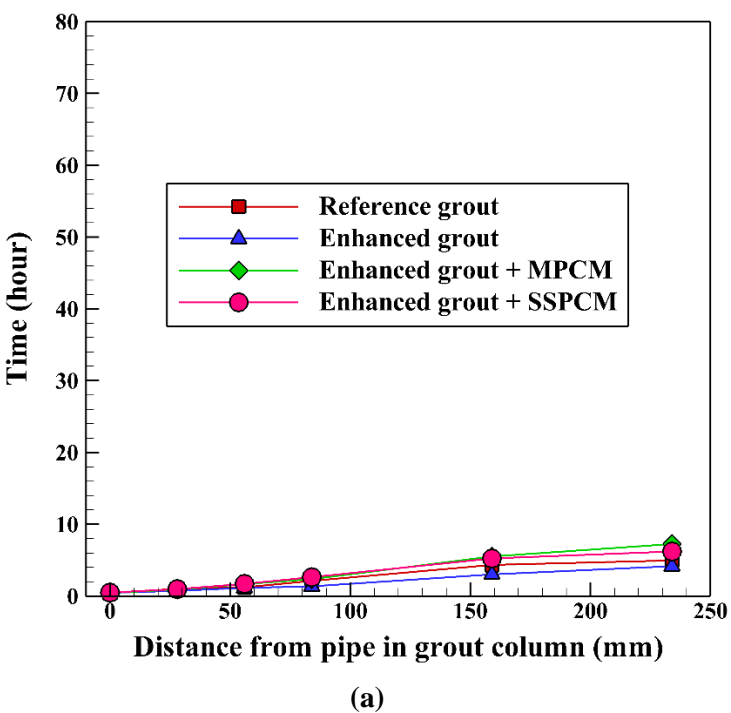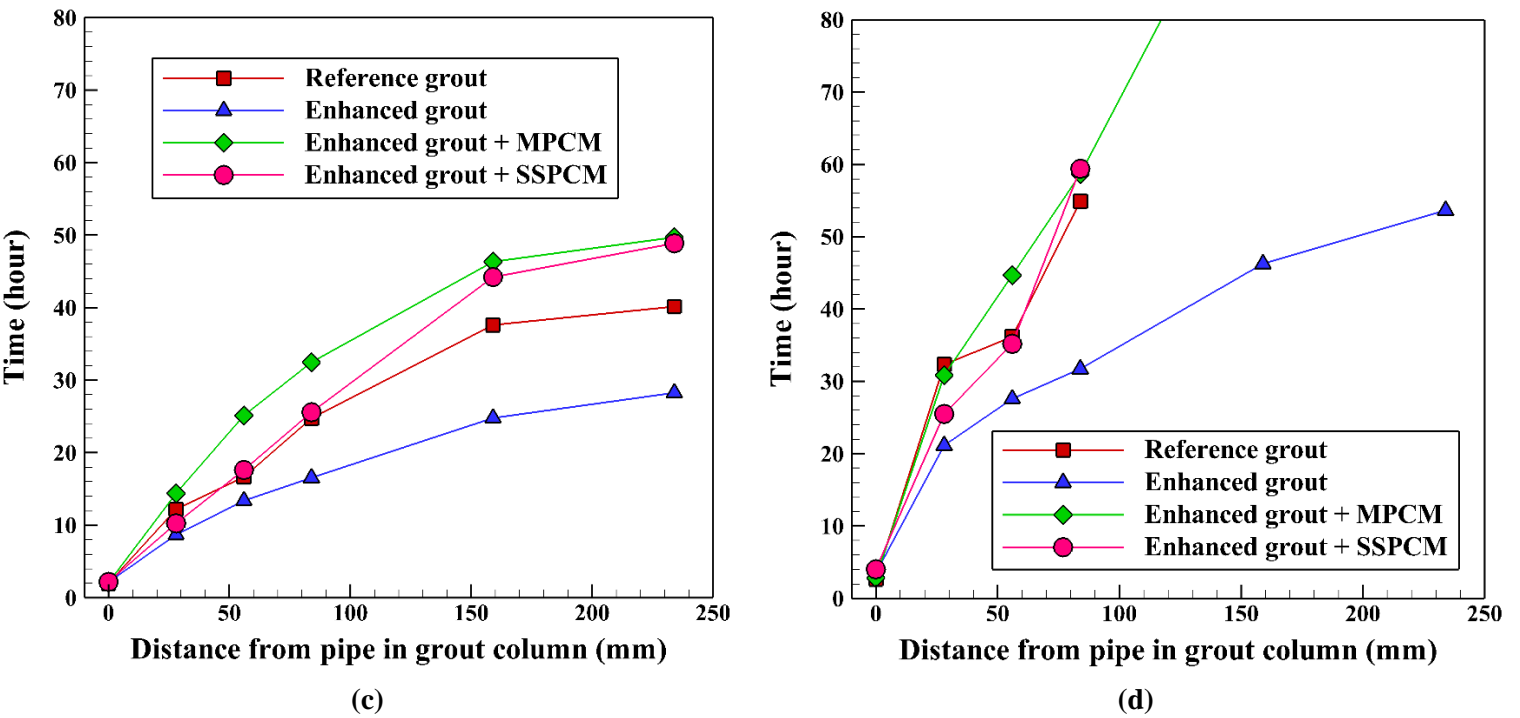
Figure 5-12: Time needed for various thermocouples in different grout columns to reach the same temperatures during the heat injection: (a) 21 °C, (b) 28.3 °C, (c) 35 °C, and (d) 40 °C.

Figure 5-13 illustrates the total surface heat flux at the borehole radius (here the lateral surface of the grout column) for different grout columns during the 30 h of the heat injection from 20 °C to 50 °C. At the beginning of the heat exchange process, the temperature difference between the system and the circulation fluid is at its maximum level, which resulted in achieving the highest values of heat flux for each grout column. Subsequently, the thermal energy transfer from the circulation fluid to the grout and sand decreases because of the reduced temperature differences between the grout and the heat carrier fluid. The presence of MPCM particles inside the enhanced grout decreases the diagram slope notably, keeping the value of heat flux per unit of grout column surface transferred to the sand more constant. On the contrary, the thermally enhanced grout significantly improves the heat dissipation rate from the working fluid to the sand. As can be seen from Figure 5-13, the maximum and minimum heat fluxes are achieved by the grout column containing enhanced grout and the grout column backfilled with the mixture of enhanced grout and MPCM, respectively. 2D contours of the temperature distribution of the sandbox in the four-column test during the heating process at different operating hours are presented in Figure 5-14 (see also Figure 8-7 (Appendix B)). The thermal radius around the pipe increases over time in all grout columns. Heat transfer has occurred mainly in the column containing enhanced grout, which shows its significant capability of heat dissipation to be used as a backfill/grout material in a BHE. In contrast, the minimum heat exchange between each working fluid and the surroundings corresponds to the column filled with a mixture of enhanced grout and MPCM (see also Figure 5-11), related to the gradual melting of the MPCM. Hence, heat storage capacity of MPCM enables it to absorb the heat from heat carrier fluid circulating inside the pipe, illustrating the notable capability of the mixture of MPCM and enhanced grout to be applied in a BTES system. Similarly, in the other column filled with a mixture of enhanced grout and SSPCM, the same trend can be observed, but with a higher rate of heat transfer from the grout column to the sand. This difference in the heat transfer can be related to the higher thermal conductivity

and lower peak melting temperature of this mixture compared with the MPCM mixture (see Table 5-1). Hence, the grout column containing the enhanced grout and SSPCM is subjected to a higher rate of heat transfer, which has caused SSPCM to be melted entirely about 6 h from the start of heat injection (see Figure 5-11 and Figure 5-15). Once the SSPCM reaches its maximum TES capacity, continuing heat injection to the grout column increases the sand temperature clearly above the level that is reached in the grout column filled with MPCM. 3D contours of the temperature distribution of the sandbox in the four-column test can be found in Figure 8-8 (Appendix B). 2D contours of the liquid fraction of the grout columns containing MPCM and SSPCM in the four-column test during the heating operation at different operation hours are illustrated in Figure 5-15. According to this figure and Figure 5-11, it can be concluded that MPCM is melted completely around 17 h after the start of the heat injection. This issue can be justified by MPCM's higher peak melting temperature than SSPCM's, which resulted in increasing the time needed for MPCM to use its maximum capacity in storing thermal energy. Thus, the time difference of a complete melting of the MPCM and SSPCM is approximately 11 h.
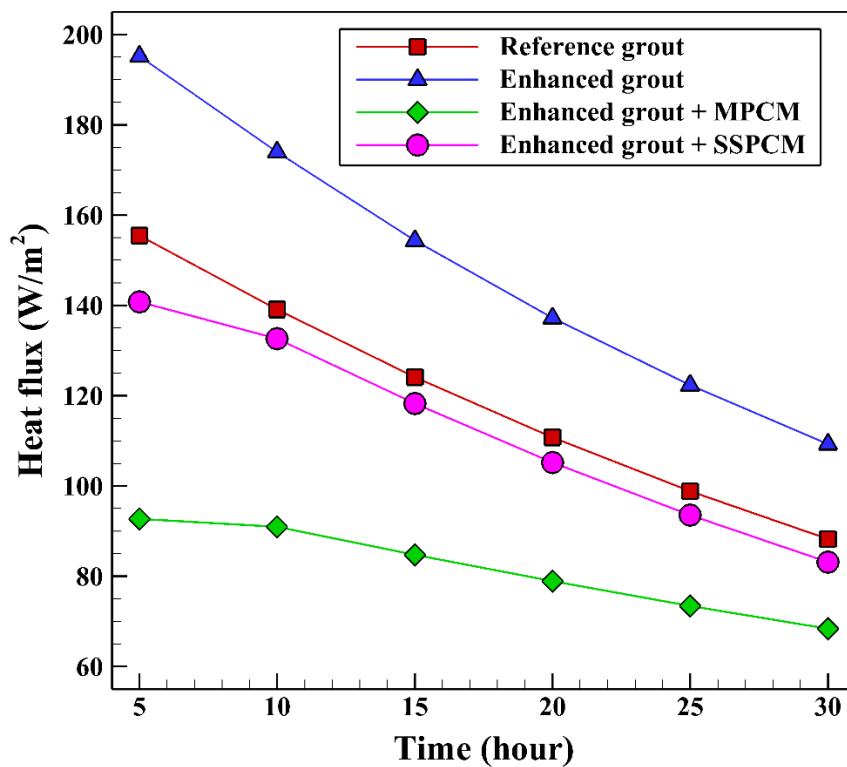
Figure 5-13: Heat flux per unit of surface area at the borehole radius for different grout columns during the 30 hours of the heating operation from 20 °C to 50 °C.
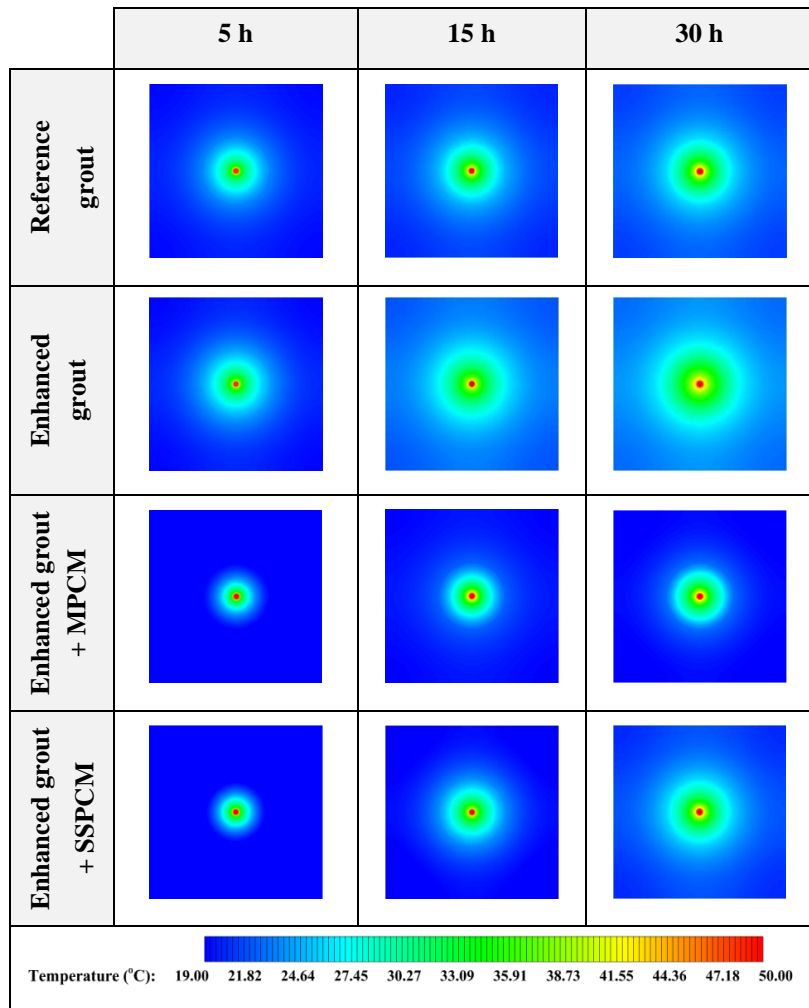
Figure 5-14: 2D contours of the temperature distribution of the sandbox in the four-column test during the heating operation at different operation hours (Top view at Z = 0).
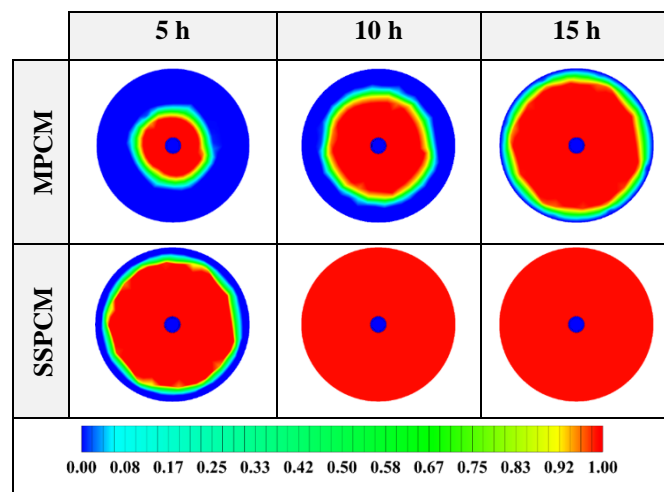
Figure 5-15: 2D contours of the liquid fraction of the grout columns containing MPCM and SSPCM in the four-column test during the heating operation at different operation hours (Top view at Z = 0)

5.5 Conclusions

In this study, different advanced grouting materials, such as enhanced grout, a mixture of enhanced grout and microencapsulated phase change material (MPCM), and a mixture of enhanced grout and shape stabilized phase change material (SSPCM), have been experimentally evaluated using a laboratory-scale prototype in combination with 3D numerical simulation. Based on the literature reviewed, there have been just a few numerical studies on implementing phase change materials in the borehole heat exchangers, and the thermal energy storage application of the borehole heat exchangers has not yet been evaluated in detail. The objective is to study the improvement in the thermal conductivity and thermal energy storage capacity of the three novel grouting formulations compared to a reference grout and investigate the potential of the developed grouts to be applied in a borehole heat exchanger and borehole thermal energy storage systems.

Verifying the numerical results with the experimental data showed good agreement indicating the reliability of the numerical simulations. The experimental and numerical outcomes showed that the grout column with enhanced grout reached the highest total surface heat flux at the borehole radius. In contrast, the grout column backfilled with the mixture of enhanced grout and microencapsulated phase change material achieved the lowest heat flux (almost 37% lower than enhanced grout), thanks to the incorporation of microencapsulated phase change material into the mixture. Despite the faster melting process of SSPCM during the beginning hours of heat injection compared to MPCM, the mushy zone thickness created in the SSPCM mixture (mutual existence of solid and liquid phases) is relatively smaller than that in the MPCM mixture, which may be related to the lower thermal conductivity, specific heat capacity and latent heat of MPCM.

In other words, the grout column with the increased thermal conductivity revealed its heat transfer effectiveness by the quickest reaction toward temperature differences compared with the other three grout columns with reference and phase change materials. Accordingly, when a GSHP system is equipped with a borehole heat exchanger backfilled with the thermally enhanced grout, the heat injection to and extraction from the ground during summer and winter will improve enormously, strengthening the whole system's performance. Moreover, when the borehole heat exchanger contains phase change materials, specifically MPCM, the objective of the GSHP system will be different from a typical shallow geothermal system. Based on the high thermal energy storage capacity of the MPCM, the system performance can be boosted daily or seasonally. In the daily mode, the MPCM stores the thermal energy during the day to minimize the peak load and then reuses the energy during the night. In seasonal operation, the heat is absorbed in the MPCM during summer, and then it can be recovered by the MPCM solidification process for winter. In both operation modes, the GSHP system performance will be improved owing to the enriched capability of MPCM in energy storage.

In conclusion, thermally enhanced grout indicated a significant increase in thermal conductivity compared with that in the reference grout column, demonstrating its ability to provide higher rates of heat transfer, which are beneficial for borehole heat exchangers. Moreover, it is concluded that adding a microencapsulated phase change material to the thermally enhanced grout improves the heat storage capacity remarkably, providing high potential for storing thermal energy for the final mixture. The mixture of enhanced grout and shape stabilized phase change material is found to be inferior to the microencapsulated phase change material solution due to the lower melting temperature and increased thermal conductivity of the mixture.

This research opens further investigation opportunities to optimize the mixture properties for a given application or scenario. Besides, the developed materials evaluated in the present paper will be applied in a real borehole thermal energy storage system to study their capability in storing heat. In future experiments, the integration of more sensitization elements will also be taken into account.

References

1. Ramos-Escudero, Adela, M. Socorro García-Cascales, Jose M. Cuevas, Burkhard Sanner, and Javier F. Urchueguía. "Spatial analysis of indicators affecting the exploitation of shallow geothermal energy at European scale." Renewable Energy 167 (2021): 266-281.
2. K.P. Tsagarakis, L. Efthymiou, A. Michopoulos, A. Mavragani, A.S. Anđelković, F. Antolini, M. Bacic, D. Bajare, M. Baralis, W. Bogusz, S. Burlon, J. Figueira, M.S. Genç, S. Javed, A. Jurelionis, K. Koca, G. Ryżyński, J.F. Urchueguía, B. Žlender. "A review of the legal framework in shallow geothermal energy in selected European countries: Need for guidelines." Renewable Energy 147 (2020): 2556-2571.
3. Javadi, Hossein, Seyed Soheil Mousavi Ajarostaghi, Marc A. Rosen, and Mohsen Pourfallah. "A comprehensive review of backfill materials and their effects on ground heat exchanger performance." Sustainability 10 (2018): 4486.
4. Javadi, Hossein, Seyed Soheil Mousavi Ajarostaghi, Marc A. Rosen, and Mohsen Pourfallah. "Performance of ground heat exchangers: A comprehensive review of recent advances." Energy 178 (2019): 207-233.
5. Badenes, B. Sanner, M.A.M. Pla, J.M. Cuevas, F. Bartoli, F. Ciardelli, R.M. González, A.N. Ghafar, P. Fontana, L.L. Zuñiga, J.F. Urchueguía. "Development of advanced materials guided by numerical simulations to improve performance and cost-efficiency of borehole heat exchangers (BHEs)." Energy 201 (2020): 117628.
6. S. Gehlin. Borehole thermal energy storage, in: Advances in Ground-Source Heat Pump Systems, Woodhead Publishing, Elsevier, 2016, 295-327.
7. M. Reuss. The use of borehole thermal energy storage (BTES) systems, in: Advances in thermal energy storage systems, Woodhead Publishing, Elsevier, 2015, 117-147.
8. Wang, Jin Long, Jing De Zhao, and Ni Liu. "Numerical simulation of borehole heat transfer with phase change material as grout." Applied Mechanics and Materials 577 (2014): 44-47.
9. Qi, Di, Liang Pu, Futao Sun, and Yanzhong Li. "Numerical investigation on thermal performance of ground heat exchangers using phase change materials as grout for ground source heat pump system." Applied Thermal Engineering 106 (2016): 1023-1032.
10. Lyne, Yi, Halime Paksoy, and Mohammed Farid. "Laboratory investigation on the use of thermally enhanced phase change material to improve the performance of borehole heat exchangers for ground source heat pumps." International Journal of Energy Research 43 (2019): 4148-4156.
11. Cortes, Douglas D., Ali Nasirian, and Sheng Dai. Smart Ground-Source Borehole Heat Exchanger Backfills: A Numerical Study, in: International Symposium on Energy Geotechnics, Springer, 2018, 27-34.
12. Aljabr, Ahmad, Andrew Chiasson, and Amr Alhajjaji. "Numerical Modeling of the Effects of Micro-Encapsulated Phase Change Materials Intermixed with Grout in Vertical Borehole Heat Exchangers." Geothermics 96 (2021): 102197.
13. Chen, Fei, Jinfeng Mao, Shangyuan Chen, Chaofeng Li, Pumin Hou, and Lu Liao. "Efficiency analysis of utilizing phase change materials as grout for a vertical U-tube heat exchanger coupled ground source heat pump system." Applied Thermal Engineering 130 (2018): 698-709.
14. Chen, Fei, Jinfeng Mao, Chaofeng Li, Pumin Hou, Yong Li, Zheli Xing, and Shangyuan Chen. "Restoration performance and operation characteristics of a vertical U-tube ground source heat pump system with phase change grouts under different running modes." Applied Thermal Engineering 141 (2018): 467-482.
15. Yang, Weibo, Rui Xu, Binbin Yang, and Jingjing Yang. "Experimental and numerical investigations on the thermal performance of a borehole ground heat exchanger with PCM backfill." Energy 174 (2019): 216-235.

16. Lei, H. Y., and C. S. Dai. "Heat transfer analysis of centric borehole heat exchanger with different backfill materials." In Proceedings of the World Geothermal Congress, Melbourne, Australia, 2015, 19-25.

17. Li, Xiangli, Cang Tong, Lin Duanmu, and Liangkan Liu. "Research on U-tube heat exchanger with shape-stabilized phase change backfill material." Procedia Engineering 146 (2016): 640-647.

18. Li, Xiangli, Cang Tong, Lin Duanmu, and Liangkan Liu. "Study of a U-tube heat exchanger using a shape-stabilized phase change backfill material." Science and Technology for the Built Environment 23 (2017): 430-440.

19. Javadi, Hossein, Javier F. Urchueguia, Seyed Soheil Mousavi Ajarostaghi, and Borja Badenes. "Numerical study on the thermal performance of a single U-tube borehole heat exchanger using nano-enhanced phase change materials." Energies 13 (2020): 5156.

20. Bottarelli, Michele, Aleksandar Georgiev, Ahmet Alper Aydin, Yuehong Su, and Charles Yousif. "Ground-source heat pumps using phase change materials." European Geothermal Congress, Pisa, Italy, 3-7 June 2013.

21. Bottarelli, Michele, Marco Bortoloni, Yuehong Su, Charles Yousif, Ahmet Alper Aydın, and Aleksandar Georgiev. "Numerical analysis of a novel ground heat exchanger coupled with phase change materials." Applied Thermal Engineering 88 (2015): 369-375.

22. Bottarelli, Michele, Marco Bortoloni, and Yuehong Su. "Heat transfer analysis of underground thermal energy storage in shallow trenches filled with encapsulated phase change materials." Applied Thermal Engineering 90 (2015): 1044-1051.

23. Zhang, Mingkan, Xiaobing Liu, Kaushik Biswas, and Joseph Warner. "A three-dimensional numerical investigation of a novel shallow bore ground heat exchanger integrated with phase change material." Applied Thermal Engineering 162 (2019): 114297.

24. Warner, Joseph, Xiaobing Liu, Liang Shi, Ming Qu, and Mingkan Zhang. "A novel shallow bore ground heat exchanger for ground source heat pump applications—Model development and validation." Applied Thermal Engineering 164 (2020): 114460.

25. Warner, Joseph Keith. "Feasibility Study of a Novel Ground Heat Exchanger using Phase-Change Materials." A Thesis Presented for the Master of Science Degree, University of Tennessee, Knoxville (2019).

26. Qin, Di, Zhengxuan Liu, Yuekuan Zhou, Zhongjun Yan, Dachuan Chen, and Guoqiang Zhang. "Dynamic performance of a novel air-soil heat exchanger coupling with diversified energy storage components—modelling development, experimental verification, parametrical design and robust operation." Renewable Energy 167 (2021): 542-557.

27. Liu, Zhengxuan, Pengchen Sun, Mingjing Xie, Yuekuan Zhou, Yingdong He, Guoqiang Zhang, Dachuan Chen, Shuisheng Li, Zhongjun Yan, and Di Qin. "Multivariant optimization and sensitivity analysis of an experimental vertical earth-to-air heat exchanger system integrating phase change material with Taguchi method." Renewable Energy 173 (2021): 401-414.

28. Hassanpour, Ammar, Mehdi Borji, Behrooz M. Ziapour, and Admin Kazemi. "Performance analysis of a cascade PCM heat exchanger and two-phase closed thermosiphon: A case study of geothermal district heating system." Sustainable Energy Technologies and Assessments 40 (2020): 100755.

29. Y. Rabin, and E. Korin. "Incorporation of phase-change materials into a ground thermal energy storage system: theoretical study." Energy Resources Technology 118 (1996): 237-241.

30. Hirmiz, R., H. M. Teamah, M. F. Lightstone, and J. S. Cotton. "Performance of heat pump integrated phase change material thermal storage for electric load shifting in building demand side management." Energy and Buildings 190 (2019): 103-118.

31. Benli, Hüseyin, and Aydın Durmuş. "Evaluation of ground-source heat pump combined latent heat storage system performance in greenhouse heating." Energy and Buildings 41 (2009): 220-228.

32. Benli, Hüseyin. "Energetic performance analysis of a ground-source heat pump system with latent heat storage for a greenhouse heating." Energy Conversion and Management 52 (2011): 581-589.

33. Zhao, Wanfang, Zhongting Hu, Wei He, Sheng Zhang, Hancheng Yu, Gaofei Xu, and Hongbing Chen. "Intermittent mode analysis of a borehole ground heat exchanger with novel phase change backfill materials." Applied Thermal Engineering 189 (2021): 116716.

34. N. Zhu, P. Hu, Y. Lei, Z. Jiang, and F. Lei. "Numerical study on ground source heat pump integrated with phase change material cooling storage system in office building." Applied Thermal Engineering 87 (2015): 615-623.

35. Eslami-nejad, Parham and Michel Bernier. "A preliminary assessment on the use of phase change materials around geothermal boreholes." ASHRAE Transactions 119 (2013): 312.

36. Mousa, M. M., A. M. Bayomy, and M. Z. Saghir. "Phase change materials effect on the thermal radius and energy storage capacity of energy piles: Experimental and numerical study." International Journal of Thermofluids 10 (2021): 100094.

37. Yang, Weibo, Binbin Yang, Feng Wang, and Naidong Jing. "Numerical evaluations on the effects of thermal properties on the thermo-mechanical behaviour of a phase change concrete energy pile." Energy and Built Environment (2021).

38. Alkhwildi, R. Elhashmi, and A. Chiasson. "Parametric modeling and simulation of Low temperature energy storage for cold-climate multi-family residences using a geothermal heat pump system with integrated phase change material storage tank." Geothermics 86 (2020): 101864.

39. Pu, Liang, Lingling Xu, Shengqi Zhang, and Yanzhong Li. "Optimization of ground heat exchanger using microencapsulated phase change material slurry based on tree-shaped structure." Applied Energy 240 (2019): 860-869.

40. McKenna, P., W. J. N. Turner, and D. P. Finn. "Thermal energy storage using phase change material: Analysis of partial tank charging and discharging on system performance in a building cooling application." Applied Thermal Engineering 198 (2021): 117437.

41. Jeon, Jun-Seo, Seung Rae Lee, and Min Jun Kim. "Benefit of phase change material on the performance of horizontal ground heat exchanger: A numerical study." In World Congress on Advances in Civil, Environmental, and Materials Research, Jeju Island. 2016.

42. Dehdezi, Pejman Keikhaei, Matthew R. Hall, and Andrew R. Dawson. "Enhancement of soil thermo-physical properties using microencapsulated phase change materials for ground source heat pump applications." Applied Mechanics and Materials 110 (2012): 1191-1198.

43. Barbi, Silvia, Francesco Barbieri, Simona Marinelli, Bianca Rimini, Sebastiano Merchiori, Barbara Larwa, Michele Bottarelli, and Monia Montorsi. "Phase change material-sand mixtures for distributed latent heat thermal energy storage: Interaction and performance analysis." Renewable Energy 169 (2021): 1066-1076.

44. Erol, Selçuk, and Bertrand François. "Efficiency of various grouting materials for borehole heat exchangers." Applied thermal engineering 70 (2014): 788-799.

45. Pu, Liang, Di Qi, Kang Li, Hongbo Tan, and Yanzhong Li. "Simulation study on the thermal performance of vertical U-tube heat exchangers for ground source heat pump system." Applied Thermal Engineering 79 (2015): 202-213.

Chapter 6

6   Discussion

Although the primary outcomes of the investigation have been deliberated in the preceding chapters, this part outlines the crucial ones and some ongoing endeavors.

6.1   Heat carrier fluid influence

Based on the author's (doctoral student) experience, previously published review articles [1,2], and the consultation with the supervisors, among various elements affecting the thermal performance of the BHE, an alternative and new type of heat carrier fluid was studied numerically at the beginning of this doctoral journey.

Initially, the Ansys Fluent commercial software was utilized to numerically examine a BHE in an unsteady state. Four categories of mixed nanofluids, Fe_3O_4-MWCNT/water, Al_2O_3-CuO/water, Ag-MgO/water, and TiO_2-Cu/water, were numerically studied to determine their viability as the working fluid in a GSHP system. The chosen hybrid nanofluid was assessed at different volume fractions and Reynolds number values.

After contrasting various scenarios at a Reynolds number of 3200 and a volume fraction of 0.15, the Ag-MgO/water hybrid nanofluid was identified as the most favorable operational fluid among the other hybrid nanofluids. This decision was reached because of its excellent efficiency, appropriate thermal resistance, and slightest pressure drop increase compared to a common heat carrier fluid (water).

The study examined the impact of varying the Ag-MgO/water mixed nanofluid's volume fraction at a Reynolds number of 3200. It was determined that all concentrations of Ag-MgO/water from 0.05 to 0.20 had better efficiency and lower thermal resistance than water but with higher pressure drops. After assessing the trade-off between efficiency, pressure drop, and thermal resistance, the Ag-MgO/water with a volume fraction of 0.10 was deemed the optimal fluid for further analysis.

Subsequently, the Ag-MgO/water mixture with a constant volume fraction ($\phi = 0.10$) was examined in terms of various Reynolds numbers. Changing Reynolds numbers from 3200 to 6200 for Ag-MgO/water reduced thermal resistance and enhanced efficiency compared to the equivalent water conditions, despite experiencing greater pressure drops.

To summarize, it was determined that the most effective heat carrier fluid applied to a single U-tube BHE for increasing the effectiveness by almost 37% and decreasing the thermal resistance by about 1.14% was the Ag-MgO/water with a volume fraction of 0.10 and Reynolds number of 3200. Despite this, all the investigated hybrid nanofluids exhibited a COP enhancement below one, signifying that utilizing them as a heat carrier fluid would not be cost-effective due to the higher pressure drop they caused compared to the heat transfer augmentation.

Derived from the initial phase of the current doctoral thesis, employing nanofluids and, more specifically, hybrid nanofluids as a working fluid in GSHP systems holds the potential for enhanced heat transfer characteristics compared to conventional fluids. Nevertheless, there remain obstacles to overcome and opportunities for further research to enhance their efficiency.

Challenges encountered with hybrid nanofluids in BHEs:

Pressure drop: An obstacle in the utilization of hybrid nanofluids is their occasional tendency to display greater viscosity than the base fluids, which subsequently results in an augmented pressure drop within the heat exchange system.

Uniform dispersion: Ensuring a consistent distribution of nanoparticles and additives in hybrid nanofluids, while also keeping it stable over time, can pose a challenge that has an impact on their overall performance.

Further research and lines of inquiry:

Hybrid additives: Conducting experiments using various hybrid additives that have the potential to enhance heat transfer efficiency without causing a substantial increase in viscosity.

Long-term stability: Investigating the enduring stability of hybrid nanofluids within BHEs, encompassing the impact of temperature fluctuations and cycling on their characteristics.

Cost-benefit analysis: Performing cost-effectiveness assessments to assess if the improved heat transfer capabilities of hybrid nanofluids warrant any potential rise in system intricacy and expenditure.

Field testing: Carrying out field experiments and real-world monitoring of ground heat exchanger systems employing hybrid nanofluids to confirm laboratory results and gauge their practical viability.

Operational parameters: Exploring how operational parameters, such as flow rates and temperature differences, affect both pressure drop and heat transfer performance to pinpoint the most favorable operational conditions.

By tackling these obstacles and delving deeper into these domains, it could become feasible to capitalize on the advantages of hybrid nanofluids while mitigating their limitations when employed within GSHP systems.

6.2   Backfill/grout materials influence

6.2.1   Nano-enhanced PCM

Many articles have been published concerning backfill/grout materials to fill the research gaps and to see how a PCM-based novelty can be created. Accordingly, nano-enhanced PCMs (NEPCMs) were found to be an exciting choice to be evaluated by numerical simulation for the first time ever applying to a BHE.

The objective of the study was to examine how Paraffin combined with different types of nanoparticles, such as SiO_2, CuO, graphene, multi-wall carbon nanotube, TiO_2, Al_2O_3, and Cu, could be used as backfill in BHE. Additionally, the study aimed to explore how altering the nanoparticles' volume fraction, which ranged from 0.05 to 0.20, affects the thermal performance of the BHE. Lastly, the research assessed how the shape of the nanoparticles, including platelet, blade, cylinder, sphere, and brick, impacted the NEPCMs' melting rate.

The research found that among the seven types of NEPCMs tested, those containing SiO_2 and Cu showed the worst and the best efficiency enhancement, respectively. Based on this finding, the Cu NEPCM was chosen for more analysis. An increase in the volume fraction of Cu impressively impacted the melting rate of the NEPCM. The optimal volume fraction was found to be 0.20, which resulted in a 55% increase in thermal conductivity compared to pure Paraffin. Regarding the nanoparticles' shape, the blade-shaped Cu nanoparticles showed expressively superior performance compared to others, causing around 85% of the PCM to melt.

In summary, when a 20% volume fraction of Cu nanoparticles was added in a blade shape to Paraffin as a NEPCM, it demonstrated remarkable potential for heat absorption from the working fluid, leading to a decrease in the outlet temperature. This outperformed other types of evaluated nanoparticles.

6.2.2   MPCM, SSPCM, and thermally-enhanced grout

Apart from the NEPCM numerical modeling, an experimental and numerical study of using new types of backfill/grout materials named microencapsulated PCM (MPCM), shape-stabilized PCM (SSPCM), and thermally-enhanced grout was conducted as part of the European project (GEOCOND), which Universitat Politècnica de València (UPV) participated in.

The research aimed to examine how BHEs could be utilized as TES systems with PCMs. Two types of studies were conducted to achieve this goal. Firstly, some materials were tested in a laboratory in Sweden to produce

three different formulas, including improved grout, a combination of improved grout and MPCM, and a combination of improved grout and SSPCM, which had favorable thermo-physical properties and TES capacity for BHE and BTES systems. Secondly, the 3D numerical simulation was conducted for better visualization and to confirm the results obtained from the laboratory experiment.

The numerical results were compared to the experimental data, and the excellent agreement between the two indicated the trustworthiness of the numerical simulations. To put it differently, among the four grout columns tested simultaneously, the one with enhanced thermal conductivity had the most rapid response to temperature differences. Suppose a BHE with thermally enhanced grout is integrated into a GSHP system. In that case, the system's overall performance can be significantly improved by increasing heat exchange with the soil surrounding the borehole for heating and cooling operation modes. Moreover, if the BHE contains PCMs, especially MPCM, the GSHP system's objective will vary from that of a standard GSHP system. The MPCM's high TES capacity can enhance the system's performance on a daily or seasonal basis. Daily, MPCM accumulates heat energy during the daytime to lessen high demands and employs it during the nighttime. In seasonal operation, MPCM absorbs heat during summer and releases it through solidification in winter. In both modes of operation, MPCM's superior TES capacity boosts the GSHP system's efficiency.

In summary, the grout column with improved thermal conductivity exhibited a noteworthy boost in heat transfer rates compared to the reference column, thereby benefiting BHEs. Further, it was concluded that adding MPCM to the thermally enhanced grout substantially improved its TES capacity, offering significant potential for BTES. However, the combination of enhanced grout and SSPCM was deemed less efficient than the MPCM option owing to the mixture's lower melting point and higher thermal conductivity.

This was the last published article included in the current doctoral dissertation. Nevertheless, worth mentioning that another part of the project is still in progress, which is both a field test study and numerical investigation of the produced materials explained above at the thermal test site of UPV.

6.2.3   Field test study and CFD modeling

6.2.3.1.   Field test study

Advanced equipment is available at the pilot site in UPV to test ground and grout properties with great accuracy, using any possible configuration of BHE. The test site is located at Camino de Vera s/n, 46022, UPV, Valencia, Spain as marked in Figure 6-1. To investigate how PCM mixtures affect the thermal efficiency of BTES systems, two such systems (BHE numbers 6 and 7 in Figure 6-2) were set up independently at the field test site. The BHEs comprise several components: heat transfer fluid, U-tube pipe, backfill/grout, casing, and soil. High-precision laboratory for thermal testing of the GHEs at UPV is illustrated in Figure 6-3.
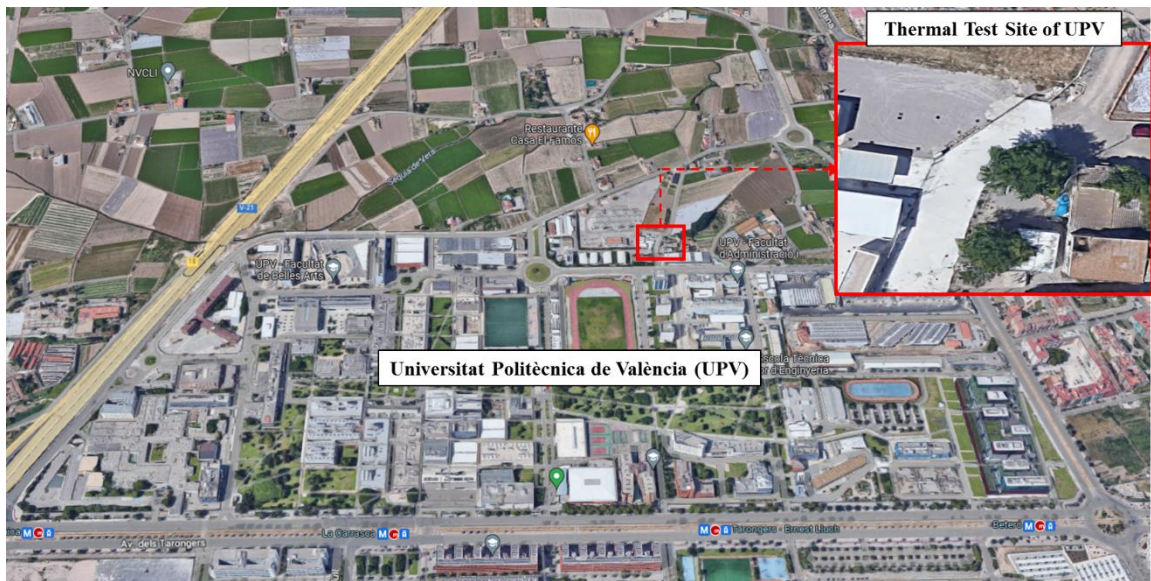
**Figure 6-1: Location of the thermal test site at UPV.**

Figure 6-2: BHE distribution on the field.

Figure 6-3: High-precision laboratory for thermal testing of the GHEs at UPV (inside).

Nowadays, in-situ thermal response tests (TRTs) are frequently used in industry to establish soil thermal characteristics and design GSHP systems. The foundation of an in-situ TRT can be defined by injecting/extracting heat to/from a BHE continuously and studying how it responds to the temperature. They then use a selected simplified model, dependent on several factors, including the soil's thermal conductivity, that must be adjusted to obtain an accurate prediction. In the first test, a total power of 944 W (80 W/m) was injected into BHE 6, which includes MPCM, for about 150 hours (see Figure 6-4).
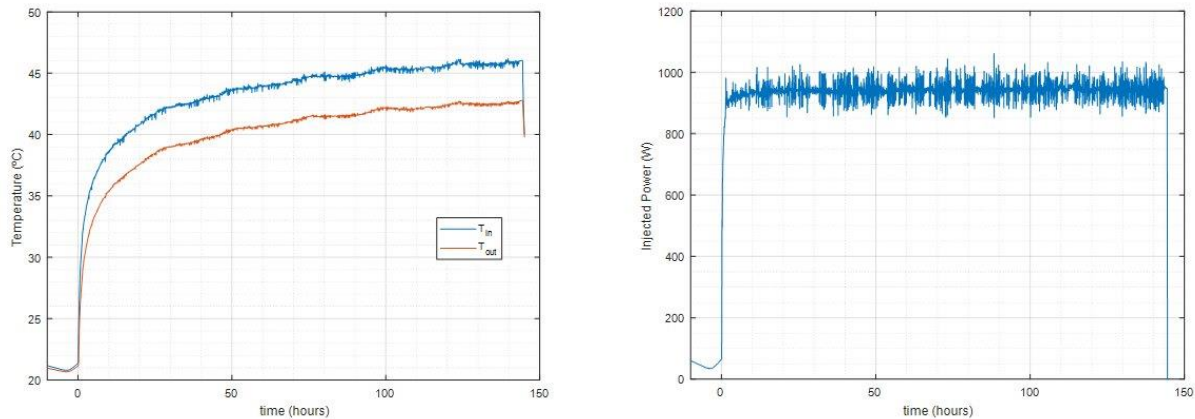

Figure 6-4: TRT on BHE 6: Tin and Tout (left) and thermal power injection (right).

6.2.3.2. CFD modeling

To study the thermal performance of BHE 6 aimed at BTES numerically, a three-dimensional unsteady computational fluid dynamics (CFD) model is created, which matches the actual profile installed in UPV thermal test site. In this work, the BHE 6 comprises the circulation fluid (water), single U-tube, backfill/grout material, casing, and the soil around the borehole (see Figure 6-5). The initial temperature of the grouting and the soil is similar to the undisturbed ground temperature. Under a velocity-inlet condition, a user-defined function (UDF) specifies a changeable temperature and fixed velocity for the inlet boundary. In contrast, the outlet boundary is subjected to a pressure-outlet condition. Geometrical parameters of the numerical model and the simulation conditions of BHE 6 components are presented respectively in Table 6-1 and Table 6-2.
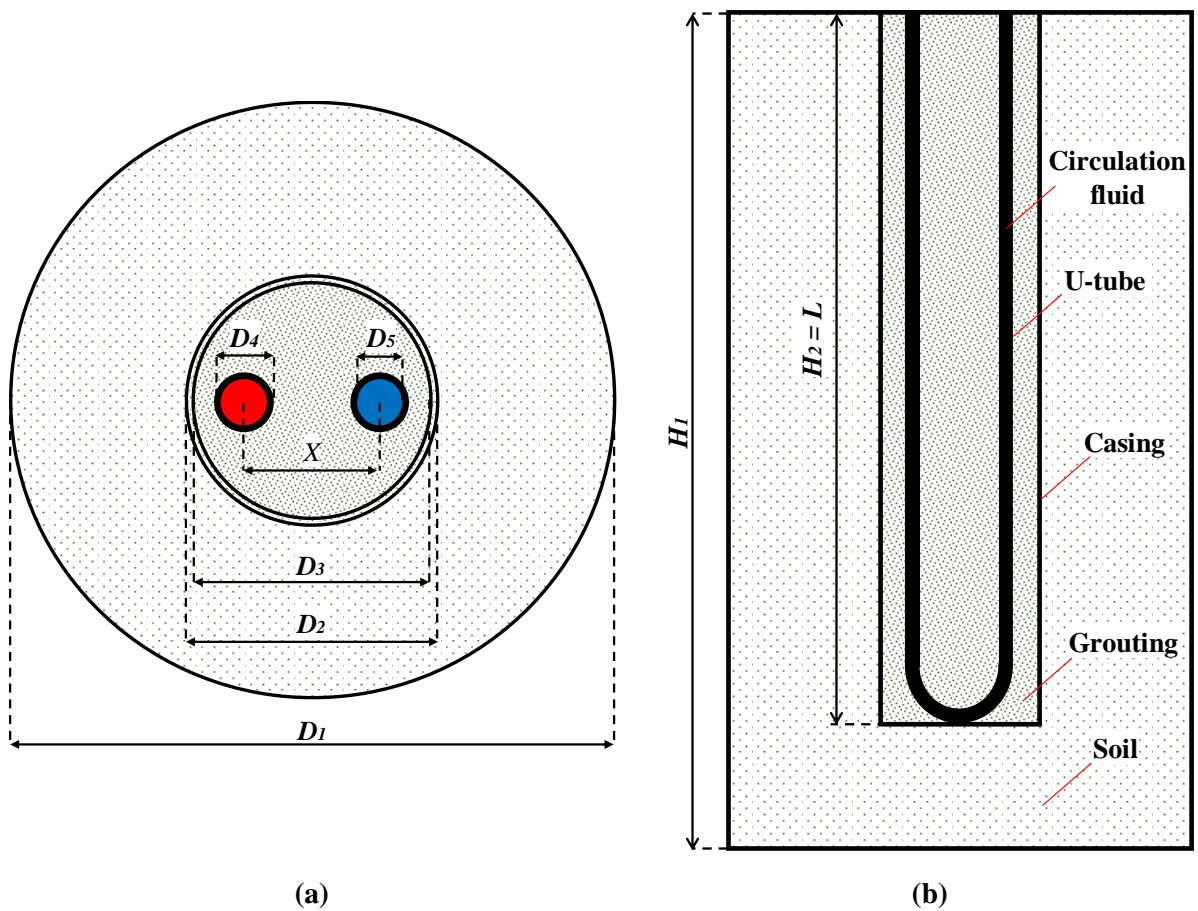
Figure 6-5: Schematics of BHE 6: (a) Top view, (b) Front view.

Table 6-1: Geometrical parameters of BHE 6.

Diameter of calculation domain, D_1	2 m
External diameter of the casing, D_2	0.14 m
Internal diameter of the casing, D_3	0.13 m
External diameter of U-tube, D_4	0.032 m
Internal diameter of U-tube, D_5	0.0262 m
Pipe spacing of U-tube, X	0.082 m
Length of U-tube, L	11.8 m
Borehole depth, H_2	11.8 m
Height of calculation domain, H_1	12.8 m

Table 6-2: Simulation conditions of BHE 6.

Inlet water velocity	250 L/h
Reynolds number	3068
Inlet water temperature	UDF
Undisturbed ground temperature	18.09 ℃
Operating time	Almost 150 h

The model meshing is conducted by Ansys Meshing software, as shown in Figure 6-6. Various parts of the model have been divided into several volumes, and then the meshes are generated applying tetrahedral unstructured and hexagonal structured methods. Unlike the volume near the elbow in which unstructured tetrahedral grids are created, other volumes are meshed by structured hexagonal grids. Finer grids have been generated for the regions inside the borehole compared to the outside. In addition, a grid independence test is carried out to compare different types of meshes, from a coarse mesh with 964,230 elements to a fine mesh with 2,916,926 elements, in terms of heat flux per unit borehole depth, as indicated in Table 6-3. According to this table, there is a minor difference between various cases compared to the experimental value; therefore, considering the precision and good skewness of 0.56, the finer mesh is chosen for the thermal performance analysis of BHE.


(a)

	(b)		(c)
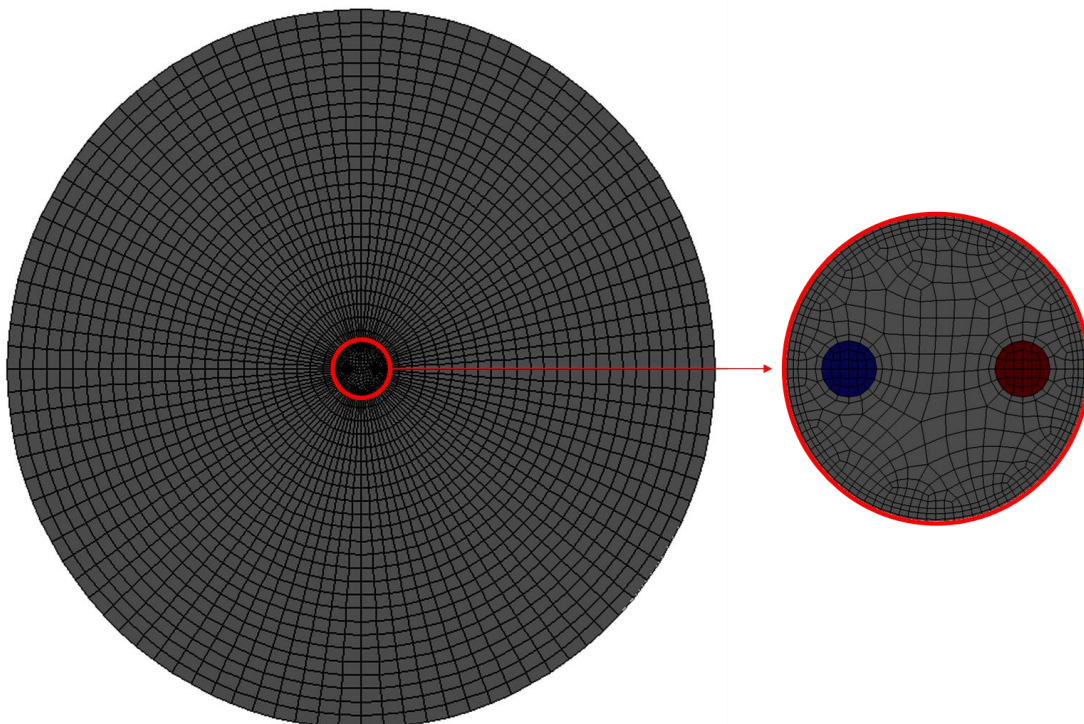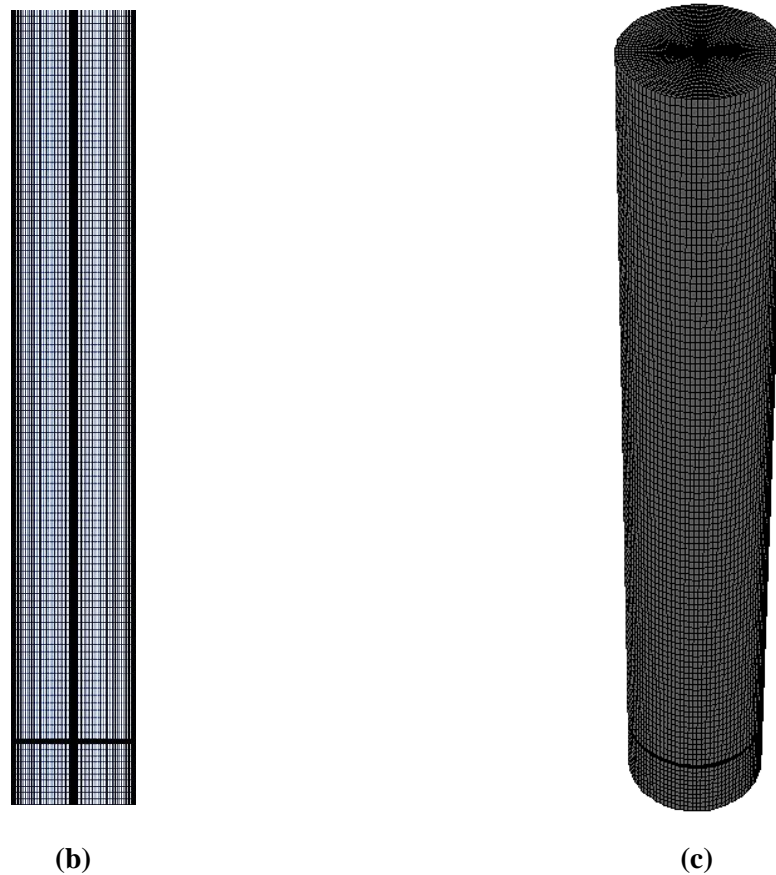
Figure 6-6: Meshing of BHE 6: (a) Top view, (b) Front view, (c) 3D view.

Table 6-3: Grid independence test.

	Coarse mesh	Medium mesh	Fine mesh	Experiment
Elements	964,230	1,881,519	2,916,926	-
Heat flux per unit borehole depth (W/m)	78.16	79.37	80.21	80

Furthermore, Figure 6-7 exhibits how the experimental test confirms the numerical study, indicating that the 3D numerical simulations are dependable. It is important to note that the Ansys Fluent commercial CFD software utilizes only the inlet water temperature data as an input and does not consider the injected power. As a result, to account for variations in the inlet temperature during the simulation of BHE 6, a custom code was developed, known as a UDF, to make the experimental inlet temperature compatible with Ansys Fluent (see Table 6-2). Regarding the continuous behavior of the outlet temperature, it is essential to acknowledge that in transient heat transfer CFD models, certain simplifying assumptions are introduced to streamline the physical model [e.g., 3-5]:

- When considering the thermal properties of both the borehole and the surrounding soil, we assume they are isotropic, homogeneous, and not dependent on temperature changes.

- We treat the undisturbed underground temperature as being consistent throughout.

110

- We do not account for thermal resistance at component joints.

- We do not take into account groundwater convection or the effects of moisture movement on heat transfer.

- We do not assess the influence of ambient temperature on the ground surface.

- We assume that the flow is driven and non-compressible.

The liquid fraction of MPCM and the average temperature of grout are presented in Figure 6-8. Based on this figure and the liquid fraction contours of BHE 6 during the heating injection (Figure 6-9), it is clear that the MPCM particles went into the phase transition once they absorbed the heat from the working fluid. By continuing heat injection to the system, the average temperature of the grout increases, resulting in reaching the total heat storage capacity of MPCM and the complete phase change from solid to liquid at about 28 hours after the start of heat injection. It is illustrated that the injection of heat into the underground continued while the MPCM reached full capacity, and consequently, it could not store more energy which led to higher rates of average grout temperature. Here is the link of the video showing the influence of PCM on the single U-tube BHE performance in summer for the first 30 hours (https://youtu.be/FPyMQGoOsP8).
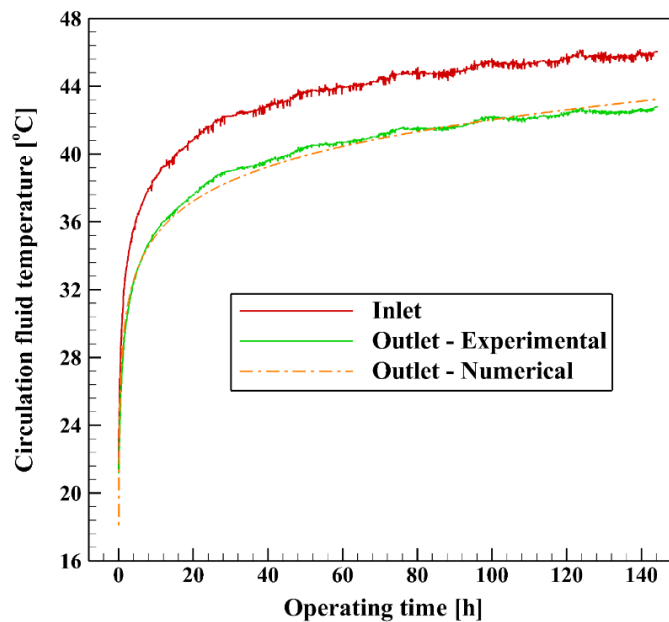

Figure 6-7: Verification of numerical simulation to the experimental test.
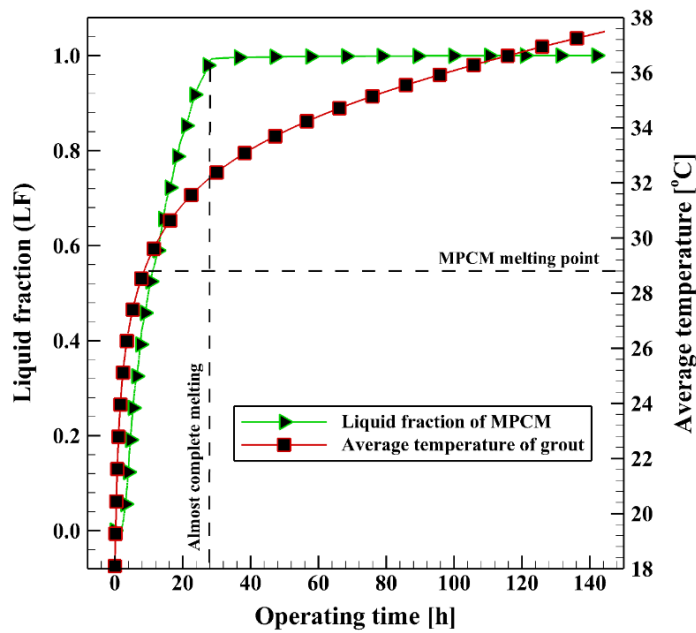
Figure 6-8: The liquid fraction of MPCM and the average temperature of grout.
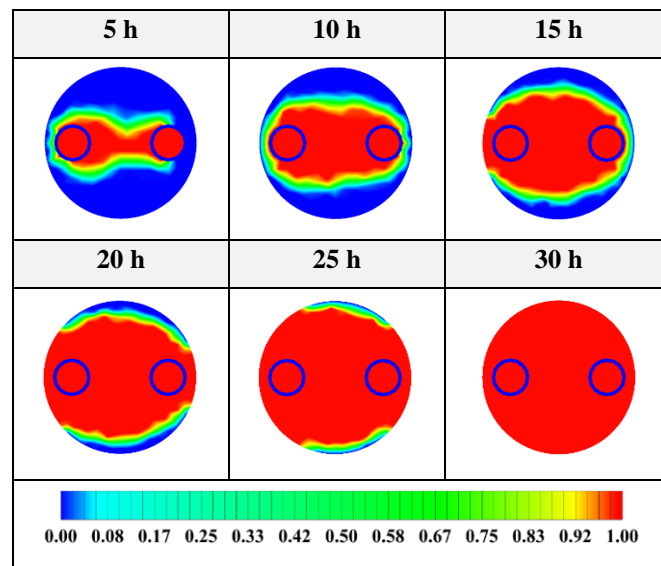
Figure 6-9: 2D contours of the liquid fraction of BHE 6 containing MPCM during the heating injection at different operation hours (Top view at Z = 0).

6.3   Borehole thermal resistance (R_b)

In TRTs, the borehole thermal resistance (R_b) measures how effectively heat is transferred between a BHE and the surrounding ground. During TRTs, a known amount of heat is applied to the BHE, and researchers monitor ground temperature changes over time to estimate R_b using this temperature data (explained in Section 6.2.3.1). For the case of a BHE with constant heat transfer rate per meter borehole depth, which is expected to have a consistent and unchanging R_b throughout its length over time, there will be an effective borehole thermal resistance (R_b). R_b can be estimated using a formula ($T_1 = T_0 + \dot{q}R_b$) involving the mean fluid temperature (T_1

in K), mean borehole wall temperature (T_0 in K), and $\dot{q}$ the heat transfer rate (from borehole to ground) per unit length (W/m) [6-8].

This resistance is affected by factors like the operational conditions (fluid mass flow rate), material thermo-physical properties (fluid, pipes, and grout), and dimensions (pipe shank spacing, number of pipes, and diameters). It should be noted that the BHE's thermal efficiency improves when R_b values are lower. It is crucial to accurately measure this resistance for designing efficient GSHP systems and understanding the impact of diverse geological conditions [9-11].

The thermal test laboratory of UPV, discussed in Section 6.2.3, evaluates PCMs developed in the European GEOCOND project. This evaluation contributes to the main objective of the doctoral dissertation, enabling a field assessment of system performance through TRT analysis. TRTs focus on obtaining the thermal conductivity of the ground and R_b. These parameters are determined using the average fluid temperature circulating in the pipes, acquired experimentally by the data logger system. Experimental data generates a model-based predicted average temperature, and parameters are estimated using direct or inverse approaches [12-14].

In Figure 6-2, BHE number 5 at the UPV thermal site is visible, featuring a single U-tube with thermally enhanced grout (Table 5-1). It has an active depth of 11.4 m and a borehole diameter of 140 mm. Due to the similarity ($\cong$) in geometrical parameters between BHE 5 and BHE 6, BHE 5 is selected to compare estimated R_b values, contrasting two BHEs with and without PCM. Like the TRT on BHE 6 (Figure 6-4), BHE 5 undergoes testing with a heat injection rate of 80 W/m (see Figure 6-10).
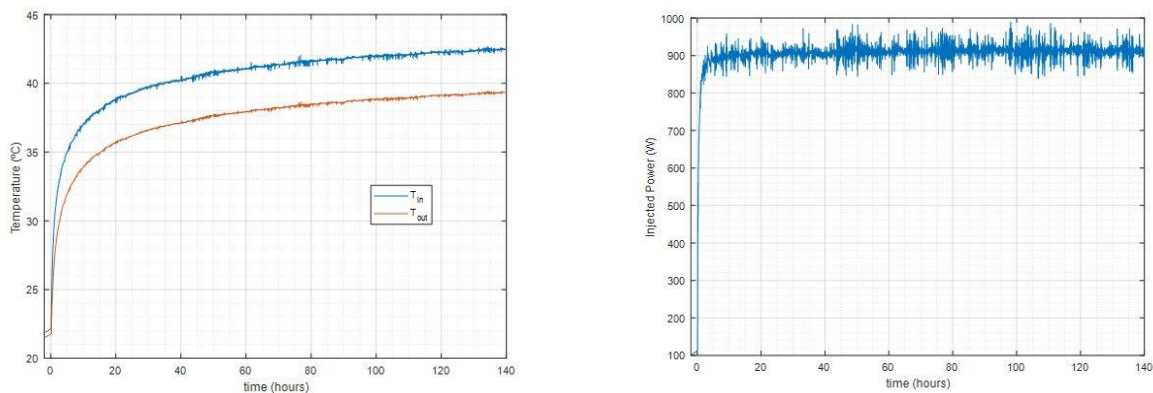

Figure 6-10: TRT on BHE 5: Tin and Tout (left) and thermal power injection (right).

In Section 6.2.3, BHE 6, a single U-tube incorporating MPCM (referring to Table 5-1), was subjected to an 80 W/m heat injection rate (see Figure 6-4). The anticipated outcome was a distinctive thermal response compared to a passive conductive material. As depicted in Figure 6-4, the outlet temperature did not follow a linear increase due to the presence of MPCM and its TES capacity, resulting in a relative temperature response different from that of BHE 5. To explore this further, 3D numerical modeling (as detailed in Section 6.2.3.2) was employed to analyze and visualize PCM activity, a characteristic not directly discernible through TRT.

Following initial TRTs conducted on BHE 5 and BHE 6, the predicted values for R_b were remarkably similar, as outlined in Table 6-4.

Table 6-4: Estimated effective borehole thermal resistance obtained for BHEs 5 and 6.

BHE no.	Effective Borehole Thermal Resistance (R_b) (m·K)/W
BHE 5	0.115
BHE 6	0.110

The TRT method aims to yield dependable thermal parameter values for the BHE/grout/soil system, particularly outside the temperature range where the PCM material undergoes melting and the heat storage capacity fraction dominates. These tests are primarily intended not for quantifying the storage capacity of PCMs during heat injection/extraction but solely for examining the PCM effect through direct comparison with TRT data from materials lacking PCM. It is essential to note that the proximity of R_b values between BHE 5 (without PCM) and BHE 6 (with PCM) justifies the use of PCM inside a borehole, serving the purpose of storing energy in the medium and minimizing heat dissipation from the borehole to the surroundings, essentially transforming the BHE into a BTES. As a result, the estimated R_b values for both boreholes were nearly identical, highlighting the foremost objective and application of the BTES system.

However, it is important to recognize that the TRT outcomes are preliminary and require further work, experiments, and analysis. The ongoing functionality of the field test site at UPV allows for additional tests, contributing to an enhanced understanding of the systems and reinforcing theoretical models for interpreting TRT results.

References

1. Javadi, Hossein, Seyed Soheil Mousavi Ajarostaghi, Marc A. Rosen, and Mohsen Pourfallah. "Performance of ground heat exchangers: A comprehensive review of recent advances." *Energy* 178 (2019): 207-233.
2. Javadi, Hossein, Seyed Soheil Mousavi Ajarostaghi, Marc A. Rosen, and Mohsen Pourfallah. "A comprehensive review of backfill materials and their effects on ground heat exchanger performance." *Sustainability* 10 (2018): 4486.
3. Cao, Shi-Jie, Xiang-Ri Kong, Yelin Deng, Weirong Zhang, Lingyan Yang, and Zi-Ping Ye. "Investigation on thermal performance of steel heat exchanger for ground source heat pump systems using full-scale experiments and numerical simulations." *Applied Thermal Engineering* 115 (2017): 91-98.
4. Yu, Xiaohui, Hongwei Li, Sheng Yao, Vilhjalmur Nielsen, and Alfred Heller. "Development of an efficient numerical model and analysis of heat transfer performance for borehole heat exchanger." *Renewable Energy* 152 (2020): 189-197.
5. Zhu, Shuiping, Jianjun Sun, Kaiyang Zhong, and Haisheng Chen. "Numerical Investigation of the Influence of Precooling on the Thermal Performance of a Borehole Heat Exchanger." *Energies* 15 (2021): 151.
6. Claesson, Johan, and Göran Hellström. "Multipole method to calculate borehole thermal resistances in a borehole heat exchanger." *Hvac&R Research* 17 (2011): 895-911.
7. Fossa, Marco, Stefano Morchio, Antonella Priarone, and Samuele Memme. "Accurate design of BHE fields for geothermal heat pump systems: The ASHRAE-Tp8 methoda compared to non aggregated schemes applied to different European test cases." *Energy and Buildings* (2023): 113814.
8. Priarone, Antonella, Stefano Morchio, Marco Fossa, and Samuele Memme. "Low-Cost Distributed Thermal Response Test for the Estimation of Thermal Ground and Grout Conductivities in Geothermal Heat Pump Applications." *Energies* 16 (2023): 7393.
9. Javed, Saqib, and Jeffrey D. Spitler. "Calculation of borehole thermal resistance." In *Advances in ground-source heat pump systems*, pp. 63-95. Woodhead Publishing, 2016.
10. Javed, Saqib, and Jeffrey Spitler. "Accuracy of borehole thermal resistance calculation methods for grouted single U-tube ground heat exchangers." *Applied Energy* 187 (2017): 790-806.
11. Spitler, Jeffrey, and Michel Bernier. "Ground-source heat pump systems: state-of-the-art." *Science and Technology for the Built Environment* 25 (2019): 945-946.
12. Urchueguía, Javier F., Lenin-Guillermo Lemus-Zúñiga, Jose-Vicente Oliver-Villanueva, Borja Badenes, Miguel A. Mateo Pla, and José Manuel Cuevas. "How reliable are standard thermal response tests? An assessment based on long-term thermal response tests under different operational conditions." *Energies* 11 (2018): 3347.
13. Bandos, Tatyana V., Álvaro Montero, Esther Fernández, Juan Luis G. Santander, José María Isidro, Jezabel Pérez, Pedro J. Fernández de Córdoba, and Javier F. Urchueguía. "Finite line-source model for borehole heat exchangers: effect of vertical temperature variations." *Geothermics* 38 (2009): 263-270.
14. Urchueguia, Javier F., Borja Badenes, Miguel A. Mateo Pla, Bruno Armengot, and Hossein Javadi. "New trilobular geometry using advanced materials for experimentally validated enhanced heat transfer in shallow geothermal applications." *Renewable Energy* (2023): 119816.

Chapter 7

7 Conclusions

Shallow geothermal energy (SGE) refers to the heat stored in the uppermost layer of the earth's surface, which can be harnessed for heating and cooling purposes using a ground source heat pump (GSHP) system. A GSHP system consists of a heat pump unit buried in the ground, which transfers heat to or from the ground using a ground heat exchanger (GHE); if vertical, it is named a borehole heat exchanger (BHE). The GHE is a closed loop of pipes filled with heat transfer fluid that circulates between the heat pump and the ground. In winter, the heat pump extracts heat from the ground and distributes it inside the building through an indoor heating system, while in summer, the heat pump removes heat from the building and discharges it into the ground. This type of renewable energy is efficient, reliable, and has a low carbon footprint, making it an increasingly popular choice for sustainable building design.

BHEs are a popular technology for geothermal heating and cooling systems that use the ground as a heat source or sink. To optimize the performance of these systems, incorporating advanced materials in BHEs for use as thermal energy storage (BTES) can be an effective solution. These materials can improve heat transfer and increase system efficiency while allowing TES during off-peak hours. Additionally, advanced materials such as phase change materials (PCM) can be integrated into BHEs to provide a higher level of energy storage and increase the system's ability to respond to changes in demand. Optimizing BHEs for use as BTES by incorporating advanced materials is a promising solution for improving the efficiency and sustainability of geothermal heating and cooling systems.

This doctoral dissertation emphasizes the alignment between numerical simulations and experimental/laboratory data. In Chapters 2 and 3, a deliberate choice is made to simulate a concise time frame of 24 and 12 hours, reflecting the temporal dynamics observed in the corresponding experimental/laboratory setting. The models used in these chapters are calibrated based on empirical data from the laboratory/experiment, ensuring their accuracy through rigorous validation against experimental observations.

Chapter 4 and, more specifically, Chapter 5 are crucial points in the research methodology, adopting a synergistic approach involving laboratory investigation and numerical modeling. The temporal scope is expanded to 300 hours, but a methodological decision is made to showcase only the initial 30 hours of the 3D modeling outcomes. This selective presentation is driven by the complexities of PCM phase transitions, requiring a focused examination within a limited temporal window.

In Chapter 6, specifically subsection 6.2.3, ongoing aspects of the research are discussed, highlighting continuous experimental efforts in Universitat Politècnica de València (UPV) thermal test laboratory. The data presented in this subsection represents the early stage of ongoing experimental tests, marking the beginning of an iterative process. As the research progresses, future iterations will extend the temporal boundaries of the experimental tests, demonstrating a commitment to thoroughly exploring the studied phenomena through longer-duration tests for a deeper scientific understanding.

Moreover, it is vital to highlight that researchers likewise adopt a 24-hour operation duration for assessing the performance of BHEs, as evidenced by references, e.g., [1-6].

In the present doctoral dissertation, a unique exploration was conducted to assess the usage of hybrid nanofluids as a working fluid in a BHE for the first time ever through numerical simulations.

This study involved investigating a numerical model of a U-tube BHE using Ansys Fluent commercial software. The purpose was to examine four types of hybrid nanofluids: Ag-MgO/water, TiO_2-Cu/water, Al_2O3-CuO/water, and Fe_3O_4-MWCNT/water as potential working fluids for the heat exchanger. Different volume fractions and Reynolds numbers were evaluated for the selected Ag-MgO/water hybrid nanofluid. Upon

comparing the various hybrid nanofluids at $\phi = 0.15$ and Re = 3200, it was found that the Ag-MgO/water hybrid nanofluid performed the best. It demonstrated higher effectiveness, lower thermal resistance, and minor pressure drop increase amongst the other hybrid nanofluids than pure water. As a result, the Ag-MgO/water hybrid nanofluid with $\phi = 0.10$ was chosen as the most suitable working fluid for further investigations. The study then examined the effect of different Reynolds numbers for the Ag-MgO/water hybrid nanofluid with a fixed volume fraction of $\phi = 0.10$. It was observed that higher Reynolds numbers resulted in greater effectiveness and lower thermal resistance compared to pure water, but they also led to increased pressure drops. In summary, the application of Ag-MgO/water hybrid nanofluid (at $\phi = 0.10$ and Re = 3200) in the U-tube borehole heat exchanger improved its effectiveness by 37.02% and reduced its thermal resistance by 1.14% compared to using pure water. Therefore, this hybrid nanofluid was identified as the most effective working fluid for enhancing the heat exchanger's thermal performance. However, it should be noted that all the hybrid nanofluids studied had a lower coefficient of performance (COP) improvement than unity, indicating that their use as working fluids might not be economically viable due to the higher pressure drop they cause in heat transfer enhancement.

Despite the potential advantages of hybrid nanofluids, the research results did not indicate any significant enhancements, concluding that this approach is not advisable for the BTES systems, thereby challenging the initial optimism.

The second step of this doctoral dissertation marks a significant advancement in exploring novel approaches for BTES. For the first time ever again, the study examined nano-enhanced PCMs (NEPCMs) as storage materials. This technique involves the incorporation of nanoparticles into PCMs to improve their thermal conductivity and energy storage capacity. The investigation aimed to identify any system performance improvements that this technique might offer. The research included evaluating seven different types of NEPCMs to explore their potential in BTES systems. The study focused on examining the influence of volume fraction and shape of the nanoparticles on the melting rate and outlet temperature.

This study aimed at analyzing the cooling operation of a GSHP using a 3D numerical model of a single U-tube BHE. The investigation used ANSYS Fluent 18.2, a commercial computational fluid dynamics (CFD) code. The research had three main objectives:

- To explore the effects of seven different types of NEPCMs (incorporating Cu, CuO, Al_2O_3, TiO_2, SiO_2, multi-wall carbon nanotube, and graphene nanoparticles) added to Paraffin as storage medium in BTES.

- To study the influence of varying volume fractions of nanoparticles, ranging from 0.05 to 0.20, on the thermal performance of BTES.

- To assess how the shape of nanoparticles (sphere, brick, cylinder, platelet, and blade) impacts the melting rate of the nano-enhanced PCM.

The results showed that among the different nanoparticles, Cu and SiO_2 demonstrated the most significant and least impact, respectively, on enhancing the thermal performance of the selected BTES. Therefore, Cu NEPCM was selected for further investigation. Increasing the volume fraction of Cu nanoparticles substantially improved the melting rate of the NEPCM. The most suitable volume fraction was found to be 0.20, which increased the thermal conductivity of the NEPCM by up to 55% compared to pure PCM. The blade shape of Cu nanoparticles proved to be the most effective in facilitating about 85% of the melting of the NEPCM.

The 3D numerical simulation results indicated that the most promising NEPCM contained Cu nanoparticles in the blade shape with a volume fraction of 20%. This particular mixture showed substantial potential to absorb thermal energy from the heat transfer fluid and reduce the outlet water temperature compared to other

nanoparticles used as additions to paraffin. The findings of this study suggest that NEPCMs could offer a practical and effective solution for BTES systems, thus contributing to the development of more efficient and sustainable energy systems.

In the final stage of the present research, as a part of a European project called GEOCOND, three different types of storage materials for BTES systems were produced and tested in a laboratory in Sweden. These materials included a thermally-enhanced material, thermally-enhanced material with microencapsulated PCM (MPCM), and thermally-enhanced material with shape-stabilized PCM (SSPSM), which were compared to a typical material. To gain a better understanding of the heat exchange process within these novel materials, numerical modeling was also conducted, which provided visual representations of the process.

SSPCM used in the sandbox test is the material developed within the GEOCOND project framework. MPCM is a commercially available PCM with comparable phase transition a) temperature interval, b) thermal effect. MPCM was benefited as a reference PCM allowing comparative evaluation of technical, technological, and thermal performance of the experimental SSPCM. The percentage of both PCMs in the formulations was targeted at 20% which should be comparable and allow detection of their thermal activity while keeping processability of the formulations acceptable for conventional grout processing equipment. However, dosage was reduced due to workability loss. Reference MPCM, having much smaller particle size, was easier to incorporate, so the target composition was prepared. Finally, both compositions differed not so much in organic phase content and showed detectable thermal activity, allowing comparative evaluation of their performance.

The objective of the research was to assess the improvement in thermal conductivity and TES capacity of the three novel grouting formulations compared to a reference grout. Additionally, the potential of these developed grouts to be utilized in the BTES systems was investigated. The experimental data were verified against numerical results, demonstrating good agreement, and confirming the reliability of the simulations. Among the grout columns, the one with enhanced grout exhibited the highest total surface heat flux at the borehole radius, indicating its superior heat transfer effectiveness compared to the other three grout columns containing reference and PCMs. The grout column backfilled with a mixture of enhanced grout and MPCM displayed the lowest heat flux, approximately 37% lower than enhanced grout, due to the incorporation of MPCM, which has a slower melting process compared to SSPCM. However, the SSPCM mixture showed a relatively smaller mushy zone thickness (a region with mutual existence of solid and liquid phases) than the MPCM mixture, likely due to the lower thermal conductivity, specific heat capacity, and latent heat of MPCM.

The results of the tests and modeling helped to provide insights into the performance of the different materials and their potential applications in either BHE or BTES. The grout material with high thermal conductivity significantly enhanced the heat transfer rate, making it beneficial for BHEs. Additionally, adding MPCM to the grout material with high thermal conductivity showed a remarkable increase in heat storage capacity, which holds excellent potential for BTES systems. However, the mixture of enhanced grout and SSPCM was less effective than the MPCM solution, mainly due to its lower melting temperature and increased thermal conductivity.

7.1   Works in progress and future scope

The investigation of the new PCM mixtures made in the laboratory in Sweden is still ongoing and currently being evaluated at the shallow geothermal test site of UPV. This is being done to conduct a field test and observe the behavior of these materials in real-world conditions. These days, thermal tests are carried out on a single U-tube BHE containing MPCM aimed at a BTES. Moreover, a three-dimensional numerical simulation

is used to model the underground thermal process. Additional tests are required for a complete analysis of this modern backfill.

In addition, the composite material consisting of SSPCM and grout, which has enhanced thermal conductivity, is being utilized in one of the boreholes situated in UPV's thermal test site. An underground U-tube BHE has been installed, and the cooling operation mode during the summer season will be evaluated on this mixture.

While the novel PCM-contained materials showed a significant influence in laboratory tests, their impact on the thermal efficiency of BHE installed in the shallow geothermal test site at UPV for TES was found to be limited. Therefore, the system is planned to be operated intermittently to evaluate its performance. However, additional research is necessary to explore the formulation and percentage of PCM in the backfill/grout material applied to a BTES system.

Moreover, the thermal test site at UPV comprises various types of BHEs, such as the coaxial, flat radiator, and trilobular geometries, each with distinct configurations, pipe materials, and grout materials. Although these boreholes have undergone occasional heat injection evaluations, additional experimental tests and 3D numerical simulations are essential to analyze them further and enhance shallow geothermal systems' performance.

References

1. Miyara, Akio, Koutaro Tsubaki, Shuntaro Inoue, and Kentaro Yoshida. "Experimental study of several types of ground heat exchanger using a steel pile foundation." *Renewable Energy* 36 (2011): 764-771.
2. Zanchini, Enzo, Stefano Lazzari, and Antonella Priarone. "Long-term performance of large borehole heat exchanger fields with unbalanced seasonal loads and groundwater flow." *Energy* 38 (2012): 66-77.
3. Miyara, Akio. "Thermal performance investigation of several types of vertical ground heat exchangers with different operation mode." *Applied Thermal Engineering* 33 (2012): 167-174.
4. Miyara, Akio. "Thermal performance and pressure drop of spiral-tube ground heat exchangers for ground-source heat pump." *Applied Thermal Engineering* 90 (2015): 630-637.
5. Yang, Weibo, Pengfei Lu, and Yongping Chen. "Laboratory investigations of the thermal performance of an energy pile with spiral coil ground heat exchanger." *Energy and Buildings* 128 (2016): 491-502.
6. Chen, Shangyuan, Jinfeng Mao, and Xu Han. "Heat transfer analysis of a vertical ground heat exchanger using numerical simulation and multiple regression model." *Energy and Buildings* 129 (2016): 81-91.

Appendix

8   Appendix

8.1   A

	3 h	12 h
NEPCM-Cu		
NEPCM-Graphene		
NEPCM-MWCNT		
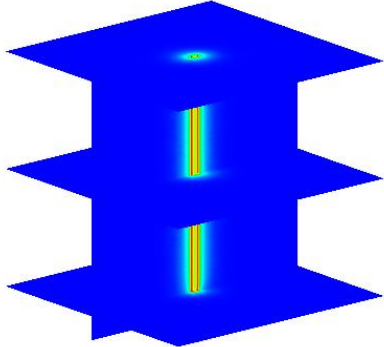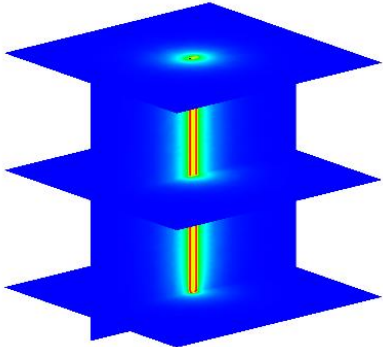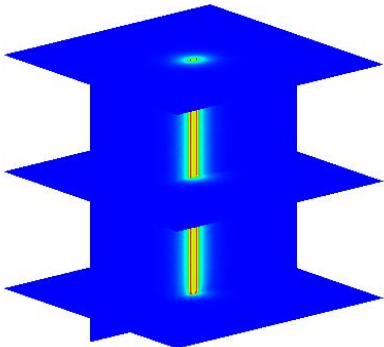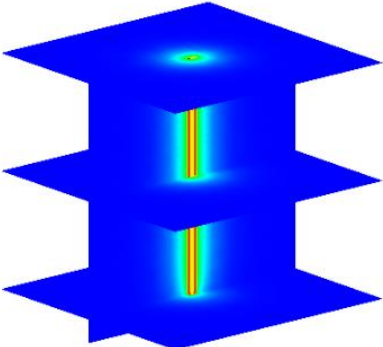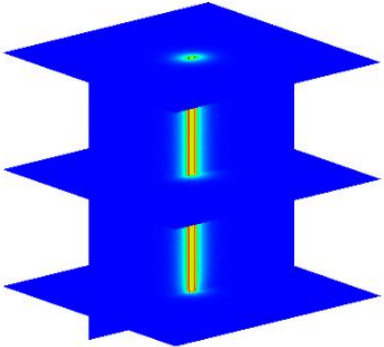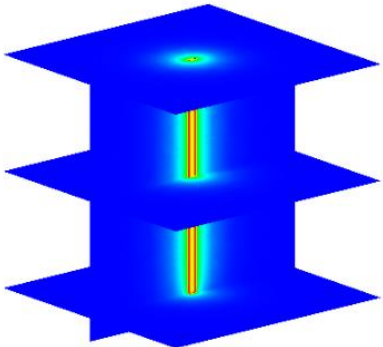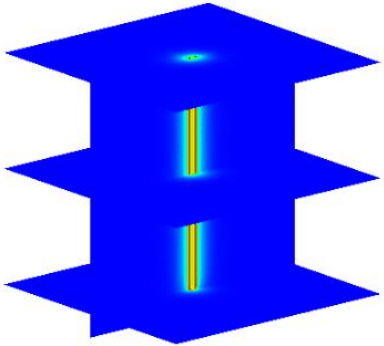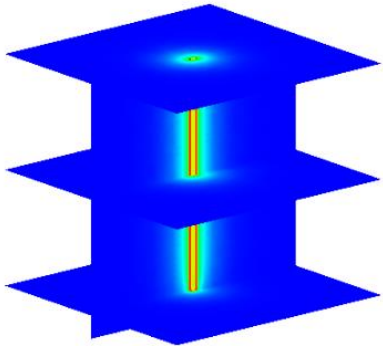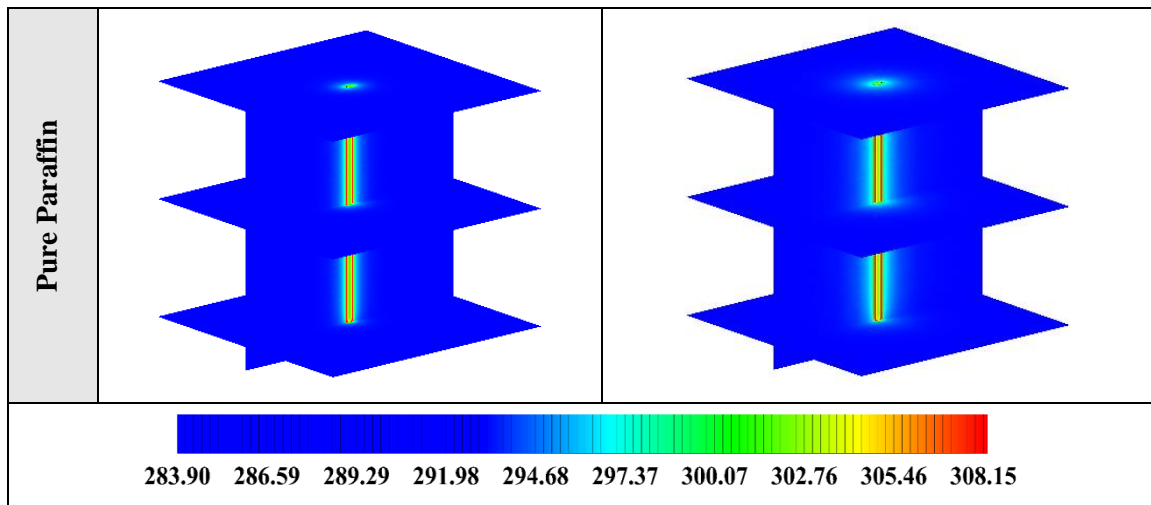
Figure 8-1: 3D contours of the temperature distribution of the BHE at various hours of operating for different NEPCMs when φ = 0.20, n = 3.

| 0.15 | | |
| 0.20 | | |

283.90 286.59 289.29 291.98 294.68 297.37 300.07 302.76 305.46 308.15

Figure 8-2: 3D contours of the temperature distribution of the BHE at various hours of operating for NEPCM containing Cu nanoparticles with different volume fractions when n = 3.

| *n* | **3 h** | **12 h** |
| 3 | | |

Figure 8-3: 3D contours of the temperature distribution of the BHE at various hours of operating for NEPCM containing Cu nanoparticles with different shape factors when ϕ = 0.20.

|	**3 h**	**6 h**	**9 h**	**12 h**
NEPCM-Cu				
NEPCM-Graphene				
NEPCM-MWCNT				
NEPCM-Al₂O₃				
NEPCM-CuO				

Figure 8-4: 2D contours of the temperature distribution of the BHE at various hours of operating for different NEPCMs when φ = 0.20, n = 3 (Front view, middle plane).
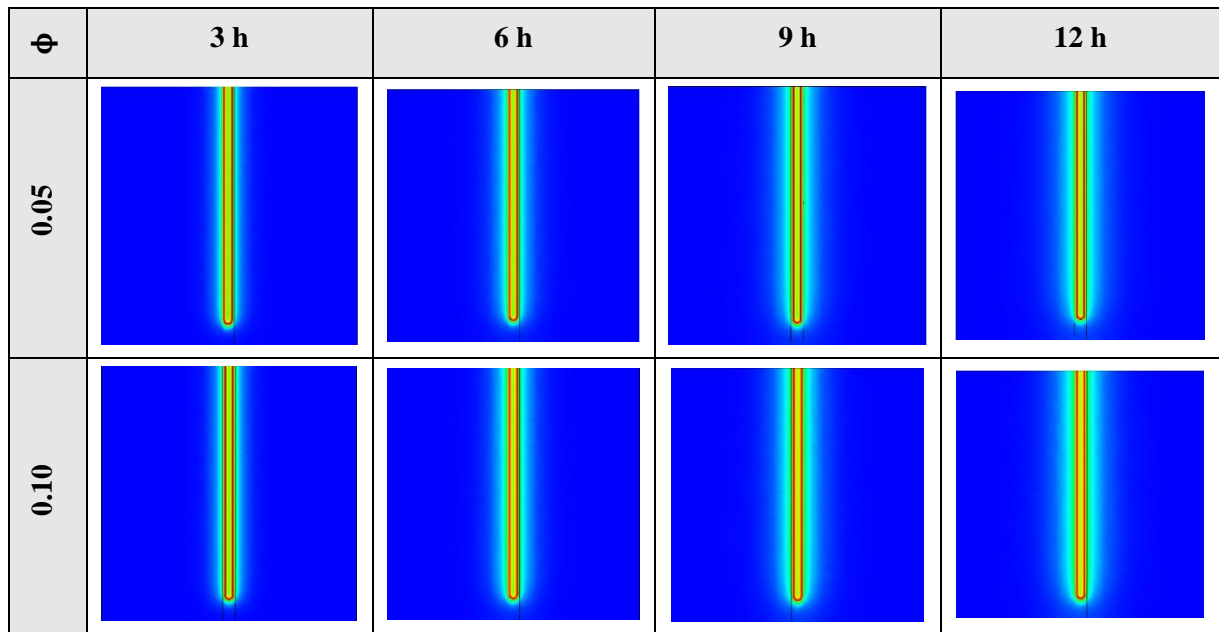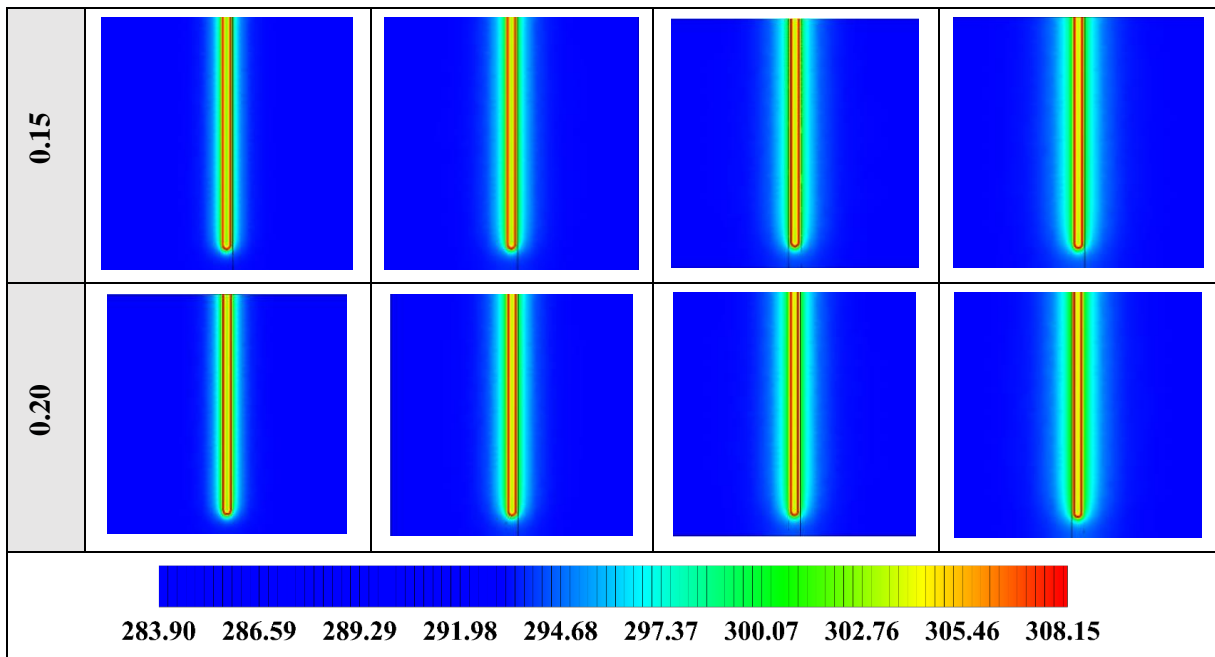
Figure 8-5: 2D contours of the temperature distribution of the BHE at various hours of operating for NEPCM containing Cu nanoparticles with different volume fractions when n = 3 (Front view, middle plane).

n	3 h	6 h	9 h	12 h
3				
3.7				
4.9				
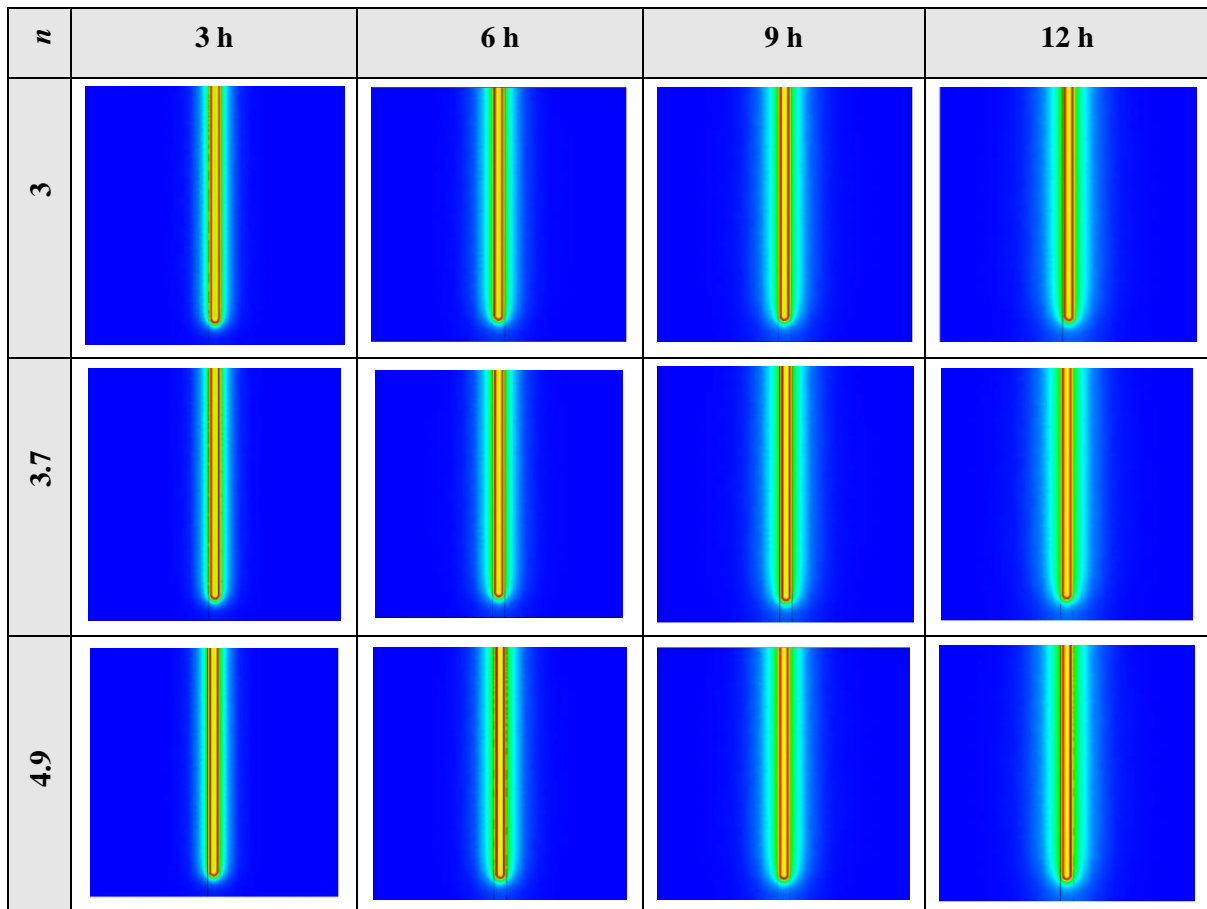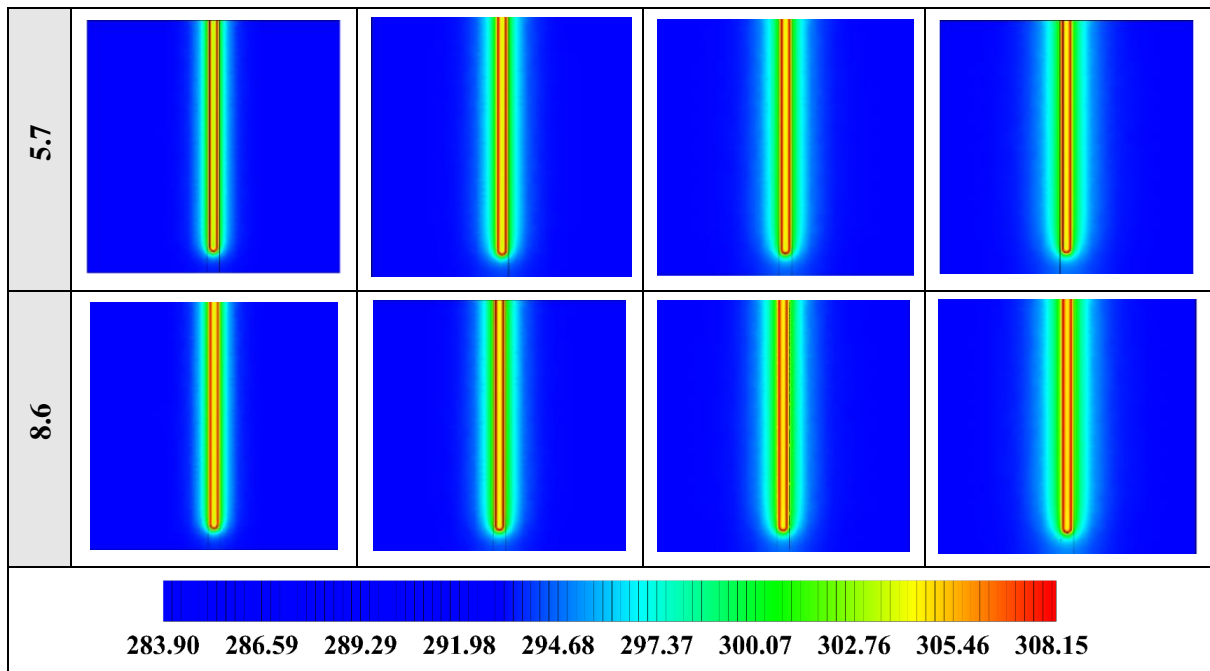
Figure 8-6: 2D contours of the temperature distribution of the BHE at various hours of operating for NEPCM containing Cu nanoparticles with different shape factors when ϕ = 0.20 (Front view, middle plane).

8.2 B

|	5 h	15 h	30 h
Reference grout			
Enhanced grout			
Enhanced grout + MPCM			
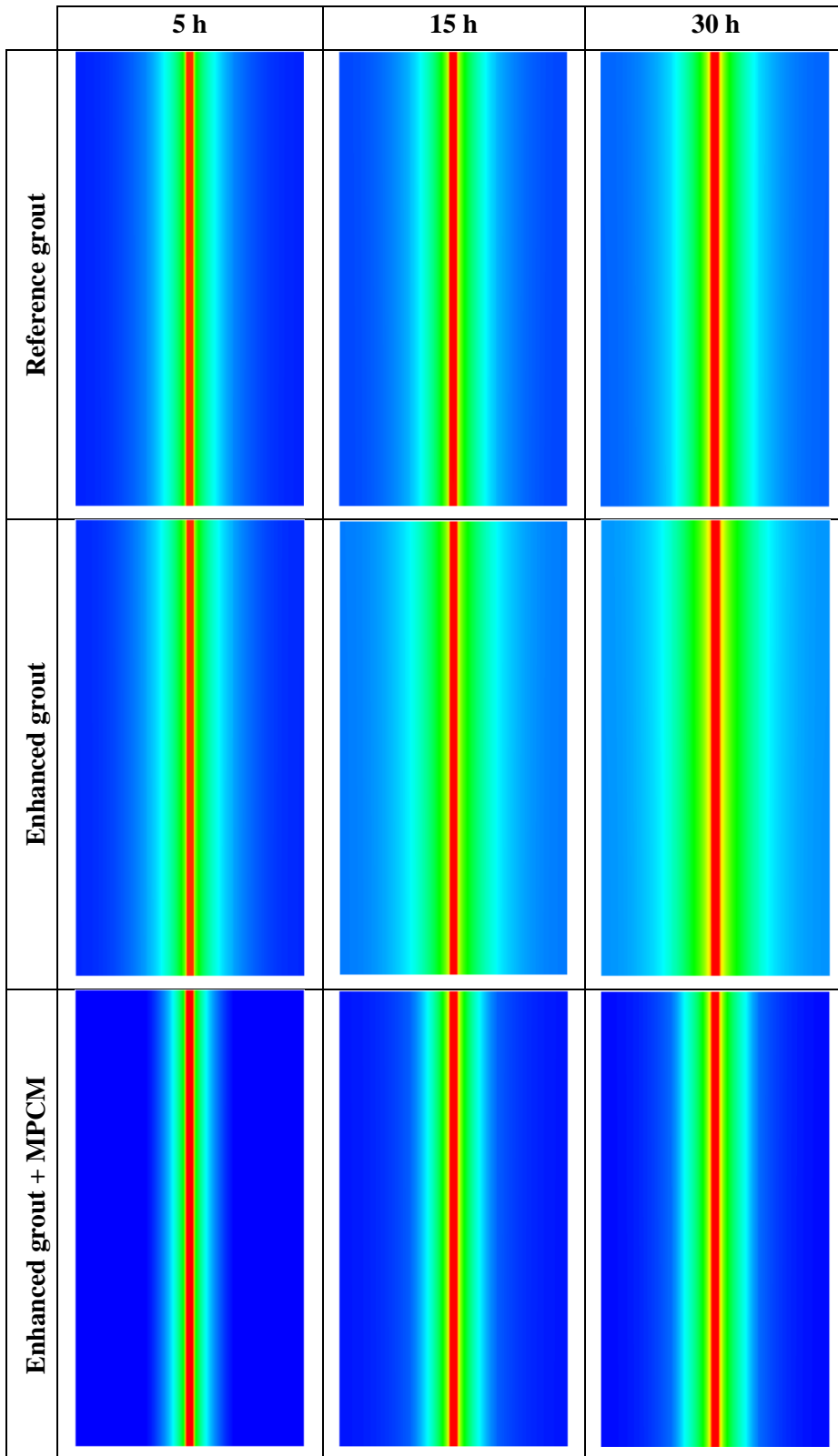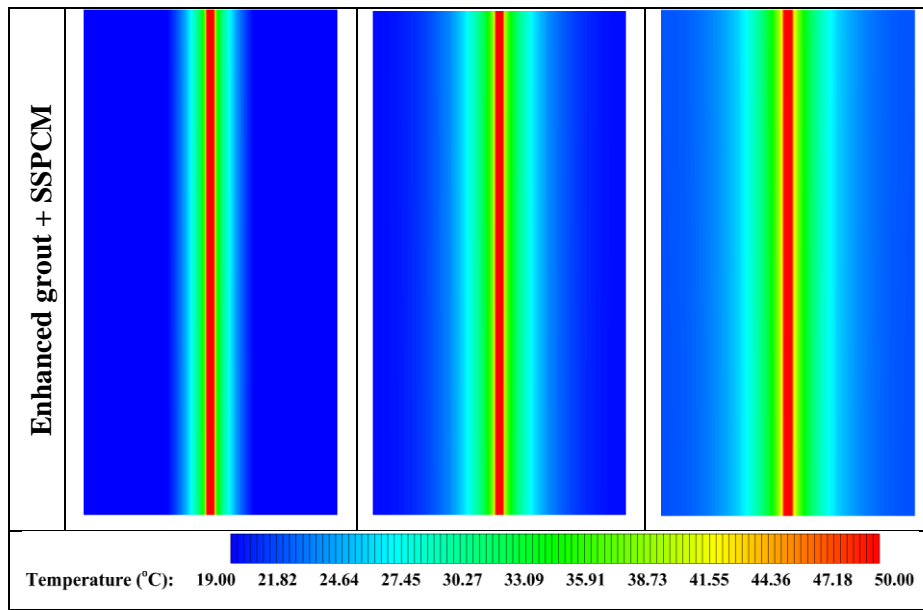
Figure 8-7: 2D contours of the temperature distribution of the sandbox in the four-column test during the heating operation at different operation hours (Front view, middle plane).
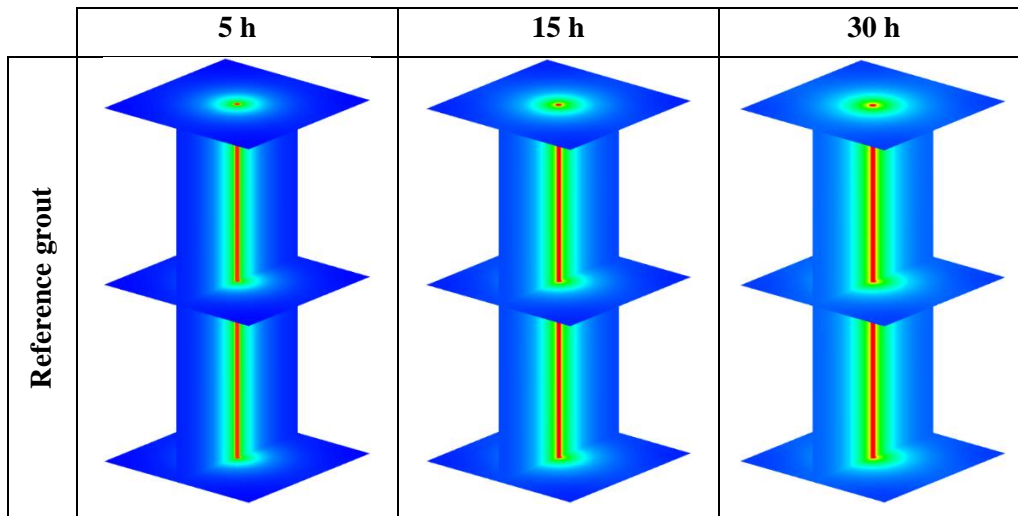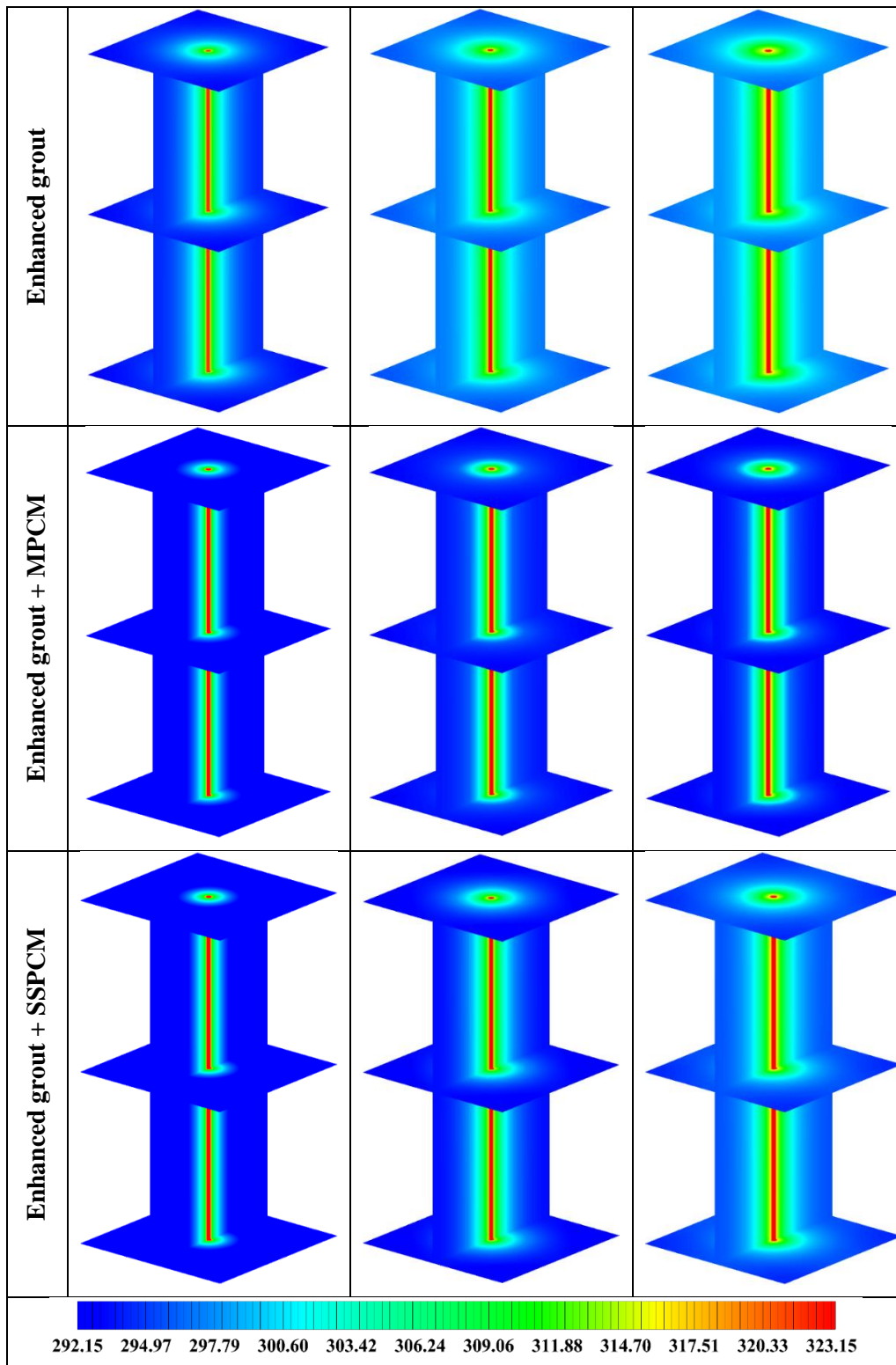
Figure 8-8: 3D contours of the temperature distribution of the sandbox in the four-column test during the heat injection at different operation hours.

134